The role of HDAC2 and Brg1 in adult neural stem cells

PhD Thesis

Submitted to the Faculty of Biology
Ludwig-Maximilian-University Munich

Prepared at the Helmholtz-Zentrum/Institute of Stem Cell Research (Prof. Dr. Magdalena Götz)

Melanie Jawerka

submitted at 31.07.2008

1. Gutachter: Prof. Dr. Magdalena Götz

2. Gutachter: Prof. Dr. Thomas Cremer

Tag der mündlichen Prüfung: 23.02.2009

Contents

1 Abstract

To understand the role of epigenetic mechanisms involved in neural stem cells during development and adulthood, I examined the localisation and function of the histone deacetylase (HDAC) 2 that affects transcriptional regulation by modifying the N-terminal ends of the histone tails resulting in decreased transcriptional activity. HDAC2 protein was detected at high levels in postmitotic neurons in the developing and adult brain. Interestingly, neuronal precursors in the developing brain did not contain HDAC2 protein, while it increased in neuronal precursors in postnatal and adult forebrain. In the two regions of adult neurogenesis, HDAC2 was contained in doublecortin-positive neuroblasts and in transit-amplifying progenitors, but not in the adult neural stem cells. In order to understand the function of HDAC2 in neurogenesis, I examined an HDAC2 deficient mouse line lacking the catalytic activity of HDAC2. While embryonic neurogenesis occurs normal in these mice, the proliferation of adult neural progenitors is increased and neurons derived from both zones of adult neurogenesis, the subependymal zone (SEZ) and dentate gyrus (DG) die at a specific maturation stage in the absence of functional HDAC2. *In vitro* cultures of neural stem cells from the adult HDAC2 deficient SEZ also showed defects in neuronal maturation while proliferation and the self-renewal capacity remained unaltered. Interestingly, these neuronal maturation deficits were not observed in neural stem cell cultures isolated from the embryonic brain. These defects in neuronal maturation from isolated neural stem cells therefore imply a cell-autonomous function of HDAC2 and transplantation experiments of WT cells into mutant mice further rule out the possibility that additional niche-dependent defects in HDAC2 deficient mice might contribute to the phenotype. Thus, the absence of functional HDAC2 reveals a rather specific function in adult neurogenesis and the maturation of adult generated neurons. As transcription is regulated by histone modifications in cooperation with the chromatin remodeling machinery, I also examined the role of the brahma-related gene (Brg) 1 that acts as the ATPase subunit in the chromatin remodeling complex SWI/SNF. Brg1 and HDAC2 were coexpressed in most brain cells, prompting the question whether deletion of Brg1 would result in a similar phenotype than loss of HDAC2-function. To examine the role of Brg1 in adult neurogenesis, I took advantage of a mouse line expressing the inducible form of Cre in adult neural stem cells. Brg1 deletion in adult neural stem cells resulted in

defects in neuronal fate acquisition and apparent fate conversion into the oligodendrocyte lineage. Furthermore, the lack of Brg1 reduces self-renewing adult neural stem cells *in vitro*. These data therefore identify for the first time a specific role of two epigenetic factors in the central nervous system, HDAC2 and Brg1, revealing their distinct functions in adult neurogenesis. HDAC2 is involved in the regulation of neuronal maturation in the adult, but not the embryonic brain. Conversely, Brg1 regulates neural stem cell maintenance and neuronal cell fate in both embryonic and adult neurogenesis. Thus, the functions of HDAC2 and Brg1 reveal the specificity by which epigenetic regulators affect key aspects of adult neurogenesis with the later regulating fate and the former regulating neuronal maturation.

2 Introduction

Neural stem cells have the ability to generate distinct cell types for the formation of the nervous system and cell replacement during development and throughout adulthood. Neural development and plasticity are determined by both extrinsic and intrinsic factors that interface to regulate gene programs controlling neural cell fate and function. The molecular mechanisms of complex processes such as proliferation and differentiation are not yet well understood. Recent reports have shown that chromatin remodeling and epigenetic gene regulation play an important role in diverse areas such as neural cell fate specification and synaptic development and function. Epigenetic mechanisms include cell-type specific transcriptional regulation, histone modifications and chromatin remodeling enzymes. In this study two epigenetic regulators and their role in neural stem cells will be introduced. First, the histone deacetylase (HDAC) 2, a small enzyme capable of deacetylating histones as well as proteins known to act as transcriptional repressors. Second, brahma-related gene (Brg) 1, an ATPase catalytically active in a chromatin remodeling complex SWI/SNF (mating type switching/sucrose nonfermenting) and known to act predominantly as a transcriptional activator. The expression analysis from embryonic to adult stages for both proteins will be presented followed by a functional study of transgenic mouse lines deficient for HDAC2 and Brg1 to examine their role in adult neural stem cells and their differentiation toward the neuronal lineage generating constantly new neurons in the adult mouse brain.

2.1 Neural stem cells

The mammalian central nervous system (CNS) is a complex structure that first arises by folding in the neural plate to become the neural tube, which comprises neuroepithelial stem cells. These cells were historically believed to produce two separate pools of committed neuronal and glial progenitors [His, 1889], which then generate neurons and glia, respectively, in the brain. Other studies support a different model in which neuroepithelial cells either produce or transform into radial glia that divide asymmetrically to give rise to neurons and glia [Schaper, 1897]. Recent data have shown that neuroepithelial cells divide symmetrically and thereby

generate two stem cells [Gotz and Huttner, 2005] followed by many asymmetric cell divisions generating a more restricted progenitor and a neuron. In the primitive neural tube neuroepithelial cells contact both the ventricular and pial surface as depicted in **Figure 2.1**. They then form the neuroepithelium and undergo interkinetic nuclear migration where the distinct area of one single layer of neuroepithelial cells forming the neuroepithelium appears as layered. As development progresses, the wall of the neural tube thickens and neuroepithelial cells transform into elongated radial glia by maintaining their ventricular and pial contacts.

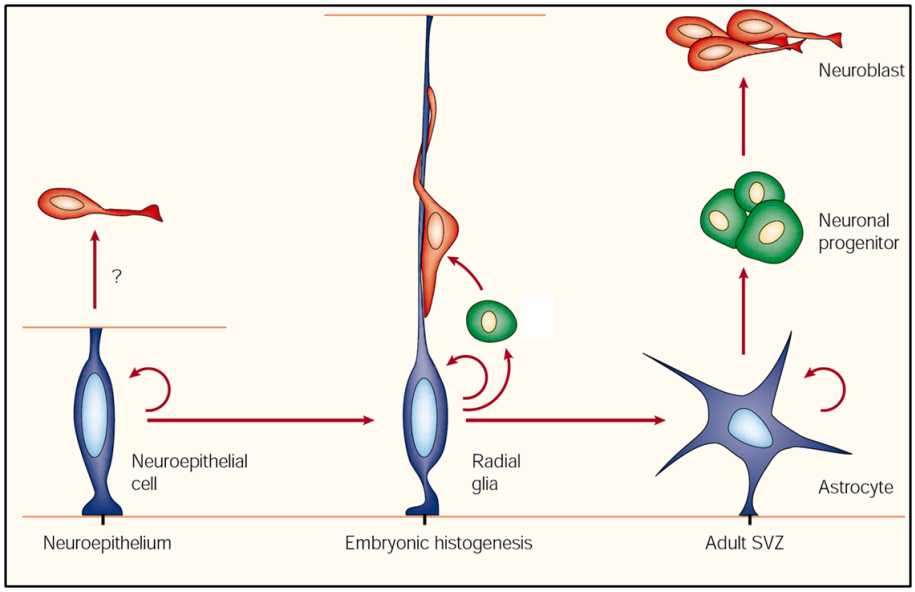

Figure 2.1: Schematic illustration of neural stem cell development

Left panel: Neuroepithelial stem cells (purple) extend from the ventricle to the pia. Middle panel: Radial glia (purple) also contact the pia and ventricular surface. These cells are known to divide either symmetrically or asymmetrically (arrows) to produce neurons that migrate into the cortex along the fiber of the radial glia. Radial glia produce neurons directly or indirectly via intermediate precursors (green). Right panel: Radial glia transform into cortical astrocytes later in development. Picture taken from Alvarez-Buylla et al., 2001

Radial glia are more fate-restricted than neuroepithelial cells [Williams and Price, 1995; Malatesta et al., 2003] but they maintain epithelial properties such as the interkinetic nuclear migration [Frederiksen and McKay, 1988; Misson et al., 1988], expression of the intermediate filament nestin [Lendahl et al., 1990; Hendry et al., 1988] and their contact to the pial and ventricular surface. Most radial glia disappear within several days to some weeks after birth. In many non-mammalian species, however, radial glia persist into adult life [Garcia-Verdugo et al., 2002; Grandel et al.,

2006]. In birds radial glia have been studied extensively, where they proved to continue to divide lifelong [Alvarez-Buylla et al., 1990], leading to the proposition that these radial glia are neuronal precursors. With the appearance of radial glial cell properties such as the expression of characteristic astrocyte molecules during neurogenesis [Kriegstein and Gotz, 2003; Campbell and Gotz, 2002; Gotz, 2003] radial glia become more fate-restricted than neuroepithelial cells. This has been supported by several studies using recombination-mediated fate mapping [Malatesta et al., 2003; Anthony et al., 2004] and retrovirus-mediated cell lineage experiments [McCarthy et al., 2000]. *In vitro* studies were also in line with the *in vivo* observations. By dissecting embryonic cortical tissue at the peak of cortical neurogenesis (E14-E16) and culturing those cells, radial glia generate primarily neuronal colonies, whereas later, when embryonic neurogenesis ends (E18), very few neuronal clones were observed [Malatesta et al., 2000]. In the adult CNS only two regions exist where neurogenesis occurs, the subgranular layer (SGL) in the dentate gyrus (DG) [Kaplan and Bell, 1984; Cameron et al., 1993; Gage et al., 1998; Seri et al., 2001, 2004] and the subependymal zone (SEZ) [Doetsch et al., 1999]. Cells that behave *in vitro* like neural stem cells were isolated from these two regions [Morshead et al., 1994; Gage et al., 1995; Palmer et al., 1997]. The identified neural stem cells in these regions possess characteristics previously attributed to fully differentiated astrocytes [Doetsch et al., 1999; Alvarez-Buylla et al., 2002]. These astrocytes have lost their connection to the pial surface and only contact the ventricular lumen by extending a thin cellular process between ependymal cells at the SEZ [Doetsch et al., 1999]. SEZ astrocytes also show several characteristics similar to neuroepithelial stem cells in the embryonic neural tube such as the expression of nestin [Filippov et al., 2003], an intermediate filament protein found in neuroepithelial stem cells [Lendahl et al., 1990]. In particular, radial glia in the adult DG have also been shown to divide in the SGL and hilus and to generate small dark cells corresponding to a transient cell type in the generation of new granular neurons, the so-called Type D cells [Seri et al., 2001].

2.1.1 Classification of adult neural stem cells

During development the potential of a neural stem cell gets more and more restricted. Neuroepithelial stem cells are multipotent and can generate undifferentiated precursors, astrocytes, oligodendrocytes and neurons [McCarthy et al., 2001]. During

brain development, neural stem cells do not generate these 3 different postmitotic cell types directly but rather indirectly via intermediate precursors that are more restricted in their potential generating only a single cell type. Adult neural stem cells in the two neurogenic niches, SEZ and SGZ, are described as Type B stem cells that show all characteristics of a stem cell: Multipotency, self-renewal capacity with the theoretically unlimited ability to produce progeny indistinguishable from themselves, and a slow division. They can be identified via their position and morphology expressing GFAP and nestin [Lendahl et al., 1990] but their identification is mainly based on morphological analysis by electron microscopy [Doetsch et al., 1999]. So far, no marker that is exclusive to stemlike cells has been identified. Lineage tracing studies in adult mice have demonstrated that newly born neurons, astrocytes and sometimes oligodendrocytes can be derived from heterogeneous populations of cells expressing a given molecular marker such as nestin, Sox2 and glutamate-aspartate transporter (GLAST) (reviewed by Breunig et al., 2007).

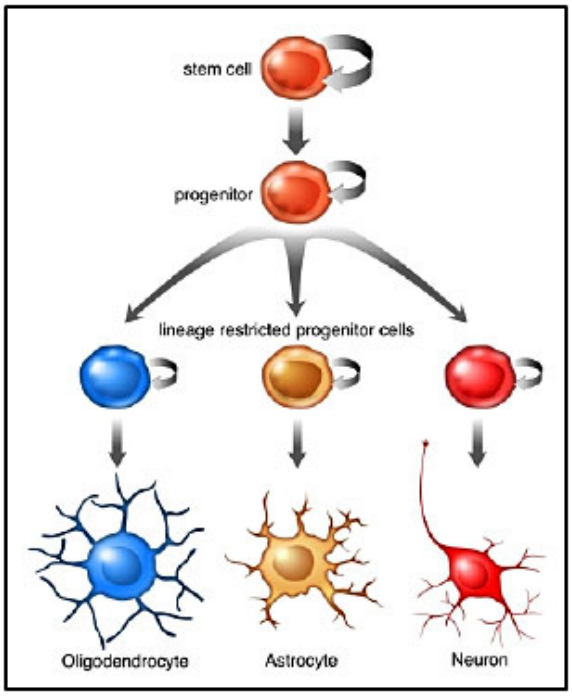

Figure 2.2: Classification of neural stem cells in the adult brain

A neural stem cell gives rise to a pool of transit-amplifying progenitors that generate lineage-restricted progenitor cells which then give rise to the three distinct cell types existing in the brain, oligodendrocytes (blue), astrocytes (yellow) and neurons (red). Picture taken from Lie, C. et al., 2004

Specific targeting of a distinct cell population is achieved by an inducible transgenic mouse line, where a gene of interest will be deleted only in cells expressing GLAST [Mori et al., 2006] after tamoxifen induction. As GLAST is expressed in SEZ astrocytes also neural stem cells will be included in the target cell population. In this study this technique will be described in more detail and the specificity of using it with regard to examining functional aspects of adult neurogenesis will be shown. The progeny of the type B stem cells are the intermediate precursors that are fast dividing and are therefore called transit-amplifying precursors or type C cells [Capela and Temple, 2002; Doetsch et al., 1999, 2002]. They can be identified by bromodeoxyuridine (BrdU) and ^{3}H-thymidine (^{3}HT) labeling, DNA-base analogues that incorporate during mitosis into the DNA. Type C cells give rise to lineage-restricted progenitor cells (**Figure 2.2**), the so-called Type A cells, either neuroblasts or glioblasts, subdivided in astroglio- or oligodendroglioblasts. Type A cells then generate postmitotitc neurons, astrocytes or oligodendrocytes [Lie et al., 2004]. For the neuronal lineage, neuroblasts of the SEZ already express neuronal traits (PSANCAM or doublecortin) and migrate via the rostral migratory stream (RMS) toward the olfactory bulb (OB). After reaching the OB, the newly born neurons detach from their chain formation, migrate radially, and progress into one of the cell layers where they undergo terminal differentiation to then become integrated into the existing network (**Figure 2.3**).

2.1.2 Regulation and maintenance of the neural stem cell fate

The expression of several key transcription factors such as the basic-helix-loop-helix (bHLH) becomes important for the transition from neuroepithelial cells to radial glia cells and the maintenance of this cell fate. For the latter, Hes genes were shown to play a crucial role [Kageyama et al., 2005]. Radial glia are still present in the neonatal mouse brain [Merkle et al., 2004; Noctor et al., 2002] and adult neural stem cells arise from these radial glia cells. The maintenance of stem cells in the adult mouse brain is based on the homeostasis between self-renewal and differentiation of these cells toward certain cell types. This balance is established by several mechanisms such as the Notch signaling pathway [Ninkovic and Gotz, 2007]. Proliferating cells and putative neural progenitors in both the SGZ and SEZ are closely associated with the vasculature, indicating that factors released from the blood vessels may have direct impact on adult neural progenitors [Palmer et al., 2000; Alvarez-Buylla and Lim,

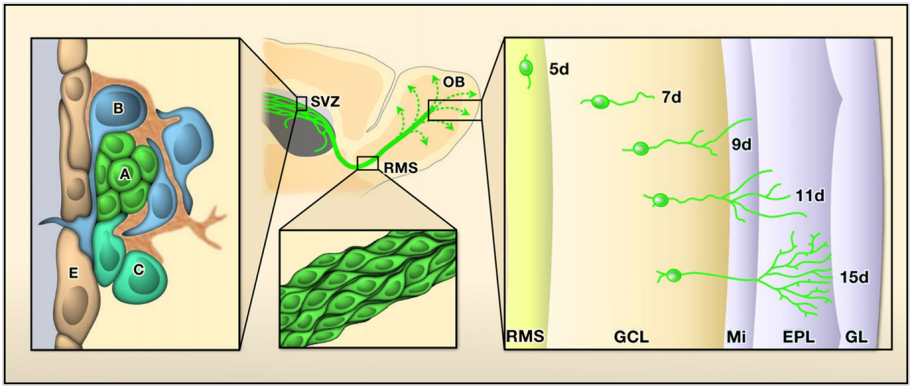

Figure 2.3: Neurogenesis in the SVZ

Progenitor cells (A-C) lining the lateral ventricle adjacent to the ependymal cells (E). Type B stem cells have contact to the ventricular lumen over a thin cellular process. Newborn neurons reach the OB through chain migrations along the RMS and integrate as granule neurons in the granular cell layer (GCL) or as periglomerular neurons in the glomerular layer (GL) after morphological and physiological development. EPL= external plexiform layer, GCL= granule cell layer, GL= glomerular layer, Mi= mitral cell layer, OB= olfactory bulb, RMS= rostral migratory stream, SVZ= subventricular zone. Picture taken from Zhao et al., 2008

2004]. The infusion of the vascular endothelial growth factor (VEGF) promotes cell proliferation in both neurogenic areas, which can be blocked by a dominant-negative VEGF receptor 2 [Cao et al., 2004]. Not only the contact between neural stem cells and blood vessels but also that between stem cells and ependymal cells proved crucial for the maintenance of the stem cell fate. Ependymal cells secrete the pigment epithelium-derived factor (PEDF) which could be shown to promote a self-renewing stem cell fate [Ramirez-Castillejo et al., 2006]. Furthermore, growth factors, in particular the epidermal growth factor (EGF) and the fibroblast growth factor 2 (FGF2), are potent factors for the maintenance of adult neural stem cells [Doetsch et al., 2002; Jin et al., 2003]. Adult neural progenitors are also regulated by a variety of other extrinsic factors that act as positive key regulators, e.g. through sonic hedgehog signaling or the neurotrophin brain-derived neurotrophic factor (BDNF) [Zhao et al., 2008; Henry et al., 2007]. The targets of many of the extrinsic factors are yet unknown. One might assume that these extracellular regulators could cause changes in other cell types within the neurogenic niches and exert an indirect effect on adult neural stem cells. Besides intracellular signaling pathways downstream of the growth factors as well as neurotrophins and morphogens, a variety of other intracellular mechanisms have been implicated in the regulation of adult neurogenesis.

The transcription factor Bmi-1, for example, is required for the maintenance of adult neural stem cells [Molofsky et al., 2005]. Pax6 promotes neuronal differentiation of SVZ progenitors, whereas Olig2 has an opposite effect [Hack et al., 2005] although these factors act similarly during embryogenesis generating different types of neurons [Gotz et al., 1998; Ono et al., 2008]. Recently it has become more and more clear that epigenetic regulation also plays an important role in adult neurogenesis. It was shown, for example, that neural stem cells lacking the methyl-CpG binding protein 1 (MBD1), which is important for the methylation of the DNA, exhibit increased genomic instability and a reduced neuronal differentiation [Zhao et al., 2003]. Histone deacetylases were shown, together with TLX, an orphan nuclear receptor essential for neural stem cell proliferation and self-renewal, to be important for neuronal differentiation [Hsieh and Gage, 2004; Sun et al., 2007]. All these studies support the notion that numerous extrinsic factors and intracellular pathways are involved in the regulation of adult neurogenesis.

2.2 Epigenetic factors involved in adult neurogenesis

Little is known about the functional role of specific epigenetic factors in molecular processes such as the proliferation or differentiation of neural stem cells to generate constantly new cells in the adult brain, respectively. Epigenetic mechanisms refer to effects that promote cellular specification by imposing a specific and heritable pattern of gene expression on the progeny of differentiating cells without altering the DNA sequence. Major epigenetic mechanisms include posttranslational histone modification such as acetylation, methylation and phosphorylation. The ability of transcription factors to access nucleosome-bound DNA is dependent upon DNA packaging [Wade, 2001] (**Figure 2.4**). Modifications of histones and/or DNA can alter the strength of their packaging and thus can modulate transcriptional activity [Strahl and Allis, 2000]. In contrast to methylation and phosphorylation, the acetylation of the core histones is probably the best understood type of modification. Interestingly, specifically this chromatin modification has also shown to play important roles in neurogenesis *per se*. Most of the studies designed in the field of neurogenesis were based on treatment with HDAC inhibitors, but the results were very controversial [Hsieh et al., 2004; Salminen et al., 1998]. In general, the maintenance of histone

acetylation has been shown to positively affect neuronal differentiation [Hsieh et al., 2004], whereas HDAC activity and hence deacetylation was shown to play a role in the progression toward the oligodendrocytic lineage [Marin-Husstege et al., 2002]. However, besides the use of general pharmacological HDAC inhibitors, the role of individual HDACs has not been examined in the central nervous system (CNS). Furthermore, the application of HDAC inhibitors in the field of cancer treatment makes it much more attractive to study their role as opposed to that of their counterplayers, the histone acetyltransferases (HATs). Therefore, the characterization and function of single HDACs selectively in a complex tissue such as the brain is of great interest, given that a single HDACs contribute to the regulation of neuronal differentiation and survival in a time-dependent manner, as it will be shown here.

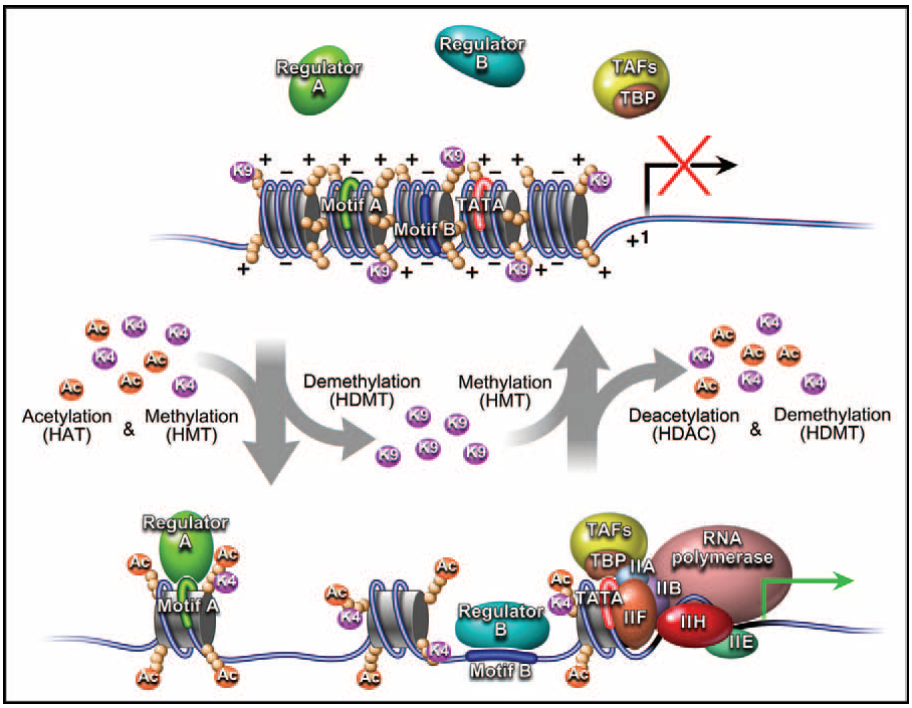

Figure 2.4: Histone modifications

Schematic illustration of changes in histone modifications results in either transcriptional repression or activation. Histone deacetylation and methylation are involved in the formation of condensed chromatin leading to an inactive chromatin state. Histone acetylation and demethylation allow relaxation of chromatin resulting in an active state. Ac= acetylation, K4= lysine 4, K9= lysine 9, HAT= histone acetyltransferases, HDAC= histone deacetylases, HDMT= histone demethylase, HMT= histone methyltransferase, TAF= TBP-associated factor, TBP= TATA-binding protein. Picture taken from Hsieh and Gage, 2005

2.2.1 Histone deacetylases (HDACs)

In order to understand the potent effects of broad-range HDAC inhibitors by pharmacological tools and the fact that the use of HDAC inhibitors brought contradictory findings in different contexts regarding neurogenesis, the analysis should be concentrated on single HDACs. The treatment of p25 overexpressing mice, for example, showed severe neuronal degeneration with a class I histone deacetylase inhibitor resulting in remarkable improvements in synaptic connections and behavior [Fischer et al., 2007]. However, several reports suggesting that HDAC inhibitors actually promote neuronal cell death stand in direct contrast to this [Salminen et al., 1998; Morrison et al., 2007]. Before examining single HDACs, the classical family of HDACs and their original requirements will be described in the following.

2.2.1.1 Classification of HDACs

The classical HDAC families are composed of two phylogenetic classes, namely class I and class II (**Figure 2.5**). Class I HDACs (HDAC1, 2, 3 and 8) are most closely related to the yeast (*Saccharomyces cerevisiae*) homologue RPD3. Class II HDACs are HDAC4, 5, 6, 7, 9 and 10. They share similarities with the yeast deacetylase, HDA1. The recently found HDAC11 [Gao et al., 2002] could not be ascribed to any of the existing classes as it does not show sufficient basic similarity with any of the members of class I and II. Therefore, it has been proposed that HDAC11 may belong to a separate subclass [Gregoretti et al., 2004]. Another class of NAD+ dependent HDACs is the sirtuin (Sir) family. These are homologues of the yeast Sir2 gene, which has been implicated in chromatin silencing, cellular metabolism and aging [Guarente, 2000].

2.2.1.2 Function and localization of HDACs

As the general function of HDACs is to deacetylate histones, they have to be localized in the nucleus. This nuclear localization of HDACs occur via a nuclear localization signal (NLS) or via transport and stabilization together with other proteins/complexes. Class I HDACs are found almost exclusively in the nucleus, with the exception of HDAC3, which can also be localized in the cytoplasm, suggesting

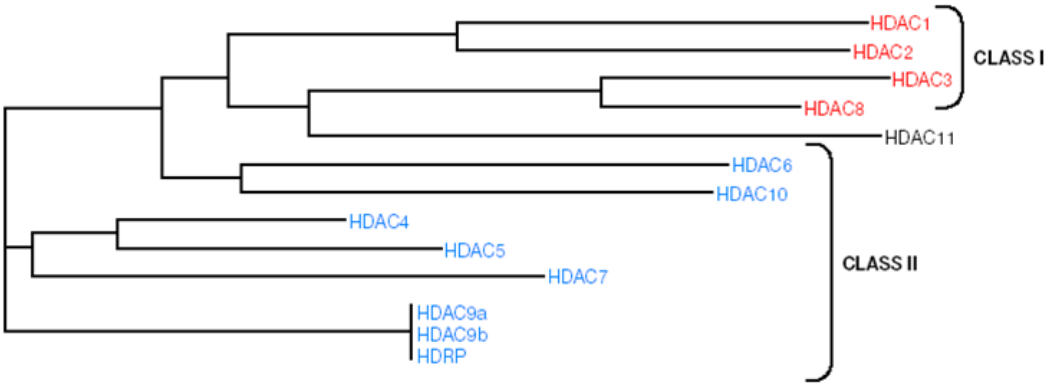

Figure 2.5: Evolutionary relationship between the HDACs

Class I HDACs contain HDAC 1,2,3 and 8, while HDAC 4,5,6,7,9 and 10 are categorized under class II. HDAC11 does not show enough identity with class I or class II to be placed in either class. Picture taken from de Ruijter, A. J. et al., 2003

that it also contains a nuclear export signal (NES) [de Ruijter et al., 2003]. Class II HDACs are able to shuttle in and out of the nucleus in response to certain cellular signals. The mechanism of action of HDAC enzymes as mentioned above is to remove acetyl groups from the N-terminal histone ends, thereby leading to a tighter wrapping of the DNA. This compaction reduces accessibility for transcription factors, resulting finally in a transcriptional repression. This function is mediated via the catalytic domain of each HDAC consisting of ≈ 390 amino acids. Crucial for the functional activity of the HDAC enzyme are two adjacent histidine residues, two aspartic residues and one tyrosine residue [Buggy et al., 2000; Finnin et al., 1999]. An essential component is a Zn^{2+} ion in the catalytic domain of the HDACs, which is the target for most HDAC inhibitors displacing it [Finnin et al., 1999]. Class I HDACs have been shown to be part of multicomponent protein complexes, which are recruited by DNA binding proteins. Three complexes containing HDAC1 and/or HDAC2 have been characterized so far: the Sin3 , NuRD (nucleosomal remodeling and deacetylation) and CoREST (Co-RE1 silencing transcription factor) complexes [Ayer, 1999; Zhang et al., 1999]. Indeed, HDAC1 and HDAC2 only display activity within a complex of proteins *in vivo*.

2.2.1.3 HDAC2

The above described discrepancy of effects observed by HDAC inhibitor treatment may also be based on differences in the expression profile of individual HDACs. In this regard HDAC expression was studied in the brain. An interesting expression pattern was observed for HDAC2 present in adult, but not embryonic neuronal precursors, besides its strong expression in postmitotic neurons in all different stages of brain development. HDAC1 showed a complementary expression pattern as it could be detected in embryonic neuronal precursors and predominantly in glial cells at later stages in brain development.

The structure of HDAC2 is very similar to that of HDAC1, in fact, they show 82 % sequence homology. As mentioned above, HDAC1 and HDAC2 are often found together in complexes [de Ruijter et al., 2003]. Several studies dealing with the function of HDAC1 in the neuronal development have been conducted. Based on these experiments it has been suggested that HDAC1 induces differentiation of retinal progenitors as well as motoneurons in the zebrafish as a result of the repression of Wnt and Notch signaling [Yamaguchi et al., 2005; Cunliffe, 2004]. Concerning HDAC2 less is known about its role in the CNS. However, it has been demonstrated that HDAC2 is involved in REST (RE1 silencing transcription factor) -mediated repression of neuronal cell fate in non-neuronal cells [Ballas et al., 2001]. The transcriptional repressor REST is a key regulator of many neuronal genes.

In this work an expressional and functional analysis of HDAC2 will be demonstrated in the developing and adult brain. The functional study was mainly performed on a HDAC2 gene trap mouse line in which the catalytic domain of HDAC2 is disrupted and, therefore, its function disappears. This construct will be explained in more detail further on. Studies that have been conducted on these HDAC2 mutant mice elucidated a role of HDAC2 in cardiac development [Trivedi et al., 2007]. This work revealed that HDAC2 regulates cardiac hypertrophy by inhibiting the (PI3K)-Akt pathway, which is important for growth control and implicated in hypertrophic signaling [Dorn and Force, 2005]. The group of Montgomery et al. (2007) generated a full HDAC2 knock-out (KO) that show a 100 % postnatal lethality within the first 24 hours after birth, while HDAC2$^{-/-}$ offspring were indistinguishable from wildtype (WT) littermates [Montgomery et al., 2007]. This suggests a potent role for HDAC2 in the early postnatal development and, moreover, a possible role of

HDAC2 in adult neurogenesis as HDAC2 immunoreactivity was found in adult but not embryonic neuronal precursors will be shown in this study.

2.2.2 Chromatin remodeling complexes

Chromatin modifications are not only important to promote cellular specifications but also insofar as the remodeling of the chromatin structure can make the DNA more accessible for the transcriptional machinery to enter regulatory sequences in the promoter region of certain genes. DNA together with histone proteins H2A, H2B, H3, and H4 form nucleosomes, comprising the basic structure of chromatin. Chromatin not only functions as DNA compaction but also contributes to the regulation of nuclear processes such as transcription. ATP-powered molecular machineries known as chromatin remodeling factors serve to modify the chromatin structure by changing histone-DNA contacts [Morettini et al., 2008]. These ATP-dependent chromatin remodeling factors are typically organized in multiprotein complexes, e.g. SWI/SNF complex, NuRD or CHRAC (Chromatin accessibility complex) complex [Vignali et al., 2000]. The most extensively studied proteins involved in chromatin remodeling are Brm (brahma) and Brg (brahma-related gene) 1. These proteins function as ATP-subunits of complexes, which are highly related to the SWI/SNF family of ATPases that are structurally related to the *Saccharomyces cerevisiae* Swi2/Snf2 protein [Eisen et al., 1995]. Brm or Brg1 either remove, reposition or assemble nucleosomes, resulting in an altered structure or positioning of nucleosomes. Thus, SWI/SNF complexes appear to function at every step in the process of transcriptional activation but can also facilitate the repression of specific genes [Sudarsanam and Winston, 2000].

2.2.2.1 Brg1

The ATPase subunits of SWI/SNF complexes Brg1 or its analogue Brm contain a single bromodomain (a protein motif associated with the binding of certain acetylated proteins) and both act as the ATPase in SWI/SNF complexes. It was suggested therefore that Brm and Brg1 are functionally redundant, as mice lacking Brm are viable and fertile [Muchardt et al., 1998]. However, *in vitro* studies have suggested that they regulate different sets of genes [Kadam and Emerson, 2003].

Moreover, Brg1-null mice die before implantation [Bultman et al., 2000], showing that Brg1 exerts specific functions early in development. Studies in *Xenopus laevis* have indicated that Brg1 is required for neuronal differentiation by mediating the transcriptional activities of the proneural bHLH genes Neurogenin (Ngn) and NeuroD [Seo et al., 2005b]. Moreover it was also shown in zebrafish that Brg1 is involved in neural crest induction, which is critical for the development of neurons, glia and pigment cells [Eroglu et al., 2006]. Recently it was shown by Lessard et al. (2007) that a switch of subunits occurs in ATP-chromatin remodeling complexes, such as SWI/SNF, which is essential for neural development. They could also show that Brg1 is essential for the self-renewal and maintenance of neural progenitor cells as well as for neuronal differentiation processes later on. As Brg1 transcripts are found to be expressed in neural stem cells in the VZ at E15 and later also at the SEZ, it may play a role in the development of the nervous system. This question was addressed by Matsumoto et al. (2006) where they used a Brg1 transgenic mouse containing loxP sites [Sumi-Ichinose et al., 1997] and crossed it with mice expressing the cre recombinase (Cre) under the control of the nestin promoter [Kellendonk et al., 1999]. By studying these mice lacking the Brg1 protein at E13-E14 they were able to show that Brg1 is sufficient for neural stem cell maintenance and also seems to be more important in astrocyte differentiation than in neuronal differentiation as reported by other research groups. These contradictory results as well as the fact that chromatin remodeling complexes, such as SWI/SNF interact with transcriptional repressor complexes, in which HDAC2 is present, imply that they recruit each other in an orchestratic manner. On the premise that the roles of HDAC2 and Brg1 in the adult neurogenic regions have, as yet, not been extensively studied it was the aim of my PhD research to shed some light onto the specific functions of the aforementioned two epigenetic regulatory elements. The expression data of HDAC2 and Brg1 turned up results that indicate a strong similarity of the protein expression patterns and a colocalization that is highly specific in both the embryonic forebrain as well as the adult brain. The resulting implications set the foundation for the further study of HDAC2 deficient mice as well as Brg1 floxed mice in order to identify the roles of HDAC2 and Brg1 in the processes of adult neurogenesis.

3 Abbreviations

AB Antibody

aSEZ adult subependymal zone

APS Ammonium persulfate

bp Base pairs

bFGF Basic fibroblast growth factor

BLBP Brain lipid binding protein

BrdU 5-bromo-2'deoxy-uridine

Brm Brahma

Brg Brahma-related gene

Calr Calretinin

CB Cerebellum

CHRAC Chromatin accessibility complex

cDNA Complementary DNA

CNS Central nervous system

CP Cortical plate

CPM Counts per minute

Casp3 Activated caspase 3

Cre causes recombination

Ctx Cortex

DAPI 4'-6-Diamidino-2-phenylindole

DCX Doublecortin

dd1 Differentiated for 1 day

dd3 Differentiated for 3 days

DIV Days in vitro

DNA Desoxyribonucleic acid

DNAse Desoxyribonuclease

dNTP Deoxynucleotide triphosphate

E Embryonic day

EGF Epidermal growth factor

eGFP Enhanced green fluorescent protein

EPL External plexiform layer

EtOH Ethanol

FACS Fluorescent activated cell sorting

FCS Fetal calf serum

FGF Fibroblast growth factor

GABA γ-aminobutyric acid

GAPDH Glyceraldehyde-3-phosphate dehydrogenase

GCL Granule cell layer

GE Ganglionic eminence

GFAP Glial fibrillary acid protein

GFP Green fluorescent protein

GL Glomerular layer

GM Grey matter

Gsk3β Glycogen synthase kinase 3β

HDRP HDAC-related protein

HC Hippocampus

HDAC Histone deacetylase

HDAC2 def Histone deacetylase 2 deficient

hGFAP human Glial fibrillary acidic protein

HRP Horse radish peroxidase

kDa Kilo Dalton

KO Knock out

Ig Immunoglobulin

Inpp5f Inositol polyphosphate-5-phosphatase f

IP Intra peritoneal

IZ Intermediate zone

IRES Internal ribosomal entry side

MEF Mouse embryonic fibroblasts

Mi Mitral cell layer

M-phase Mitosis phase of the cell cycle

mRNA messenger ribonucleic acid

n.d. not defined

Ngn Neurogenin

NS neurospheres

OB Olfactory bulb

OPC Oligodendrocyte progenitor cell

P Postnatal day

PBS Phosphate buffered saline

PCR Polymerase chain reaction

PDL Poly-D-lysine

RMS Rostral migratory stream

RNA Ribonucleic acid

rpm Rounds per minute

RT Room temperature

RT-PCR Realtime- polymerase chain reaction

SCWM Subcortical white matter

SEM Standard error of the mean

SEZ Subependymal zone

STDV Standard deviation

SWI/SNF mating type switching/sucrose nonfermenting

TAP Transit-amplifying precursor

TSA Trichostatin A

ud undifferentiated

VPA Valproic acid

VZ Ventricular zone

WM White matter

WT Wildtype

Zli Zona limithans intrathalamica

4 Materials and Methods

4.1 Animals

4.1.1 Mouse lines

The inbred mouse strain C57BL/6J was used as wildtype (WT). The day of vaginal plug was considered as embryonic day 0 (E0), the day of birth as postnatal day 0 (P0). Here we used an HDAC2 deficient mouse line. The Hdac2 gene-trap clone was obtained from the German Genetrap Consortium (ES clone no. W035F03). The genomic locus of HDAC2 was interrupted by insertion of the pT1-βgeo vector, which integrated into intron 8. Chimeric mice were produced by blastocyst injection according to standard protocols [Zimmermann et al., 2007] on a C57BL/6J background. Additionally, a Brg1 floxed/floxed transgenic mouse line was generously provided by Pierre Chambon, Universitè Louis Pasteur, Strassbourg, France was used [Sumi-Ichinose et al., 1997]. For the deletion of Brg1 in the adult brain the inducible mouse line GLASTCreER^{T2} was used [Mori et al., 2006] and crossed with Brg1 floxed/floxed mice. To follow the recombined cells over time a reporter mouse line Z/EG was crossed in [Novak et al., 2000].

4.1.2 Genotyping of mutant and transgenic mice

Genotyping was performed by PCR on genomic DNA extracted from mouse tails. DNA was obtained following the protocol by [Laird et al., 1991]: Tail biopsies of less than 5 mm length were transferred in 0,5 ml lysis buffer and incubated rotating for several hours or overnight at 55 °C in a modified hybridization oven. Following complete lysis, hairs and tissue residues were removed by centrifugation in an Eppendorf centrifuge at maximum speed (13,1 $\times$ 103 rpm $\approx$ 16.000 g) for 10 -20 minutes. The supernatant was transferred into 0,5 ml isopropanol and mixed well. After precipitation DNA pellets were transferred in 200 μl TE-buffer. To solve the DNA, tubes were again rotated at 55 °C for several hours.

4.1.2.1 HDAC2 deficient genotyping protocol

PCR was carried out using about 80 ng of genomic DNA ($\approx 2\,\mu$l) and 0,5 μM of the HDAC2 primers (**Table 4.1**) in a 20 μl reaction containing 0,25 mM dNTPs, 1,5 U of Taq-DNA-polymerase, 2 μl 10× PCR-buffer and 0,5 μl Q-solution. Cycling conditions were: preheat to 94 °C, 2 minutes at 94 °C, followed by 39 cycles at 94 °C for 30 seconds, at 58 °C for 1 minute and at 72 °C for 2 minutes. Finally, amplicons were extended at 72 °C for 7 minutes. 15 μl of each PCR-product was analyzed on a 2 % agarose-TAE-gel. The amplicon obtained from normal WT DNA is 514 bp long and the amplicon obtained from HDAC2 deficient-DNA is 290 bp long (**Figure 4.1**).

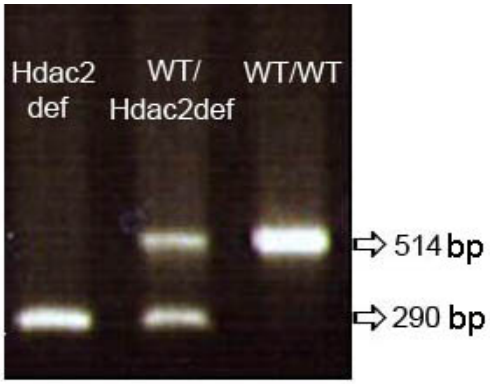

Figure 4.1: Genotyping HDAC2

4.1.2.2 Brg1 floxed/floxed genotyping protocol

The PCR protocol for Brg1 floxed/floxed mice was adapted from [Sumi-Ichinose et al., 1997]. PCR was designed by using about 80 ng of genomic DNA ($\approx 2\,\mu$l) and 1 μM of the primers TG57, TH185 and TB82 (**Table 4.1**) in a 20 μl reaction containing 0,25 mM dNTPs, 1,5 U of Taq-DNA-polymerase, 2 μl 10× PCR-buffer and 0,5 μl Q-solution. Cycling conditions were: 5 minutes at 94 °C, followed by 35 cycles at 94 °C for 30 seconds, at 55 °C for 30 seconds and at 72 °C for another 30 seconds. Finally, amplicons were extended at 72 °C for 7 minutes. 15 μl of each PCR product was analyzed on a 2 % agarose-TAE-gel. The various Brg1 alleles were identified with the recommended primers TG57 and TH185 for the WT (+) allel (241 bp), the L2-allel containing the loxP-sites (387 bp) (**Figure 4.2**).

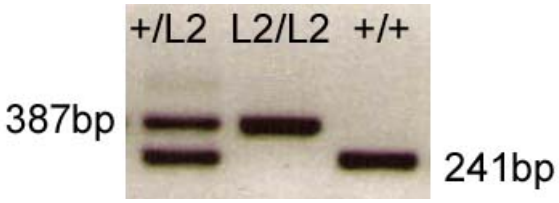

Figure 4.2: Genotyping Brg1

4.1.2.3 GLASTCreER^{T2} genotyping protocol

For detection of GLASTCreER^{T2} PCR was designed by using about 80 ng of genomic DNA ($\approx 2\,\mu$l) and 1 μM of the primers Glast F8, Glast R3 and CER1 (**Table 4.1**) in a 30 μl reaction containing 0,25 mM dNTPs, 1,5 U of Taq-DNA-polymerase, 3 μl 10× PCR-buffer and additionally 3 μl MgCl and 6 μl Q-solution. Cycling conditions were: 5 minutes at 94 °C, followed by 35 cycles at 94 °C for 30 seconds, at 55 °C for 30 seconds and at 72 °C for another 30 seconds. Finally, amplicons were extended at 72 °C for 7 minutes. 15 μl of each PCR product was analyzed on a 2 % agarose-TAE-gel. The GLAST locus before recombination can be indentified with the recommended primers GLAST F8 and R3 (700 bp) and the insertion of the CreER^{T2} was detected with the primers GLAST F8 and CER1 (400 bp) (**Table 4.1**).

4.1.2.4 Z/EG genotyping protocol

PCR was carried out to detect eGFP in the Z/EG reporter mice by using about 80 ng of genomic DNA ($\approx 2\,\mu$l) and 0,5 μM of the primers (**Table 4.1**) in a 25 μl reaction containing 0,25 mM dNTPs, 1,5 U of Taq-DNA-polymerase, 2,5 μl 10× PCR-buffer and additionally 0,5 μl MgCl. To optimize the PCR result 1 μl Glycerol and 1 μl DMSO was added. Cycling conditions were: 9 minutes at 95 °C, followed by 37 cycles at 95 °C for 20 seconds, at 56 °C for 30 seconds and at 72 °C for another 30 seconds. Finally, amplicons were extended at 72 °C for 10 minutes. 15 μl of each PCR product was analyzed on a 2 % agarose-TAE-gel. The PCR product has a size of 400 bp and can be detected if mice are positive for the reporter.

Table 4.1: PCR primers

Primer name	Primer sequence
HDAC2 WT For	5'-TgATggAgATgTACCAgCCTAgCgCgg-3'
HDAC2 WT Rev	5'-gCgCTgACATgCAACAAACTACTCATgg-3'
HDAC2 Mut For	5'-CTggAgAAggCCCgACCATCC-3'
HDAC2 Mut Rev	5'-CATgCgCTgCCACATgCAACTTTgC-3'
TG57	5'-gCCTTgTCTCAAACTgATAAg- 3'
TH185	5'-gTCATACTTATgTCATAgCC-3'
TB82	5'-gATCAgCTCATgCCCTAAgg-3'
GLAST F8	5'-gAggCACTTggCTAggCTCTgAggA-3'
GLAST R3	5'-gAggAgATCCTgACCgATCAgTTgg-3'
CER1	5'-ggTgTACggTCAgTAAATTggACAT-3'
eGFP F2	5'-CTACggCAAgCTgACCCTgAAgTTC-3'
eGFP R2	5'-gCCgATgggggTgTTCTgCTggTAg-3'

4.2 Tamoxifen administration

Tamoxifen (SIGMA, T-5648) was dissolved in pre-warmed corn oil (SIGMA, C-8267) at 20 mg/ml concentration on a shaker at 37 °C overnight. 10 mg tamoxifen is required to achieve recombination efficiently. Following a previously established protocol [Mori et al., 2006], 1 mg tamoxifen was injected intraperitoneally (i.p.) twice a day for 5 consecutive days. Each time an amount of 50 μl was injected. The solution was kept in darkness at 4 °C for maximum 1 month to avoid precipitation.

4.3 Histology

Pregnant animals were sacrificed with diethylether or increasing CO_2 concentrations followed by cervical dislocation. Embryos (day 14) were removed by hysterectomy and transferred to Hanks buffered salt solution (HBSS) with 10 mM HEPES. Embryonic brains were removed and fixed for 2 hours in 4% paraformaldehyde (PFA) in 0,1 M phosphate-buffered saline (PBS), pH 7,5 . Postnatal day 0-5 old pups were decapitated, brains removed and fixed for 5-7 hours in 4 % PFA. Adult animals were first anaesthetized with 5 % chloralhydrate and then transcardially perfused with

4 % (PFA) and postfixed at 4 °C in the same fixative overnight.

4.3.1 Cryosections

After post fixation brains were incubated for 24 hours in 30 % sucrose in PBS, embedded in Tissue Tek and stored at −20 °C. Cryosections were cut sagitally at 12 μm (embryonic brains) and 20 μm thickness (adult brains), mounted on glass slides and processed for immunohistochemistry.

4.4 Immunostaining

The following primary antibodies were used in a PBS solution containing 0,5 % Triton X100 and 10 % serum as listed in **Table 4.2**. Usually the antibody mix was applied and incubated overnight at 4 °C in a humid chamber, but for some antibodies special pretreatments were necessary. For the immunodetection of BrdU, pretreatment with 2 N HCl for 60 minutes was required to denature double-stranded DNA. This was followed by two washes with 0,1 M sodium-tetraborate-buffer (pH 8,5) for 15 minutes at RT. After three further washes in PBS the staining with the mouse anti-BrdU or rat anti-BrdU was performed. Intermediate filament and microtubuli stainings like anti-nestin-, anti-β-IIItubulin- and anti-GFAP-staining required a special pre-treatment for better visualization of intermediate filaments and microtubuli before the application of the primary antibodies. Therefore, cells were incubated in ethanol (EtOH) glacial acetic acid for 15 minutes at -20 °C followed by three washes in PBS for 10 minutes at RT. After the washing steps in PBS cells were incubated in blocking solution (PBS+Triton+serum) with specific subclasses of secondary antibodies coupled to FITC- or TRIC at a dilution of 1 :100 , Cy2- or Cy3-coupled antisera at 1 :200 or Alexa 488 or Alexa 594 at 1 :400 for 45 minutes at RT (**Table 4.3**). For triple-stainings, biotinylated secondary antibodies (dilution 1 :100) followed by incubation in Streptavidin-AMCA at a 1 :100 dilution was used. After three further washes in PBS, glass coverslips with cells or sections were mounted in Aqua Poly/Mount, a glycerol-based mounting medium. To rule out any unspecific binding of the secondary antisera, control experiments were performed by either leaving out the primary antibody or by using a primary antibody against an antigen that is not present in the representative tissue or at the respective developmental

stage. Nuclei were visualized with DAPI (4 ', 6 ' diamino-2 -phenylindole, Sigma) by incubating cells or sections for 10 minutes with a concentration of 0,1 g/ml DAPI in PBS.

4.4.1 Tyramide signal amplification

Some stainings were enhanced using the tyramide amplification kit (Perkin Elmer) as described in the tyramide signal amplification (TSA) handbook (Perkin Elmer). Briefly, the TSA system uses horse radish peroxidase coupled to a secondary antibody to catalyze the deposition of fluorescein or rhodamine labeled tyramide amplification reagent onto tissue sections (**Table 4.4**). This reaction results in the deposition of numerous fluorescein or rhodamine labels immediately adjacent to the immobilized horse-radish-peroxidase (HRP). Since this technique results in a significant enhancement of the signal it was used for weak signals in immunostainings (on adult sections for HDAC2, Olig2 or GFP).

4.5 Quantitative analysis

Quantifications (absolute cell numbers, marker coexpression) were performed by means of Neurolucida connected to an Axiophot Zeiss microscope (40 × objective). The analysis was performed on sagittal sections at medio-lateral levels from 0,6 to 1 mm relative to midline (3-7 sections per animal) in 3 pairs of WT and HDAC2 deficient mice, if it is not indicated differently in the figure legends. For all data sets, the arithmetic average $\overline{x} = \frac{1}{n}\sum_{i=1}^{n} x_i$ standard deviation $s = \sqrt{\frac{\sum_{i=1}^{n}(x_i - \overline{x})^2}{n-1}}$ and standard error of the mean $SEM = \frac{s}{\sqrt{n}}$ was calculated. The error bars in the diagrams showing the SEM. To test the data for significance the student's T-test was used. The p-value (p) of this test declares the probability of the conclusion being correct. There is a 95 % chance of the means to be **significant** different if $p = 0{,}05$, a 99 % chance of the means to be **highly significant** different for $p = 0{,}01$ and a 99,9 % chance of the means to be **very highly significant** different for $p = 0{,}001$. The calculations and constructions of the diagramms were carried out with GraphPadPrism 4,0 .

Table 4.2: Primary antibodies

Name	**Host-animal**	**Marker for**	**Supplier**
anti-Blbp	Rabbit 1:1500	Radial glia	Nataniel Heintz Rockefeller Univ. New York, USA
anti-BrdU	Rat 1:10 Mouse IgG1 1:300	S-phase	Abcam Bio-Science
anti-Brg1	Mouse IgG1 1:100	ATPase of a chromatin remodelling complex	Santa Cruz
anti-Calretinin	Mouse IgG1 1:100	Subset of mature neurons	Chemicon
anti-act. caspase 3	Rabbit 1:100	Apoptosis	Promega
anti-CC1	Mouse IgG2b 1:200	Immature oligodendrocytes	Calbiochem
anti-DCX	Guineapig 1:2000 Rabbit 1:200	Immature neurons (Neuroblasts)	Chemicon Chemicon
anti-GFAP	Rabbit 1:1000 Mouse IgG1 1:200	Precursor subtypes, Astrocytes	DAKO Sigma
anti-GFP	Rabbit 1:500 Mouse IgG1 1:200	Reporter gene	Clontech Chemicon
anti-HDAC1	Rabbit 1:100	HDAC1	Cell Signaling
anti-HDAC2	Rabbit 1:100	HDAC2	Santa Cruz
anti-NeuN	Mouse IgG1 1:50	Postmitotic neurons	Chemicon
anti-Ki67 (Tec-3)	Rat 1:50	Precursor cells	Dianova Immundiagnostics
anti-NG2	Rabbit 1:300	Oligodendrocyte precursors	Chemicon
anti-Olig2	Rabbit 1:300	Immature Oligodendrocytes	Chemicon
anti-PH3	Rabbit 1:100	M-phase marker	Upstate Biotech
anti-Prox1	Rabbit 1:200	Immature neurons DG	Santa Cruz
anti-Sox2	Rabbit 1:1000	precursor-and postmitotic cells	Santa Cruz
anti-β-IIItubulin	Mouse IgG2b 1:100	Young neurons	Sigma

Table 4.3: Secondary antibodies

Name	**Supplier**
anti-rabbit Ig FITC/TRITC/biotinylated	Boehringer Ingelheim (Vector Laboratories)
anti-rabbit Ig Cy2/Cy3	Dianova
anti-rabbit Alexa 488 / 564	Invitrogen
anti-rat Ig Cy3	Dianova
anti-rat Ig Alexa 488	Invitrogen
anti-mouse IgG1 FITC/TRITC /biotinylated	Southern Biotech
anti-mouse IgG2b FITC/TRITC/biotinylated	Southern Biotech
Streptavidin AMCA	Boehringer Ingelheim (Vector Laboratories)

Table 4.4: Tyramid Signal Amplification Reagents

Name	**Content**
TN Buffer (pH 7,5)	0,1 M Tris-HCl (pH 7,5 and 0,15 M NaCl
TNT Buffer	0,1 M Tris-HCl (pH 7,5 , 0,15 M NaCl, 0,005 % Tween 20
Blocking Reagent	Milk Powder
TNB Buffer	0,1 M Tris-HCl (pH 7,5 , 0,15 M NaCl and Blocking Reagent
SA-HRP	Horseradish Peroxidase-labelled reagent
Amplfication Diluent	
Amplification reagent	Fluorophore

4.6 Tissue culture

4.6.1 Cultures of primary dissociated neural precursors

Embryos at day E14 were removed by caesarean section from time-pregnant mice plug positive at day EO and anaesthetized by an overdose of diethylether (Sigma). The meninges of the embryonic brains were removed, the telencephalic hemispheres separated, the hippocampi and the olfactoric bulbi removed. The cortex (Ctx) and the ganglionic eminence (GE) were dissected and collected in separate tubes under sterile conditions in HBSS (Invitrogen) containing 10 mM HEPES (Invitrogen) on ice.

To show the forebrain morphology with the separation into Ctx and GE a picture of an E16 embryonic forebrain was used, what is also valid for E14 (**Figure 4.3**). The tissue was then allowed to settle and HBSS medium was removed and replaced by trypsin-EDTA and incubated for 15 minutes at 37 °C. The enzyme activity was stopped by the addition of twice the volume of Dulbecco's modified eagle medium (DMEM; Invitrogen) supplemented with 10 % fetal calf serum (FCS; Sigma) and penicillin/streptomycin (100 units/ml streptomycin; Invitrogen). The tissues were mechanically dissociated with a fire-polished Pasteur pipette coated with serum, twice pelleted for 5 minutes at 172 g and resuspended in FCS containing medium. Cells were plated at 10^6 cells/ml in DMEM/FCS (0,5 ml/well) in a 24-well plate in poly-D-lysine (PDL) coated coverslips and incubated at 37 °C and 5 % CO_2. Acutely dissociated cells were fixed after 2 hours with 4 % PFA for 15 minutes. Long-term cell cultures were maintained in SATO-medium which was changed by half every second day with gradually reducing serum concentration in the medium and then fixed after 5-7 days in vitro (DIV) with 4 % PFA for 15 minutes. After three washes with PBS at room temperature (RT) cells were processed for immunocytochemistry.

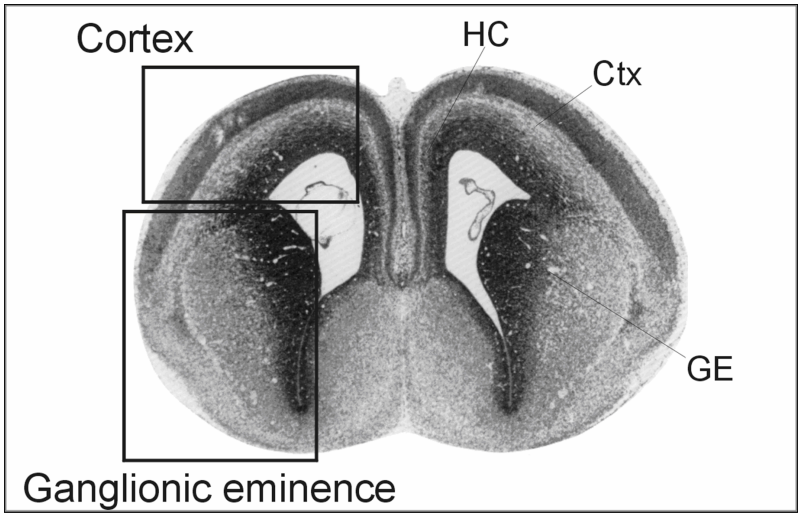

Figure 4.3: Frontal section of an E16 brain [Schambra et al., 1991]. Rectangles schematically mark regions that were used for the primary cell preparations.

4.6.2 Neurosphere cultures

4.6.2.1 Embryonic neurosphere preparation

Embryonic neurosphere cultures where prepared from the Ctx or GE of WT and HDAC2 deficient littermates at E14 as described above with the exception that these cells were dissociated mechanically without enzymatic digestion, then pelleted and cultured after dissociation at clonal density (10 cells/μl) in a T75 flask in 15 ml serum-free DMEM/F-12 medium (Invitrogen) containing B-27 supplement (concentration 1 :50) at 37 °C and 5 % CO_2. Cells were passaged once a week by centrifugation at 172 g for 10 minutes, followed by mechanical redissociation and replating in 50 % neurosphere-conditioned medium and 50 % fresh medium. Cells were fixed for immunostaining 2 or 7 days after passage 3 or 4 . This ensures that contaminating aggregates of cells that are not neurosphere-forming are removed from the culture.

4.6.2.2 Adult neurosphere preparation

Adult neurospheres were obtained from the lateral wall of the lateral ventricle of adult (about 10 week old) mice. The SEZ was prepared after sagittal sectioning of the brain. The SEZ was cut in pieces and these pieces were incubated in a dissociation solution in HBSS with 2 mM glucose at 37 °C for 30 minutes and gently triturated. The cells were then centrifuged at 200 g for 5 minutes, resuspended in 0,9 M sucrose in 0,5 × HBSS, and centrifuged for 10 minutes at 750 g. The cell pellet was resuspended in 2 ml of culture medium, placed on top of 10 ml 4 % BSA in HBSS solution, and centrifuged at 200 g for 7 minutes, followed by washing in DMEM/F12 . The culture conditions were identical to those described above for neurospheres from embryonic brains.

4.6.2.3 Adult neurosphere cultures

Dissociated cells were cultured at low density (10 cells/μl) to ensure the clonal origin of neurospheres [Morshead et al., 1994] in a 24 well plate (Falcon, well size: $\approx$ 2 cm^2). Every second day EGF and FGF2 were added to the cultures. Primary neurospheres were quantified after 7 days and the spheres were dissociated mechanically

into single cells again in order to get secondary neurosphere formation. Single cells were cultured again for clonal density at 10 cells/μl in the same conditions in 24 well plates. Secondary neurospheres were quantified 7 days after taken in culture.

4.6.2.4 Differentiation of neurosphere cultures

For differentiation of cells from adult and embryonic neurospheres, spheres were spun down 7 days after the last passage, trypsinized at 37 °C for 3 minutes or mechanically dissociated only. For mechanic dissociation a 200 μl tip was used to triturate the cells (30 times up and down). Dissociated cells were plated in PDL-coated glass coverslips at a density of 1-2 $\times$ 10^5 cells/ml and cultured in DMEM-F12 medium with B27 supplement (differentiation medium) for maximum 7 days without growth factors.

4.6.2.5 Transduction of cultured cells

Cultured cells were infected in neurospere medium with retroviral vectors at a concentration of 0,5 μl/ml either in the floating state or 2 hours after plating. After 24 hours medium was changed to differentiation medium. Then the cells were cultured as described above for 2-7 days.

4.7 *In vivo* injections

4.7.1 Anaesthesia

Animals were anaesthetized by intraperitoneal injection of Medetomidine (Domitor, 0,5 mg/kg body weight), Midazolam (Dormicum, 5 mg/kg body weight) and Fentanyl (Fentanyl Hexal, 0,005 mg/kg body weight). The anesthesia was antagonized by intraperitoneal injection of Atipamezol (Antsedam, 5 mg/kg body weight) and Naloxon (Narcanti-vet, 1,2 mg/kg body weight). All animal experiments were revised and approved by the state of bavaria under the license number 209-211-2531-23/04 .

4.7.2 Stereotactic injections in adult mice

Injections of retroviral particles were done stereotactically on 9 -10 weeks old WT and HDAC2 deficient mice as described [Carleton et al., 2003]. Briefly, the head of adult mice was fixed in a stereotactic apparatus. Then a 1 cm midline cut was performed and the skull was opened at the anterior-posterior and medio-lateral coordinates (see below) using a drill (Multipro395 PR, Dremel). About 500 nl of virus were injected at one site of each hemisphere by means of a glass micropipette or a Hamilton syringe. The solution with viral particles was injected very slowly (100 nl/min). The following coordinates were used for virus injections (relative to bregma): WT dentate gyrus (DG) = anterior-posterior = 2,0 ; medio-lateral = 1,6 ; dorso-ventral = 2,0 . HDAC2 deficient DG = anterior-posterior = 1,8 ; medio-lateral = 1,4 ; dorso-ventral = 1,8 . For the subcortical white matter (SCWM) in WT, anterior-posterior = 1,9 ; medio-lateral = 1,32 ; dorso-ventral = 1,1 . HDAC2 deficient SCWM = anterior-posterior = 1,7 ; medio-lateral = 1,1 ; dorso-ventral = 0,8 .

4.7.3 Transplantations

Cells isolated from the SEZ of mice expressing myristolated Venus [Rhee et al., 2006] were dissociated as described [Seidenfaden et al., 2006] and injected into the SEZ of HDAC2 deficient mice at 0,6 (anterior-posterior), 1,1 (medio-lateral) and 1,6 (dorso-ventral) relative to Bregma.

4.8 BrdU administration

4.8.1 BrdU pulse labeling

For some experiments WT and HDAC2 deficient mice were injected intraperitoneally with a DNA synthesis marker, 5 -bromo-2 'deoxyuridine (BrdU; 50 mg/kg of body weight, dissolved in 0,9 % NaCl with 0,4 N NaOH) 1 hour prior to transcardial perfusion of the animal. Cryosections were then prepared and stained as described above.

4.8.2 BrdU label retaining analysis

To study the number of stem cells and the generation of postmitotic cells within a specific time window BrdU was applied in drinking water (1 mg/ml in H_2O) for 2 weeks followed by 1 week without BrdU. Afterward mice were sacrificed and brains were treated as described above.

4.9 *In situ* hybridization

4.9.1 Plasmid preparation and *in vitro* transcription

10 ng plasmid DNA was added to 25 μl chemically competent Top10 cells and incubated for 30 minutes on ice. Cells obtained a heat shock at 42 °C for 45 seconds. After bacteria recovered for 10 minutes on ice, 1 ml LB-medium was added and cells were incubated on a bacterial shaker for 45 minutes at 37 °C. Then 50 - 100 μl of bacterial suspension were plated on e.g. ampicillin containing (50 g/ml) LB-agar plates, depending on the resistance encoded by the plasmid, and incubated at 37 °C overnight. One colony was picked the next day and grown for about 4 hours in 5 ml antibiotica-containing LB-medium. This preculture then was added to 50 ml LB-ampicillin-medium and was incubated overnight at 37 °C on the rotary shaker. Plasmid-DNA was harvested following the Qiagen-Midiprep protocol using a midi Tip100 column. The DNA pellet was dissolved in 200 μl ddH_2O and 20 μg of plasmid-DNA, quantified by spectrophotometry at 260 nm, were linearized with the appropriate enzyme (40 U) in a total volume of 50 μl of the appropriate buffer for 2 - 3 hours at 37 °C. The plasmid-DNA then was purified by phenol extraction. First, water was added to a total volume of 200 μl, then 200 μl phenolchloroform-isoamylalcohol (50 :49 :1) was added and strongly vortexed for about 1 minute. After 5 minutes of centrifugation in an Eppendorf-centrifuge at maximum speed, the water phase was recovered and 1 /10 × volume 3 M sodium acetate and 0,7 volume Isopropanol were added and incubated for 10 minutes at RT for precipitation. After a centrifugation at maximum speed in an Eppendorf-centrifuge for 15 minutes the pellet was washed shortly with 70 % EtOH and resuspended in 18 μl TE (pH 8 , RNAse-free). For *in vitro* transcription of the linearized plasmid, 1 μl (about 1 μg) of the plasmid-DNA was mixed with 2 μl dNTP-mix containing Digoxygenin labeled UTP (DIG-UTP,

Roche; concentration was 10 mM ATP, 10 mM CTP, 10 mM GTP, 6,5 mM UTP and 3,5 mM DIG-UTP), 4 μl 5 $\times$ transcription buffer (Fermentas), 1 μl RNAse inhibitor (Fermentas; 40 U/μl, 2500 U) and 1 μl (20 U/μl, 5000 U) of the respective RNA-polymerase (T7, Stratagene). Pure RNAse-free ddH_2O was added up to a final volume of 20 μl and the plasmid-mix was incubated for 2 hours at 37 °C. To stop the reaction 2 μl 0,2 M EDTA was added followed by addition of 2,5 μl 4 M LiCl and 75 μl pure EtOH to precipitate the RNA either at −20 °C overnight or at −80 °C for 2 hours. The RNA probe was centrifuged for 7 minutes at 37 °C. RNA precipitation was repeated by addition of 2,5 μl 4 M LiCl and 75 μl 100 % EtOH, incubation for 2 hours at −20 °C and centrifugation for 7 minutes at 4 °C. The pellet was resuspended in 20 μl ddH_2O and hybridization buffer was added to a final RNA concentration of around 100 ng/μl.

4.9.1.1 Plasmids

Mouse cDNAs of NeuroD and Cux2 in pBluescript II KS were used as templates for *in situ* hybridization probes (**Table 4.5**).

Table 4.5: *in situ* plasmids

Name	**Digestion**	**Transcription**
NeuroD	HindIII	T7
Cux2	SalI	T7

4.9.2 Non-radioactive *in situ* hybridization

In situ hybridizations were performed on 20 μm thick cryostat sections with 1-2 μg of the respective probe in hybridization buffer (1 $\times$ Salt Solution), 50 % Formamid, 10 % Dextran Sulfate (Sigma), 1 mg/ml wheat germ tRNA (Sigma, R7876), 1$\times$ Denhard's solution (Sigma, D2532), 0,5 % CHAPS (3-[(3-cholamidopropyl)dimethylammonio]-1-propanesulfonic acid) and ddH_2O) at 65 °C overnight. The next day slides were washed first with washing solution containing 1 $\times$ SSC, 50 %Formamid, 0,1 % Tween 20 at 65 °C followed by washing with 1 $\times$ MABT (100 mM Maleic Acid, 150 mM NaCl-pH 7,5 , 0,02 % Tween 20). Slides were incubated 1 hour at room temperature in blocking solution in 1 $\times$ MABT and blocking reagent (Boehringer

Mannheim), and 20 % heat inactivated sheep serum (Sigma, G6767). Anti-digoxygenin FAB fragments coupled to alkaline phosphatase were diluted 1 :2500 in blocking solution and applied on slides for overnight incubation. At the third day slides were again washed with 1 × MABT and kept in staining solution containing the substrates for alkaline phosphatase, NBT and BCIP (Sigma) in a concentration of 350 g/ml for NBT and BCIP.

4.10 Western Blotting

4.10.1 Cell lysates and tissue preparation

4.10.2 Protein detection

Prtotein detection was performed according to Bradford (1976) with the "BioRad Proteinassay" following the manufactors instructions. Calf-serumalbumine was used as a protein standard.

4.10.3 Protein analysis

4.10.3.1 SDS-Polyacrylamidgelectrophoresis

The following reagents are needed:

5 x sample buffer

10 % w/v SDS
10 mM β-mercaptoethanol
20 % v/v Glycerol
0,2 M Tris-HCl, pH 6,8
0,05 % Bromophenolblue

1 x Running buffer

25 mM Tris-HCl
200 mM Glycine
0,1 % SDS

1 x Running Gel solution

	7 %	**10 %**	**12 %**	**15 %**
H_2O	15,3 ml	12,3 ml	10,2 ml	7,2 ml
1,5 M Tris-HCl, pH 8,8	7,5 ml	7,5 ml	7,5 ml	7,5 ml
20 % (w/v) SDS	0,15 ml	0,15 ml	0,15 ml	0,15 ml
Acrylamide	6,9 ml	9,9 ml	12,0 ml	15,0 ml
10 % APS	0,15 ml	0,15 ml	0,15 ml	0,15 ml
TEMED	0,02 ml	0,02 ml	0,02 ml	0,02 ml

The percentage of acrylamide is according to the molecular weight of the proteins of interest. In the case of HDAC2 that is 55kDa, a 10 % gel gave the best resolution. After adding TEMED and APS the gel polymerized fairly quick.

Stacking Gel solution (4 % acrylamide)

H_2O	3,075 ml
0,5 M Tris-HCl, pH 6,8	1,25 ml
20 % (w/v) SDS	0,025 ml
Acrylamide	0,67 ml
10 % APS	0,025 ml
TEMED	0,005 ml

After mixing the ingredients needed for the chosen percentage and pouring the solution quickly into the gel casting form, it is important to leave enough space for the stacking gel. The top of the gel layer was loaded with water saturated isopropanol to remove bubbles at the top of the gel and ensure this part won't dry out. After 30 minutes the gel was polymerized completely. Then the stacking gel solution was added together with desired combs after removing the isopropanol. After 1 hour the gel is polymerized fully and ready for loading the samples. The samples were

prepared by mixing the protein of interest with sample buffer 4:1 . For denaturation the mixture was heated for 5 minutes at 95 °C. The gel run was done at 100 - 150 V for 1 - 3 hours at RT.

4.10.3.2 Western Blot analysis

The Western Blot method was designed to transfer extracted proteins on a membrane. Proteins were before uploaded with SDS, so they can now travel in the electric field to the Anode and can be separated from the gel matrix onto the membrane. Membranes used here were exclusively PVDF-membranes (Milipore) that were incubated prior to the blotting for 1 minute in methanol to activate them. In the so called "'semi-dry"' method, membranes and filter papers (Whatman-3MM-Chromatography papers) were cut to the exact size of the gel and soaked in transfer buffer. Now a blot-sandwich was built out of: anode, four soaked filter papers, activated PVDF membrane, SDS gel, four soaked filter papers, cathode. The blot was run with 0,8 - 1 mA/cm^2 for 90 minutes. After successfully transferred the proteins onto the membrane, proteins of interest could be detected by immunostaining.

4.11 Viral vectors

4.11.1 Retroviral vectors and retrovirus production

For lineage tracing experiments retroviral vectors expressing the green fluorescent protein (GFP) were used, that were either pMXIG or CMMP [Hack et al., 2004]. For viral infection of adult Brg1 floxed neurospheres a retrovirus containing CreIRES-GFP was used. This virus expresses Cre and GFP behind an IRES (internal ribosomal entry side) [Hack et al., 2005; Colak et al., 2008]. Gpg293 cells [Ory et al., 1996] were cultured in DMEM (Gibco) containing 10 % (v/v) FCS (heat inactivated for 30 minutes at 56 °C; Gibco), 1 % (v/v) penicillin-streptomycin in DMEM (Gibco), 1 g/ml tetracycline (Sigma), 2 g/ml puromycin (Sigma) and 0,3 mg/ml G418 (Gibco). Cells were passaged once per week with PBS and trypsin containing 1 g/ml tetracycline. These cells allow the production of high titer amphotropic retrovirus. Many retrovirus packaging cell lines lose packaging efficiency as they are cultured due to

the gradual loss of expression of the packaging genes. The packaging plasmids introduced to this cell line were chosen using different selection markers (gentamycin (G418), puromycin). Therefore, expression of packaging proteins can be fairly well maintained by culturing the cells continuously in media containing the corresponding antibiotics. In addition, the vesicular stomatitis virus G (VSV-G) protein is toxic to gpg293 cells, so expression of this gene is controlled by tetracycline. Therefore, these cells are maintained in tetracycline, puromycin and G418 containing medium. Retroviral vectors pseudotyped with VSV-G differ from standard murine retroviruses by their very broad tropism and the capacity to be concentrated by ultracentrifugation without loss of activity. Gpg helper-free packaging cells were used for viral production [Pear et al., 1993]. For retrovirus production 90 -95 % confluent gpg cells were transfected using Lipofectamin 2000 (Invitrogen) and Opti-MEM I reduced serum medium (Invitrogen) as described in the Lipofectamin 2000 transfection protocol for adherent cells (Invitrogen). Transfection medium was replaced after 8 - 10 hours, and gpg cells were further cultured in DMEM containing 10 % (v/v) FCS (heat inactivated for 30 minutes at 56 °C; Gibco), 1 % (v/v) penicillin-streptomycin in DMEM (Gibco). After 48 hours the virus containing medium was collected and filtered through a 0,4 μm filter to remove the cell debris but maintain the viral particles (Becton Dickinson) and centrifuged at 50000 x g for 90 minutes at 4 °C. The virus pellet was resuspended in TNE (50 mM Tris-HCl pH 7,8 , 130 mM NaCl, 1 mM EDTA) and aliquoted. Virus aliquots were stored at −80 °C. Virus titers (viral particles/ml) were measured by adding viral vectors serially diluted to primary cerebral Ctx cells isolated from embryonic day 14 cortices. Cells were cultured for 2 days to allow the expression of the transgene and then the number of infected clones (clusters of GFP-positive cells) was counted. The number of infected clones corresponds to the viral particles used for transduction of primary cells and was then referred to viral particles.

4.12 Fluorescence-activated cell sorting (FACS)

For FAC sorting, SEZ and OB of 5 WT and 5 HDAC2 deficient mice were dissected separately and enzymatically dissociated in 0,7 mg/ml hyaluronic acid, 1,33 mg/ml trypsin in HBSS with 2 mM glucose at 37 °C for 15 minutes. After the first 15 minutes of trypsinization the cells were triturated very strongly with a fire polished and

fetal calf serum coated Pasteur pipet to avoid clumps. This step was followed by one more digestion for 15 minutes at 37 °C. The cells were centrifuged at 200 g for 5 minutes, resuspended in 0,9 M sucrose in 0,5 ×HBSS and centrifuged for 10 minutes at 750 g. The cell pellet was resuspended in 2 ml of culture medium, placed on top of 10 ml 4 % BSA in EBSS solution, and centrifuged at 200 g for 7 minutes, followed by washing in Dulbecco's modified eagle medium: F-12 nutrient mixture (DMEM/F12; Gibco). Then cells were dissolved in staining medium containing PSANCAM antibody. PSANCAM+ cells were then isolated using a FACSAria (BD). Flow cytometry is a method to characterize cells on single-cell level according to their light scattering qualities and emitted fluorescence radiation. Cells pass in a liquid flow hydrodynamically focussed one after the other a laser beam. The FACSAria is set at purity mode and the appropriate sort rate (below 1000 cells per second for high purity and recovery of cells). The forward scatter (FSC) is determined by the light dispersion of 3 to 10ř and correlates with cell size. The sideward scatter (SSC) is determined by a 90ř reflection of the light and correlates with the granularity of the cell. These gating parameters determined by side and forward scatter are used to eliminate debris, dead and aggegrate cells. After sorting, the cells were centrifuged for 30 minutes at 1000 rpm and resuspend in 100 μl of lysis buffer (RLT from QIAGEN containing β-mercaptoethanol) for RNA isolation.

4.13 RNA extraction and microarray

4.13.1 RNA extraction

For microarray analysis either RNA from FAC sorted cells or RNA was prepared from SEZ and OB of WT and HDAC2 deficient animals. RNA was extracted from selected cells/tissue with Qiagen RNAeasy Kit. FAC sorted cells or tissue were stored in lysis buffer (RLT) containing β-mercaptoethanol after sorting/dissection. After 15 minutes centrifugation at maximum speed (13100 rpm) the supernatant was collected in a QIAshredder (purple) spin columns placed in 2 ml collection tubes. Following a 2 minutes centrifugation at maximum speed the supernatant of the flow-through fraction was transferred to a new RNase-free 1,5 ml microcentrifuge tube without disturbing the cell-debris pellet. 0,5 volume (half of initial lysis volume) of room temperature 96 -100 % EtOH was added to the clear lysate and mixed

immediately. The mixture was applied to a RNeasy (pink) mini column placed in a 2 ml collection tube. This was followed by a 15 seconds centrifugation at 11.000 rpm. At this stage RNA and DNA arebound to silica gel membrane in the RNeasy column. DNA was digested in the same column with DNase I for 15 minutes. After proper washing steps the columns were transferred into RNase-free 1,5 ml microcentrifuge tubes. 30 μl of RNase-free water (supplied with the kit) was put directly on the center of the silica-gel membrane of the RNeasy columns for elution. The samples were then centrifuged twice for 1 minute at maximum speed. The eluted RNA was measured at Nanodrop Spectrophotometer.

4.13.2 Microarray

The quality of purified RNA was examined using the Agilent Bioanalyser and revealed high quality of all RNA preparations. 80 ng of total RNA was used for each microarray from 3 biological replicates of control and HDAC2 deficient mice in the case of HC analysis (tissue preparation). FACS sorted cells from OB were isolated in two independent preparations from 5 WT and 5 HDAC2 deficient mice. The RNA amplification was performed with MessageAmp II-Biotin Enhanced Kit (Ambion, 1791). This single round RNA amplification kit was used for all samples to avoid variations resulting from multiple rounds of amplification. Hybridization to Affymetrix MOE430 2.0 GeneChips (46 k probe sets) was performed according to standard protocols provided by Affymetrix. All housekeeping genes were present and number of present calls was determined as 40 % or higher. To process the data we calculated probe set summaries (according to RMA) [Bolstad et al., 2003] and normalized the data (lmp, nonlinear transformation employing the loss smoother [Cleveland, 1981]. To test the quality and reproducibility of the samples, hierarchical clustering was used to find (dis)similarities between the samples showing that the replicates of each group of cells analyzed were clustering together. Hierarchical clustering was performed on normalized data (RMA) using packages available from http://cran.r-project.org. For statistical analysis of the expression data the Bioconductor software package implemented in Carma web was employed using the moderated limma test. The Benjamini-Hochberg algorithm [Benjamini, 1997] was used to identify genes with a false discovery rate $< 5\,\%$.

4.14 cDNA preparation and Real Time (RT) PCR

4.14.1 cDNA synthesis

To confirm the expression differences as predicted by the microarray analysis mRNA expression levels of some of the genes of interest by RT-PCR were compared. For complementary DNA preparation RNA was reverse transcribed by SuperScript^{TM} III Reverse Transcriptase Kit from Invitrogen. As shown below (components and their amounts for 1 reaction) after mixing the RNA template with Oligo(dT) and dNTPs the samples were kept at 65 °C for 5 minutes for annealing of oligo(dT)s to the messenger RNA. This was followed by addition of reverse transcriptase together with other components which were listed below (**Table 4.6**). Transcription took place for 50 minutes at 50 °C. The samples were then incubated at 85 °C for 5 minutes for the inactivation of the reverse transcriptase. cDNA was stored at −20 °C.

Table 4.6: cDNA Reaction Mix

Components	**ONE Reaction**
dNTPs	1 μl
Oligo(dT)	1 μl
10 × RT buffer	2 μl
25 mM $MgCl_2$	4 μl
0,1 M DTT	2 μl
RNaseOUT	1 μl
SuperScriptIIIRT	1 μl
RNA template	X μl
Total volume	**20 μl**

4.14.2 Real Time (RT) PCR

Real-time PCR was done using iQSYBRGreen kit from BIO-Rad in an Opticon qPCR machine. For 1 reaction see the components listed in **Table 4.7**. 2 × iQSYBR Green Supermix contains 100 mM KCl, 40 mM Tris-HCl, pH 8,4 , 0,4 mM of each dNTP, iTaq DNA polymerase, 50 units/ml, 6 mM $MgCl_2$, SYBR Green I, 20 nM

fluorescein and stabilizers. Primers used for genes of interest were listed in **Table 4.8**. The observed expression levels were all normalized to GAPDH.

Table 4.7: Real Time PCR reaction mix

Components	**ONE Reaction**
iQSYBR Green Supermix	12,5 μl
Primer 1	0,5 μl (100 nM)
Primer 2	0,5 μl (100 nM)
Sterile water	X μl
DNA template	2-5 μl (10 ng)
Total volume	**25 μl**

Table 4.8: RT PCR primers

Primer Name	**Primer Sequence**
HDAC1 forward	5 '-tgttccagcctagtgcagtg-3 '
HDAC1 reverse	5 '-aacattccggatggtgtagc-3 '
HDAC2 forward	5 '-tggaggaggctacacaatcc-3 '
HDAC2 reverse	5 '-caccaggtgcatgtggtaac-3 '
Brg1 forward	5 '-aggttcagctcatggattgg-3 '
Brg1 reverse	5 '-cacactgcttccctccttct-3 '

4.15 HDAC activity assay

The HDAC activity assay was performed in collaboration with Sabine Lagger (Max F. Perutz Laboratories, Medical University of Vienna, Institute of Medical Biochemistry, Dr. Bohr-Gasse 9/2, A-1030 Vienna) using 10 μg total protein extract from freshly isolated hippocampus (HC), OB and cerebellum (CB) of WT and HDAC2 deficient mice. First isolation buffer (Hunt buffer) was added to a final volume of 20 μl and then 10 μl of tritium labeled chicken erythrocyte histones (1,5 mg/ml) and incubated at 30 °C for 1 hour. After this incubation step reactions were stopped with 35 μl Histone Stop and 800 μl ethylacetate followed by a vortex step of 15 seconds and spin down 4 minutes at 10.000 rpm in a swing out bucket rotor. Measurement was done using 600 μl of the organic upper phase in 3ml Scintillation solution. Counts were measured on a Scintillation counter for 1 minute.

4.16 Materials

4.16.1 Microscopy

The following microscopes were used:
- AxioPhot fluorescent microscope, AxioCam HRc camera and AxioVision software with the objectives from Plan Neofluar series (Objective Plan Neofluar 5 x/0,15 ; 10 x/0,30 ; 20 x/0,50 ; 40 x/0,75).
- Olympus BX61 fluorescent microscope, F-view II camera and Olympus Cell^F software with the objectives U Plan S Apo 4 x, 10 x, 20 x, 40 x oil and 60 x oil.
- Olympus FV1000 confocal laser microscope, inversiv stativ Oplympus IX81 and FV12 software with the objectives U Plan Semi Apo Objective 4 x, 10 x, 20 x, 40 x, 40 x oil and 60 x oil.

4.16.2 Complex media, buffers and solutions

Alkaline-phosphatase staining buffer (AP-buffer) for ISH

100 mM NaCl
50 mM $MgCl_2$
100 mMTris pH9,5
0,1 % Tween-20
1 mM Levamisole in dd H_2O

AP-NBT/BCIP (ISH)

AP
350 μg/ml NBT
175 μg/ml

APS10 %

100 mg Ammoniumpersulfat
in 1 ml ddH_2O

Blocking solution (ISH)

MABT
2 % blocking reagent
20 % heat inactivated sheep serum

Differentiation medium for adult neurospheres

DMEM/F12
B27 1:50
2 mM glutamine
100 U/ml penicillin
10 μg/ml streptomycin

Di-sodium-tetraborate-buffer (0,1 M, pH 8,5)

0,1 M $Na_2B_4O_7$
in ddH_2O

Dissociation solution for adult neurospheres

0,7 mg/ml hyaluronic acid
0,2 mg/ml kynurenic acid
1,33 mg/ml trypsin
2 mM glucose
in HBSS

Electrophorese buffer (10 X)(Western Blot)

30,3 g TRIZMA
144 g Glycine
10 g SDS
in 1 ml ddH_2O

0,5 M EDTA, pH 7,6 , 50 ml

9,31 g disodium dihydrate (M=373,2 g/mol)
add 30 ml DEPC-H_2O
adjust pH with 5 N NaOH

FCS-PS-medium

10 % (v/v) FCS (heat inactivated 30 minutes at 55 °C
1 % (v/v) Penicillin-Streptomycin
in DMEM

HCl (2,4 N)

2,4 N HCl (37 % (w/v)
10 mM β-mercaptoethanol
20 % v/v Glycerol
0,2 M Tris-HCl, pH 6,8
0,05 % Bromophenolblue

LB (Luria-Bertani) medium

20 g/l LB broth base
in ddH_2O

LB-agar

LB-medium
10 mM β-mercaptoethanol
15 g/l agar

Lysis buffer pH 8,5

100 mM TrisHCl
5 mM EDTA
0,2 % SDS
200 mM NaCl
100 μg/ml Proteinase K

MABT (5 x pH 7,5)

500 mM maleic acid
750 mM NaCl
0,1 % Tween-20
ddH_2O

NaAc (3 M), pH 5,2

24,61 g NaAc (M= 82,03 g/mol)
in 100 ml ddH_2O

NaN_3-PBS (0,05 %)

0,05 % (w/v) NaN_3
in 1 x PBS

Neurosphere medium

DMEM/F12 (glucose 1,8 g/l
3,5 mg glucose)
1 % (v/v) Penicillin-Streptomycin
B27 1:50
EGF 20 ng/ml
FGF 20 ng/ml

NP40 (0,1 %)

0,1 % NP40 (w/v)
in 1 x PBS

PBS (Phosphate buffered salt solution, 1 x) pH 7,4

137 mM NaCl
2,7 mM KCl
80,9 mM Na_2HPO_4
1,5 mM KH_2PO_4
in ddH_2O

Poly-D-lysin-hydrobromide solution

1 % (w/v) PDL solved (1 mg/ml PDL in ddH_2O)
in 0,1 M sodium-tetraborate buffer

Preparation buffer

10 mM HEPES
in HBSS

Saline

0,9 % (w/v) NaCl
in ddH_2O

Salt solution (10 x)(ISH)

2 M NaCl
90 mM Tris HCl, pH 7,5
10 mM Tris base
70 mM NaH_2PO_4
50 mM Na_2HPO_4

50 mM EDTA
ddH_2O

SATO-medium

DMEM
1 g/l Glucose
2 mM Glutamine
10 μg/ml Insulin (bovine)
100 μg/ml Transferrin (human)
0,0286 % BSA-pathocyte
0,2 μM Progesterone
0,1 μM Putrescine
0,45 μM Thyroxine
0,224 μM Selenite
0,5 μM Tri-iodo-thyronine

Sodium-citrate buffer

10 x 0,1 M sodium-citrate, pH 6,0 in ddH_2O

SSC (20 x)(ISH)

3 M NaCl
0,3 M sodium citrate
in ddH_2O

Sucrose-PBS-solution (30 %)

30 % (w/v) sucrose
in 1 x PBS

TAE (Tris-acetate-EDTA)(50 x)

242 g Tris base
57,1 ml acetic acid
100 ml 0,5 M EDTA
in ddH_2O

TBE (10 x)

450 mM Tris base
440 mM boric acid
10 mM EDTA
in ddH_2O

TE pH 8,0

10 mM Tris HCl
1 mM EDTA
in ddH_2O

TE-buffer pH 7,5

10 mM Tris HCl
0,1 mM EDTA
in ddH_2O

Triton X-100 10 %

10 % (w/v) Triton X-100
in 1 x PBS

Trypsin-EDTA

0,05 % trypsin
0,02 % EDTA
in HBSS

Washing solution (ISH)

1 x SSC
50 % formamide
0,1 % tween-20

4.16.3 Product list

Acrylamide BioRad

Agarose Biozym

Ampicillin Sigma

Anti-DIG-FAB-fragments alkaline phosphatase Roche

APS Sigma

Aqua Poly Mount Polyscience

BCIP(5-bromo-4-chloro-3-indolyl-phosphate, 4-toluidine salt) Roche

beta-mercaptoethanol Sigma

Blocking reagent Roche

BrdU Sigma

BSA Sigma

cDNA-synthesis Kit Invitrogen

Chloralhydrate Sigma

Corn oil Sigma

DAPI Sigma

Denhardt's solution Sigma

Dextran sulfate Sigma

diethylether for anaesthesia Merck

DIG-RNA labeling mix Roche

Di-Sodiumhydrogenphosphate Na_2HPO_4 Merck

dNTP Pharmacia Biotech

Dulbecco's modified Eagle medium (DMEM) Invitrogen

EDTA Sigma

Ethanol absolute Roth

Fetal Calf serum(FCS) Sigma

Formamide Merck

Geneticin (G418-sulfate) Invitrogen

Gentamycin Invitrogen

Glucose Merck

Glycerol (87%) Sigma

Glycin Sigma

Hank's buffered salt solution (HBSS) Invitrogen

Heat inactivated sheep serum Sigma

HEPES-Buffersolution 1M, pH 7,2-7,5 Invitrogen

Hydrochlorid acid (37%) HCl Merck

Insulin Sigma

iQSYBRGreen Kit BioRad

Isopropanol Roth

Kaliumchloride KCl Merck

Kaliumdihydrogenphosphat KH_2PO_4 Merck

LB broth base Invitrogen

Lipofectamine 2000 Invitrogen

L-glutamine Invitrogen

LiCl Merck

MessageAmp II-Biotin Enhanced Kit Ambion

Methanol absolute (MetOH) Merck

$MgCl_2$ Sigma

MidiPrep-Kit Qiagen

Molecular weight marker (1 kb ladder) Invitrogen

NaCl Merck

Natriumdihydrogenphosphat $NaKH_2PO_4$ Merck

$NaHCO_3$ Merck

Natriumtetraborate (borax) $Na_2B_4O_7$-H_2O Merck

NBT (Nitroblue tetrazolium chloride) Roche

Normal goat serum (NGS) Vector Laboratories

NP40-Igepal Sigma

Oligo(dT) primers Roche

Olympus immersion oil Olympus

Opti-MEM I reduced serum medium Invitrogen

Paraformaldehyde(PFA) Merck

PCR-buffer (10x) Qiagen

Penicillin/Streptomycin solution Invitrogen

Phenol-chloroform-isoamylalcohol (50:49:1 Roth

Poly-D-Lysine Hydrobromide (PDL) Sigma

Progesterone Sigma

Proteinase K Roche

Putresine Sigma

PVDF membranes (Western Blot) Milipore

Q-solution (5x) Qiagen

Reverse transcriptase kit Invitrogen

Restriction enzymes New England Biolabs

RNA polymerase T7 Stratagene

RNase inhibitor Fermentas

RNeasy kit Qiagen

SDS Roth

Selenite Sigma

Sodium citrate Sigma

Sodium acetate Merck

Sucrose Merck

Tamoxifen Sigma

Taq-DNA-polymerase Qiagen

TEMED BioRad

Top10 cells Invitrogen

Transcription buffer (5x)(ISH) Fermentas

Transferrin Sigma

TrisBase Merck

TrisHCl Merck

Triton X-100 Roth

Trizol Invitrogen

Trypsin Type XII, 9000 BASF units/mg Sigma

Trypsin-EDTA (1x) Invitrogen

Tyramide amplification kit Perkin Elmer

5 Results

5.1 Expression analysis of HDAC1, HDAC2 and Brg1

5.1.1 mRNA analysis of HDAC1, HDAC2 and Brg1

Microarray data from FAC sorted cells of embryonic cortices of the transgenic mouse line hGFAPeGFP were analyzed to figure out chromatin modification genes which are involved in neurogenesis. In this mouse line eGFP is expressed under the hGFAP promoter active in astrocytes [Nolte et al., 2001]. According to the intensity and levels of GFP expression two populations of cells were separated. One population of radial glial cells expresses GFP intensively and is supposed to contain the gliogenic precursors (GP) whereas in the other neurogenic population the hGFAP promoter is downregulated and hence expresses less GFP (NP) [Pinto et al., 2008]. This study is also described in the PhD work of Michael A. Hack (2006). In these microarray data sets certain genes were found to be differentially regulated which are involved in chromatin remodeling, such as Brg1 or chromatin modification such as HDAC1 and 2. Therefore, the expression of these candidate genes was examined by the real time RT-PCR method to evaluate whether differential expression can be detected. The expression of HDAC1, HDAC2 and Brg1 was studied in undifferentiated versus differentiated cell populations and in more specified populations, such as astrocytes cultured in the presence or absence of the growth factors EGF and FGF (see Materials and Methods 4.6.) and FAC sorted neurons from TauGFP transgenic mice [Jacobs et al., 2007]. HDAC2 and Brg1 mRNAs are enriched in neurogenic and gliogenic precursors compared to HDAC1 (**Figure 5.1**). The increase was 6-7x higher (all normalized to GAPDH, see Materials and Methods 4.14.2.). HDAC1 and HDAC2 were both highly expressed in postmitotic neurons, not tested for Brg1 (**Figure 5.1 a,b**). Brg1 was not only enriched in both progenitor populations but also in the population of undifferentiated neurospheres (**Figure 5.1 c**).

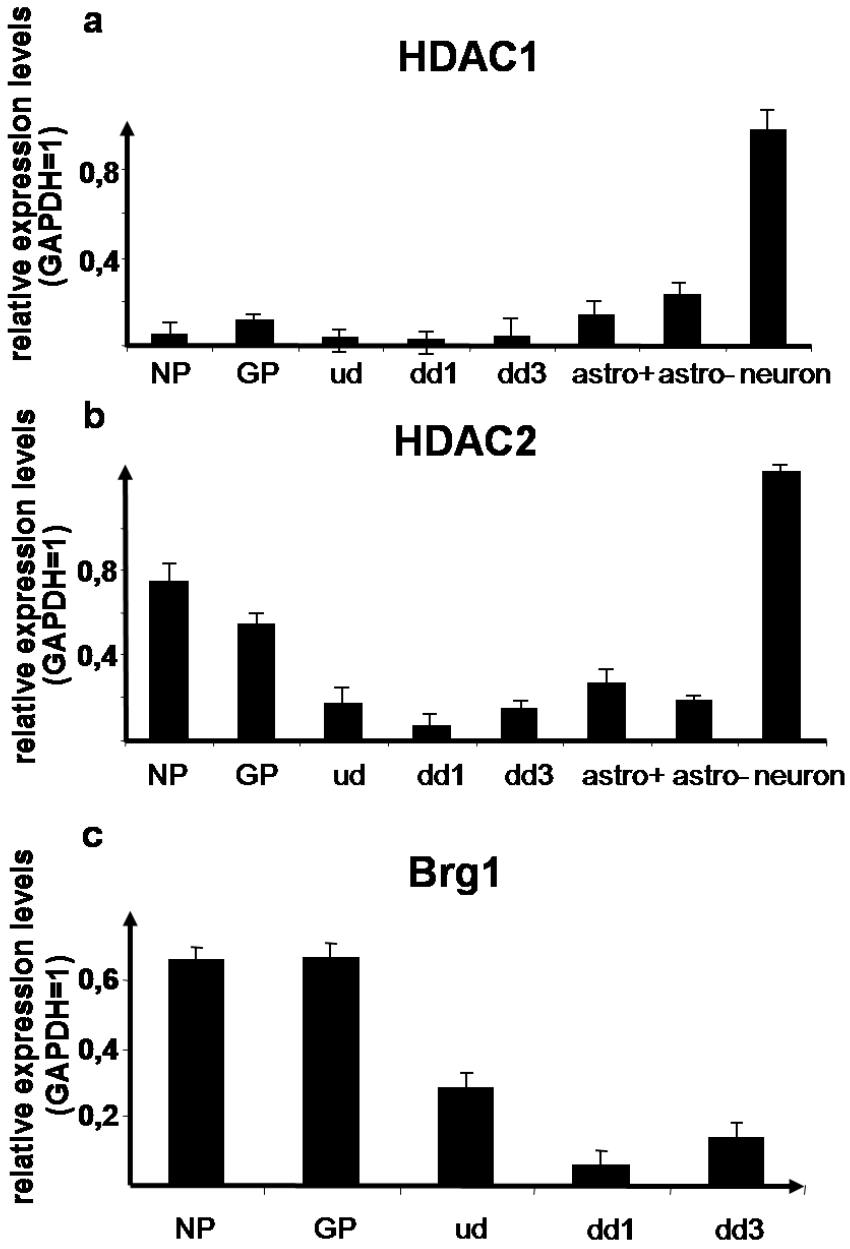

Figure 5.1: RT-PCR expression levels of candidate genes found in the Microarray studies

a-c Histograms of expression levels of HDAC1 (a), HDAC2 (b) and Brg1 (c) in specific cell populations relative to GAPDH=1. Brg1 and HDAC2 are intensively enriched in gliogenic and neurogenic precursors compared to HDAC1. Both HDACs are highly expressed in neurons. **NP**= neurogenic precursors, **GP**= gliogenic precursors, **ud**= undifferentiated neurosphere cultured cells, **dd1**= neurospheres differentiated for 1 day, **dd3**= neurospheres differentiated for 3 days, **astro+**= astrocyte cultures with growth factors, **astro-**= astrocyte cultures without growth factors, **neuron**= postmitotic neurons from E14 Ctx.

5.1.2 Protein expression analysis of HDAC1, HDAC2 and Brg1 *in vitro*

First, the expression of the three candidate genes *in vitro* was examined to underline the RNA expression results. Neurosphere cultured cells from E14 cortices were stained by immunocytochemistry using, besides the antibodies to detect the candidate proteins, β-IIItubulin for young born neurons and GFAP for astrocytes and neural progenitors. HDAC1 protein was expressed at overall weak levels, but detectable in GFAP+ astrocytes and in β-IIItubulin+ young neurons (**Figure 5.2 a**). HDAC2 immunoreactivity was high in β-IIItubulin+ neurons and weak in GFAP+ cells (**Figure 5.2 b**). This suggests that HDAC2 protein is not as highly expressed in neural progenitor cells as implicated in the mRNA levels, whereas the higher immunoreactivity in postmitotic neurons is consistent with the high mRNA levels in neurons. By contrast, Brg1 was high in the progenitor populations and in undifferentiated neurospheres at mRNA level. In order to examine this at the protein level, embryonic neurospheres fixed 2 hours after plating were stained for Brg1. Most of the cells were not yet differentiated at all, but showed stem cell properties. These undifferentiated cells show high levels of nuclear Brg1 immunostaining (**Figure 5.2 c**). After 3 days of differentiation Brg1-immunoreactivity is still present in GFAP+ astrocytes and also in β-IIItubulin+ neurons (**Figure 5.2 d**), suggesting that Brg1 is present in neural precursor cells as well as in differentiated cells.

5.1.3 HDAC1 immunoreactivity *in vivo*

5.1.3.1 HDAC1 immunoreactivity during embryonic and postnatal brain development

In addition to the studies on mRNA- and protein levels *in vitro*, the HDAC1 protein expression *in vivo* was studied by immunocytochemistry. In contrast to previous reports of an ubiquitous expression of HDACs, a very specific expression pattern was observed already at E14. The HDAC1 protein was expressed at high levels in neural precursor cells which are located in the ventricular zone (VZ) during embryonic neurogenesis and are positive for Ki67, a protein expressed in all dividing cells. Besides the prominent existence of the protein in neural precursors, it was also

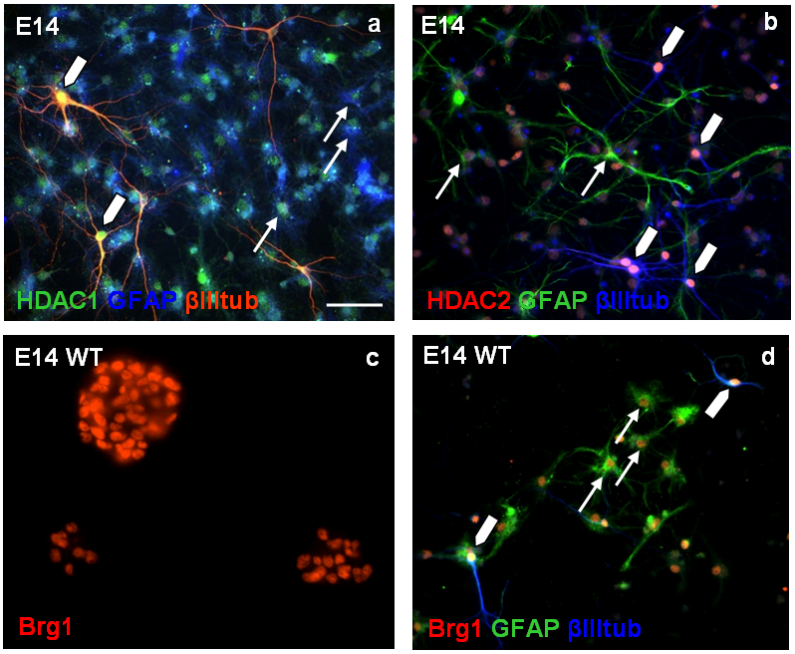

Figure 5.2: Cell-type specific localization of HDAC1,2 and Brg1 *in vitro*

Neurosphere cultures of E14 cortices. **a** HDAC1 immunoreactivity (green) is weak in E14 NS cultures, detectable in some β-IIItubulin+ neurons and a bit more enhanced in GFAP+ astrocytes. **b** HDAC2 (red) is strongly expressed in postmitotic neurons that are β-IIItubulin+ and weakly in GFAP+ astrocytes. **c** Brg1 immunoreactivity is high in undifferentiated neurosphere cells. **d** After 3 days of differentiation, Brg1 immunoreactivity is present in GFAP+ cells as well as in β-IIItubulin+ neurons. Small arrows depict cells double-positive with GFAP, bold arrows depict cells double-positive with β-IIItubulin. Scale bar: 20 μm.

weakly expressed in postmitotic neurons that are NeuN+ in the cortical plate (CP) (**Figure 5.3 a**). At neonatal stages HDAC1-immunoreactivity was mainly found in glial cells but could not be detected in neurogenic regions, such as the HC anlage, except for a low remaining expression in glial cells (**Figure 5.3 b**). Later, at P5, the HDAC1 protein was not detectable in neuronal cells immunopositive for NeuN (**Figure 5.3 d**). Around P21, when postnatal development ends, HDAC1 is expressed in the WM, the only region where a partial overlap of HDAC1 and 2 in the same cell can be observed. No change compared to earlier stages in the postnatal development can be found in the Ctx with HDAC1 not expressed in NeuN+ cells (**Figure 5.3 f**). To prove the fact that the HDAC1 protein can only be observed in glial cells, glial markers were stained such as GFAP labeling astrocytes and Olig2 labeling oligodendrocyte progenitors. **Figure 5.3 g,h** shows the presence of HDAC1 protein in both cell types.

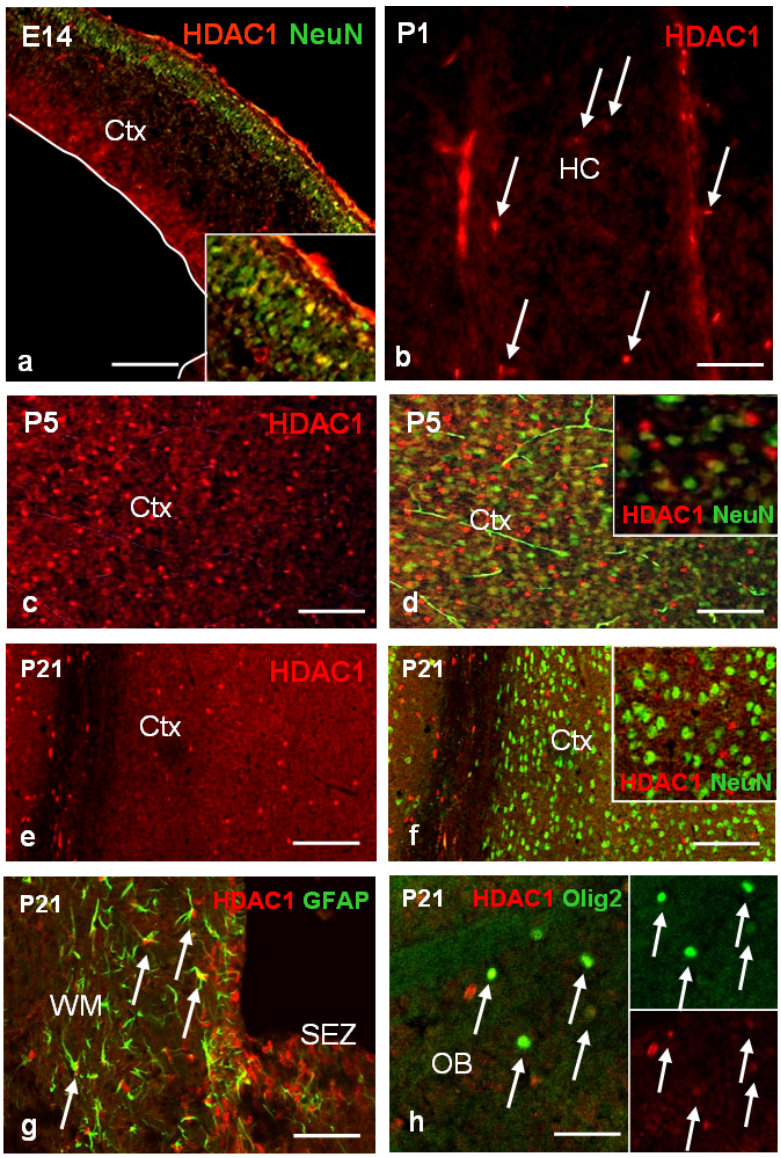

Figure 5.3: HDAC1 immunoreactivity during developmental stages

a HDAC1 immunoreactivity at E14 is highly present in neural precursors located in the VZ and weakly expressed in NeuN+ neurons in the CP. **b** At neonatal stages HDAC1 is not expressed in neurogenic regions, such as the HC anlage except presumably in glial cells. **c,d** HDAC1 is expressed in a scattered pattern and does not colocalize with NeuN at P5. **e,f** HDAC1 expression at P21 in the Ctx is not detectable in NeuN+ cells. **g** Overlay of HDAC1-immunoreactivity . **h** HDAC1 is detectable in Olig2+ cells. Arrows depict double-positive cells. Ctx= cortex, HC= hippocampal anlage, OB= olfactory bulb, SEZ= subependymal zone. Scale bars: a, c-f 50 μm; b, g-h 20 μm.

5.1.3.2 HDAC1 immunoreactivity in the adult brain

At adult stages the expression of HDAC1 is still detectable in glial cells and is absent in postmitotic neurons that are NeuN+ (**Figure 5.4**). This scattered pattern of HDAC1 indicative of the expression in glial cells was also observed in other brain regions, such as the Ctx, OB or the CB. A summary of HDAC1 immunoreactivity at different stages as reported is depicted in **Table 5.1** at the end of this chapter.

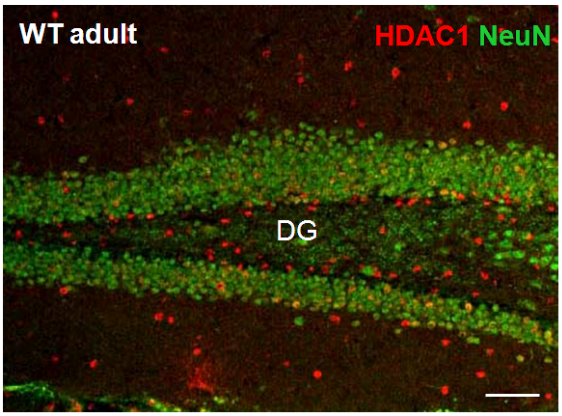

Figure 5.4: HDAC1 immunoreactivity in the adult brain

In the adult brain, here in the DG, HDAC1 is not present in NeuN+ neurons. Scale bar: 50 μm.

5.1.4 HDAC2 expression *in vivo*

5.1.4.1 HDAC2 immunoeactivity during embryonic neurogenesis

To examine whether the cell-type specific immunoreactivity of HDAC1 was also consistent for other HDACs, the expression pattern of the second candidate gene, HDAC2, was studied. HDAC2 immunoreactivity at E14 (midneurogenesis) was restricted to postmitotic neurons identified by NeuN-immunostaining in the forebrain, e.g. in the cortical plate (CP) and in the differentiating parts of the GE, while it was absent in progenitor cells identified by the Ki67 antigen, labeling all proliferating cells at the VZ, in contrast to the observed pattern of HDAC1 (**Figure 5.5 a-c**). Another region in the embryonic forebrain that shows a specific expression of HDAC2, was the Zona limitans intrathalamica (ZLi), a region in the diencephalon composed of neural precursor cells at E14 and one of the few regions where HDAC2 was found

in progenitor cells. This supports the tight regulation and cell-type specific expression of HDAC2 (**Figure 5.6**). Later on, at E18, when embryonic neurogenesis is about to finish, HDAC2 was still highly present in postmitotic neurons, but now a weak presence of the protein was observed in the VZ in Ki67+ cells (**Figure 5.5 d-f**), suggesting the fact that HDAC2 starts to be expressed in another cell type except postmitotic neurons in the Ctx.

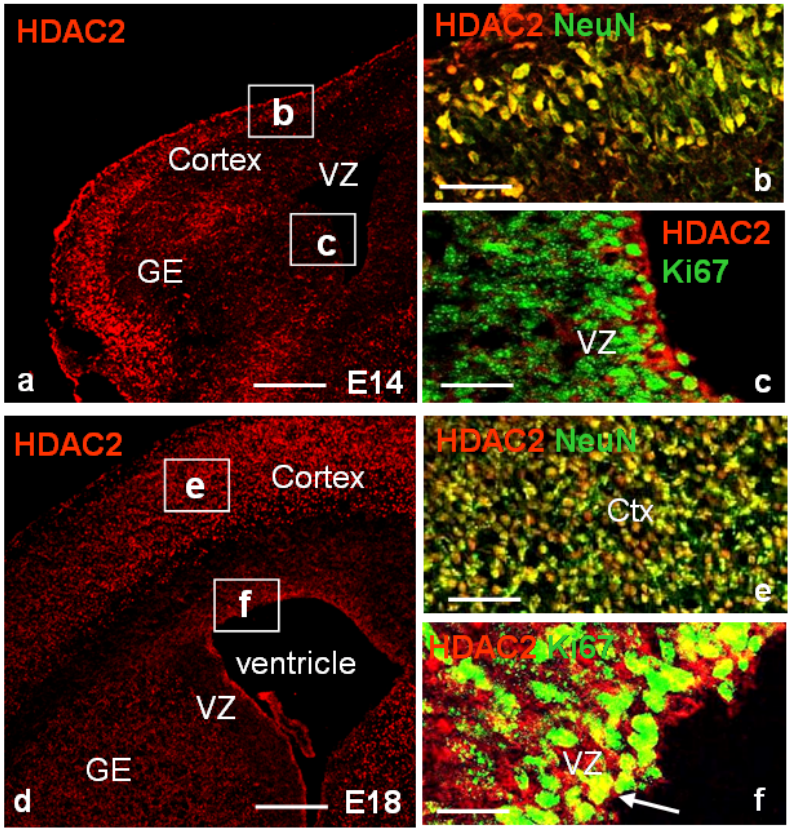

Figure 5.5: HDAC2 immunoreactivity at embryonic stages

a-c HDAC2 immunoreactivity in the E14 telencephalon. High levels of HDAC2 protein were observed in NeuN+ neurons in the CP (b), but were absent in Ki67+ precursors lining the VZ (c). **d-f** HDAC2 immunoreactivity at E18. HDAC2 is still expressed in NeuN+ cells in the CP (e). Weak expression of HDAC2 is also detectable in Ki67+ cells (f). The arrow depicts a double-positive cell. GE= ganglionic eminence, VZ= ventricular zone. Scale bars: a, d 100 μm; e 50 μm; b, c 20 μm; f 10 μm.

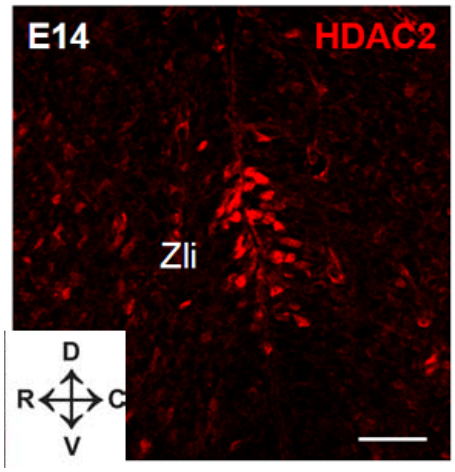

Figure 5.6: HDAC2 immunoreactivity at E14 in the Zona limithans intrathalamica

HDAC2 is expressed specifically in the Zli in the diencephalon. Zli= zona limithans intrathalamica. C, D, R, V= caudal, dorsal, rostral, ventral. Scale bar: 20 μm.

5.1.4.2 HDAC2 immunoreactivity during postnatal development

HDAC2 immunoreactivity is maintained during the postnatal development of the brain starting on postnatal day 0 (P0) and ending at around P21. While neurogenesis is restricted to embryonic stages in the developing brain, gliogenesis starts after birth (P0). Cells that are proliferating and can be detected by immunoreaction against the antigen Ki67 have gliogenic potential. The first glial precursors arise around E18, when HDAC2 was observed to switch from its restricted presence in postmitotic neuronal cells to an existence in proliferating cells that were presumably glial precursors. The same pattern of immunostaining for HDAC2 could be observed at the different stages P0, P5 and P21 during postnatal development. At P0, HDAC2 immunoreactivity is high in NeuN+ neurons (**Figure 5.7 b**). Moreover it is expressed in Ki67+ cells in the HC, one of the regions where neurogenesis continues lifelong (**Figure 5.7 c**), as well as in the white matter (WM) full of gliogenic precursors that are Ki67+ and GFAP+ (**Figure 5.7 d,e**).

At P5 HDAC2 showed a similar expression pattern to that at P0. High expression was still maintained in neurons. Furthermore, specifically gliogenic precursors in the WM showed weaker HDAC2 immunoreactivity (**Figure 5.8 b,c**) compared to doublecortin (Dcx)+ neuroblasts and Ki67+ precursors in the HC which showed increased HDAC2 immunoreactivity (**Figure 5.8 d,e**).

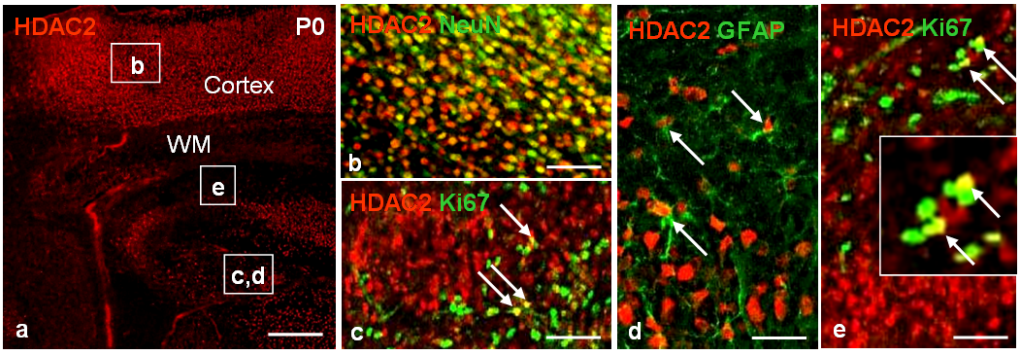

Figure 5.7: HDAC2 immunoreactivity at postnatal day 0

a Overview of HDAC2 immunoreactivity at P0. **b,c** HDAC2 is highly expressed in NeuN+ neurons (b) and in Ki67+ cells in the HC (c). **d,e** In a gliogenic region, the WM, HDAC2 is expressed in GFAP+ (d) and in Ki67+ cells (e). Arrows depict double-positive cells. White rectangle shows higher magnification. WM= white matter. Scale bars: a 100 μm; b, c 50 μm; d, e 20 μm.

The last time point to be discussed in postnatal development is P21, when the brain development is about to be completed. The HDAC2 expression is still identical to that at P0 or P5. The prominent postmitotic expression is detectable in neurons (**Figure 5.9 d**) as well as in GFAP+ astrocytes (**Figure 5.9 a**) and in CC1+ oligodendrocytes (**Figure 5.9 b**). In the WM where glial progenitors can be found, HDAC2 was also expressed in neurogenic progenitor cells that are Dcx+ located in a stream between HC and Ctx, the so-called subcortical white matter (SCWM) (**Figure 5.9 c**). In contrast to the normal neurogenic potential of Dcx+ cells, these cells have glial progenitor properties and can also be labeled by a short pulse BrdU 1 hour before sacrificing the animal. At early postnatal stages neural progenitor cells were described to generate Dcx+ cells in this region [Takemura, 2005]. Later, at adult stages, Dcx+ cells in the subcortical white matter (SCWM) have almost disappeared.

5.1.4.3 HDAC2 immunoreactivity in the adult brain

In the adult brain HDAC2 immunoreactivity was found in most cell types, including neurons, glia and progenitors (**Figure 5.10 a**). Interestingly, a high expression was also observed in the two regions of adult neurogenesis, SEZ/RMS/OB and the subgranular zone (SGZ) in the DG. This raised the question, in which cell

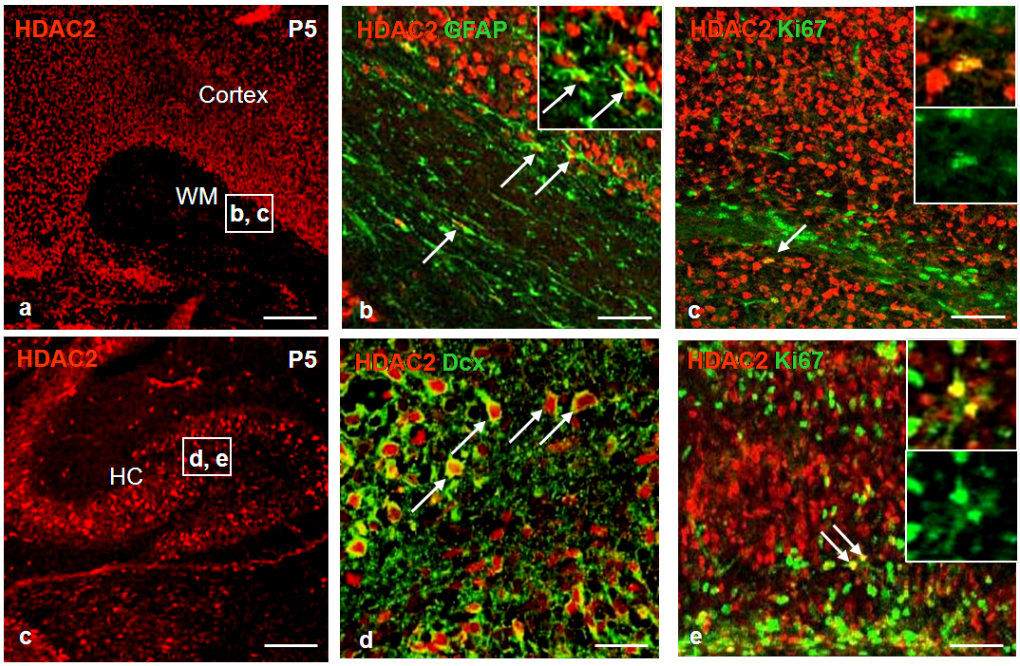

Figure 5.8: HDAC2 immunoreactivity at postnatal day 5

a,d HDAC2 immunoreactivity at P5 in the regions of the Ctx and WM (a) and the HC (d). **b,c** Immunostaining of HDAC2 is weakly found in GFAP+ cells (b) and in Ki67+ cells in the WM (c). **d,e** Strong HDAC2 immunoreactivity is observed in Dcx+ neuroblasts (d) and in Ki67+ precursors (e) in the HC. Arrows depict double-positive cells. White rectangles show higher magnifications. HC= hippocampus, WM= white matter. Scale bars: a 100 μm; c 50 μm; b, d, e, f 20 μm.

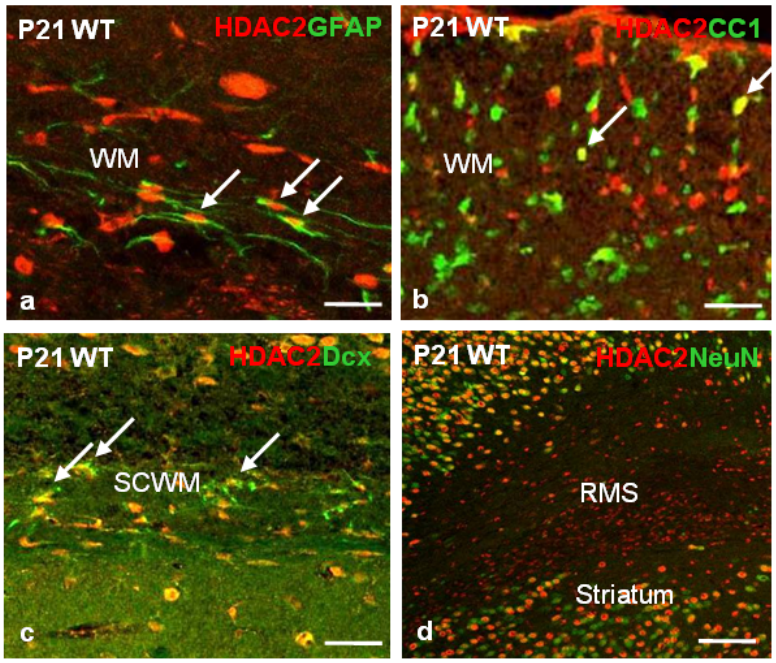

Figure 5.9: HDAC2 immunoreactivity at postnatal day 21

a HDAC2 immunoreactivity is observed in postmitotic GFAP+ astrocytes. **b** The HDAC2 protein is found in CC1+ oligodendrocytes. **c** HDAC2 is detectable in Dcx+ cells in the SCWM. **d** HDAC2 stays on in postmitotic neurons. Arrows depict double-positive cells. RMS= rostral migratory stream, SCWM= subcortical white matter, WM= white matter. Scale bars: a 10 μm; b, c 20 μm; d 50 μm.

type HDAC2 is expressed there? To answer this, a lineage analysis using specific markers to label each cell type existing in the adult neurogenic niches was performed. As shown in P21 old animals, the HDAC2 protein was found in postmitotic glial cells such as CC1+ cells, and it was still high in postmitotic neurons similar to earlier stages (**Figure 5.10 b**). Dcx as a marker for neuroblasts was found to be coexpressed with HDAC2 from postnatal day 0 on until adult stages in both neurogenic regions (**Figure 5.10 c,d**; **Figure 5.9 c**; **Figure 5.8 d**). HDAC2 could also be detected in transit-amplifying progenitor cells that are Dcx- negative but divide fast and can be labeled by a short pulse of the DNA-base analogue 5-bromo-2'deoxyuridine (BrdU)(**Figure 5.10 e,f**). BrdU is incorporated in the DNA of dividing cells [Nowakowski et al., 1989]. In contrast, no HDAC2-immunoreactivity could be observed in adult neural stem cells that show astroglial properties and are labeled by the green fluorescent protein (GFP), whose expression is driven by the human GFAP promoter [Doetsch et al., 1999; Nolte et al., 2001](**Figure 5.10 g,h**). These cells can also be identified according to their location in the adult neurogenic zones as well as their morphology. Therefore stem cells do not show HDAC2 expression in the adult brain, whereas all other cells are HDAC2+. All results for the expression analysis of HDAC2 are summarized in **Table 5.1**.

5.1.5 Overlap of HDAC2 and Brg1 immunoreactivity

Having analyzed the expression pattern of HDAC1 and HDAC2, the expression pattern of Brg1 was examined *in vivo*. Interestingly, there was an almost complete overlay in the immunoreactivity of both proteins after double stainings for HDAC2 and Brg1 in the adult brain. While the expression pattern of Brg1 and HDAC2 were different in the embryonic neurosphere cultures, with Brg1 being highly expressed in neural precursors and HDAC2 mainly in postmitotic cells, the picture in the adult brain was rather different. The coexistence of the HDAC2 and Brg1 proteins was present in all regions in the brain, in particular in the DG and SEZ as the zones of adult neurogenesis (**Figure 5.11**).

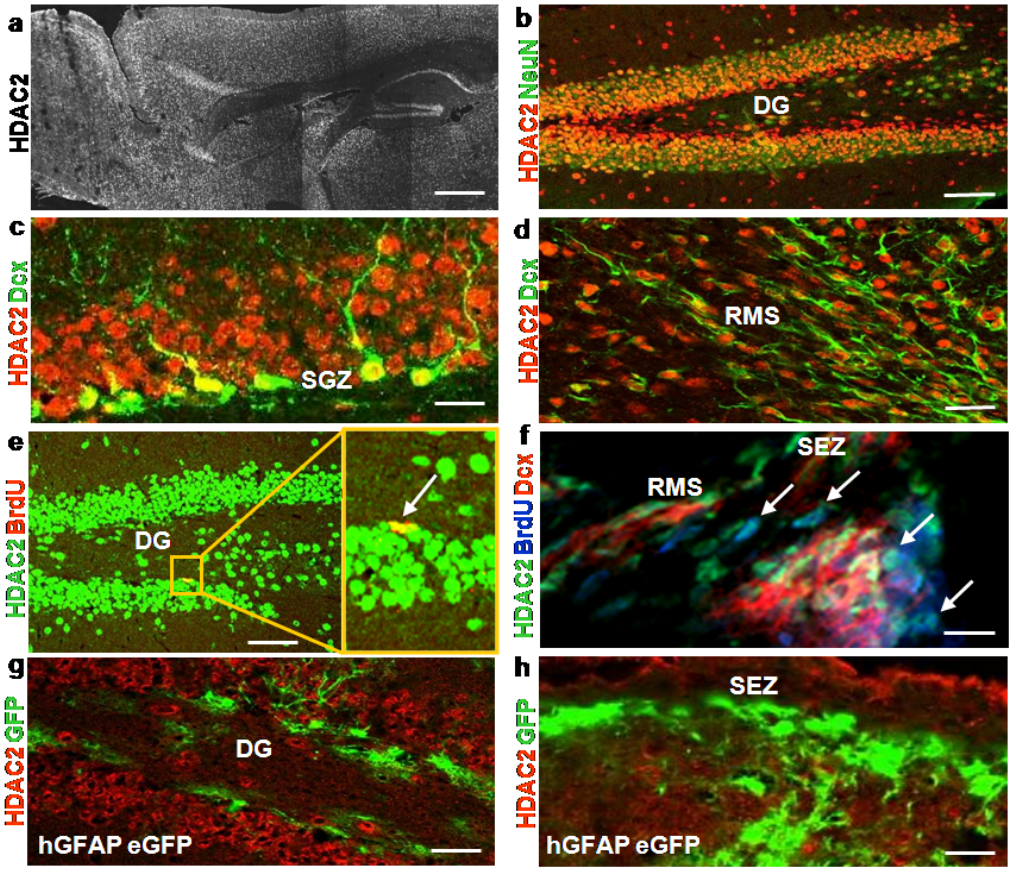

Figure 5.10: HDAC2 immunoreactivity in the adult brain

a HDAC2 immunoreactivity depicted in an overview. **b** HDAC2 is found in NeuN+ neurons in the granule cell layer (GCL) of the DG. Note the HDAC2 presence in the inner cell layer of the DG, the subgranular zone (SGZ). **c,d** HDAC2 is detectable in Dcx+ cells in the SGZ (c) as well as in the RMS (d). **e,f** HDAC2 immunoreactivity in BrdU+ transit-amplifying precursors in the DG (e) and at the SEZ, which are DCX- (f). **g,h** No coimmunoreactivity detectable on hGFAPeGFP sections with GFP labeling neural stem cells in both regions. Arrows depict double-positive cells. DG= dentate gyrus, RMS= rostral migratory stream, SEZ= subependymal zone, SGZ= subgranular zone. Scale bars: a 100 μm; b, e 50 μm; c, d, f, g, h 20 μm.

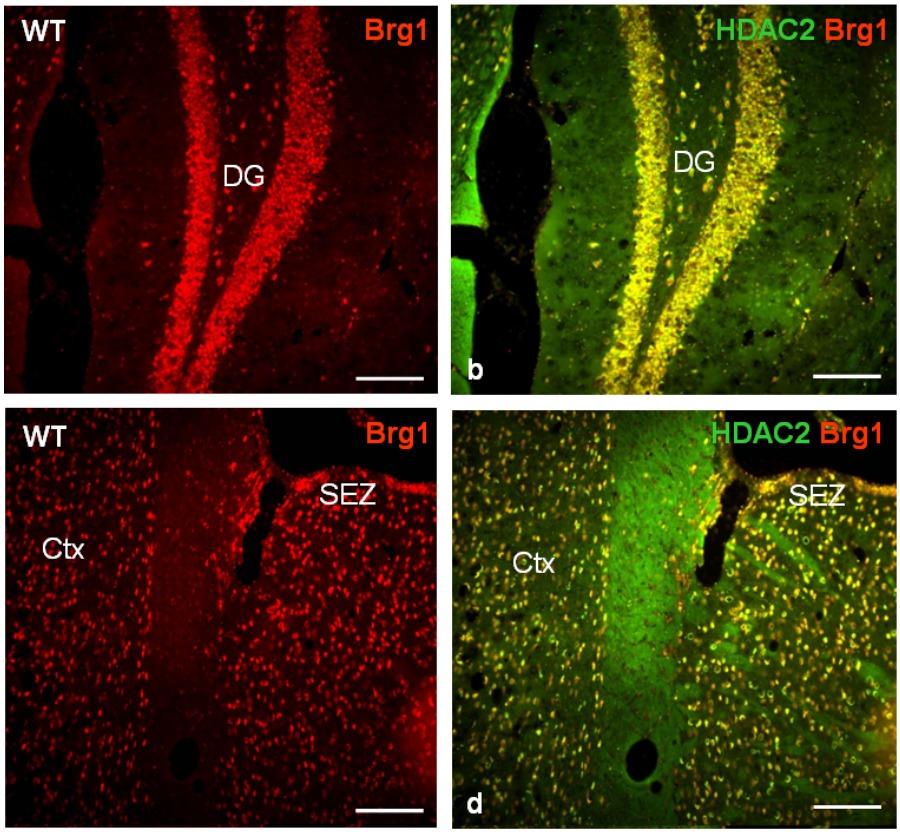

Figure 5.11: HDAC2 and Brg1 immunoreactivity in the adult brain

a,b Immunoreactivity of Brg1 and HDAC2 in the DG. Note the virtual overlap of HDAC2 (green) and Brg1 (red) immunostaining in the same cells. **c,d** Colocalization of Brg1 and HDAC2 at the SEZ and Ctx. Scale bars: a-d 50 μm.

5.1.5.1 Brg1 immunoreactivity in adult neural stem cells

Given the almost complete overlay in the immunoreactivities for HDAC2 and Brg1, it was also examined whether the Brg1 protein was absent in adult neural stem cells equal to HDAC2. Therefore immunohistology on sections from the transgenic mouse line hGFAPeGFP was performed, in which eGFP is expressed under the hGFAP promoter that is only active in astrocyte-like cells and stem cells. In both regions of adult neurogenesis Brg1 immunoreactivity in GFP expressing cells could be detected (**Figure 5.12 a,b**).

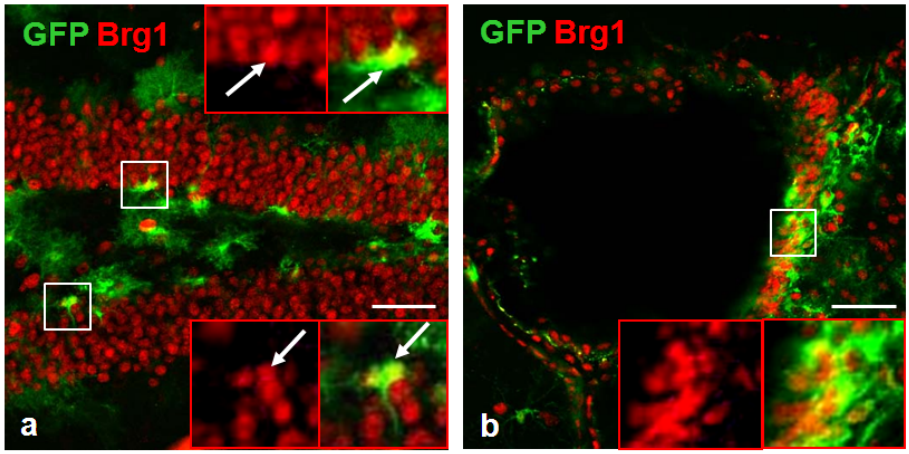

Figure 5.12: Brg1 immunoreactivity in adult neural stem cells

Brg1 is detectable together with eGFP on sections of hGFAPeGFP mice in both adult neurogenic regions, the DG (a) and the SEZ (b). Arrows depict double-positive cells. White rectangles depict regions of higher magnification. Scale bars: a 20 μm; b 50 μm.

5.1.5.2 Brg1 immunoreactivity at embryonic stages

The near identical expression of HDAC2 and Brg1 in the adult brain, with the exception of the additional presence of Brg1 protein in adult neural stem cells, called for an examination of the expression pattern during embryonic neurogenesis. In comparison to the HDAC2 expression at E14, Brg1 was also observed in the CP, where postmitotic neurons are located. In contrast to HDAC2, however, Brg1 was also present in the VZ progenitor cells (**Figure 5.13 a**). At the end of embryonic neurogenesis at E18 the Brg1 protein was, like HDAC2, observed at high levels in the

Ctx but was downregulated in the VZ (**Figure 5.13 b**) where HDAC2 immunoreactivity increased from E18 on in precursor-like cells (**Figure 5.5 d-f**). A summary of Brg1 immunoreactivity at different stages as reported is depicted in **Table 5.1**.

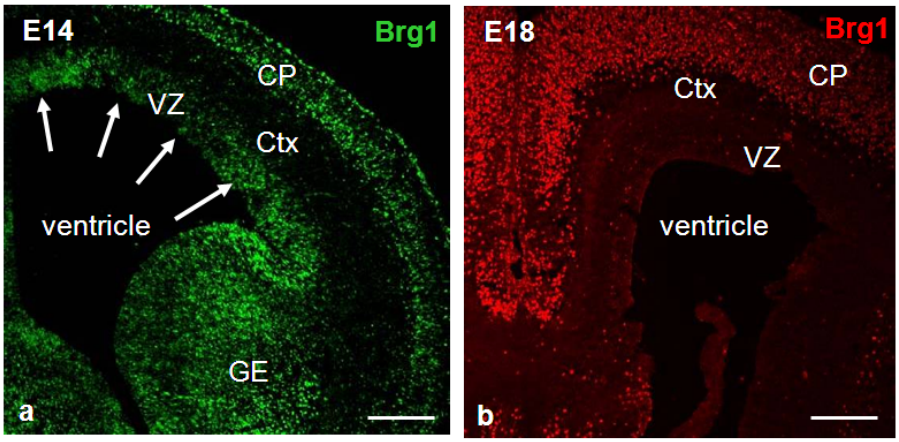

Figure 5.13: Brg1 expression at embryonic stages

a Expression of Brg1 at E14. Note the high amount of the Brg1 protein in the VZ, but also in the CP and in the GE. **b** At E18 the expression remains high in the Ctx, whereas it is redundant in the VZ. Arrows point to high levels of Brg1 protein at the VZ. CP= cortical plate, Ctx= cortex, GE= ganglionic eminence, VZ= ventricular zone. Scale bars: 100 μm.

5.2 Functional analysis of HDAC2

The high levels of HDAC2 in postmitotic cells at all stages analyzed during brain development and the differential expression of HDAC2 protein in adult, but not embryonic neurogenic precursors prompted us to study the function of HDAC2 in the central nervous system (CNS).

5.2.1 HDAC2 deficient mice - construct design

In order to perform a functional analysis, a mouse line deficient of HDAC2 was used that will be referred to as HDAC2 deficient (HDAC2 def) in the following. This mouse line was obtained from a gene trap clone (ES clone no. W035F03) from the German Genetrap Consortium. The gene trap was performed by an insertion of a pPT1-βgeo vector in the genomic locus of HDAC2 on chromosome 10 integrating in

Table 5.1: Summary expression analysis

Time	Cell type	HDAC1	HDAC2	Brg1
E14	neuronal progenitors	++	−	++
	postmitotic neurons	+	++	++
P0	neuronal progenitors	−	+	n.d.
	glial progenitors	++	+	n.d.
	astrocytes	++	+	++
	neurons	−	++	++
P5	neuronal progenitors	−	++	n.d.
	glial progenitors	++	+	n.d.
	astrocytes	++	+	++
	neurons	−	++	n.d.
P21	Type B cells	n.d.	−	+
	Type C cells	n.d.	+	n.d.
	Type A cells	n.d.	++	++
	astrocytes	++	+	++
	oligodendrocytes	++	+	n.d.
	neurons	−	++	++
adult	Type B cells	n.d.	−	+
	Type C cells	n.d.	+	+
	Type A cells	n.d.	++	++
	astrocytes	++	+	++
	oligodendrocytes	++	+	++
	neurons	−	++	++

the region of intron 8 (**Figure 5.14 a**). This leads to an interruption of the gene in the catalytic domain thereby creating a fusion protein. This can be detected by βgalactosidase staining and is responsible for the loss of functional protein tested by Western Blot as well as Southern Blot to reveal the partial deletion of HDAC2 gene [Trivedi et al., 2007; Zimmermann et al., 2007]. As the HDAC2 antibody binds to the C-terminal end of HDAC2 protein and the mutant protein lacks the normal C-term, it cannot be detected by normal immunostaining for HDAC2 (**Figure 5.14 b**).

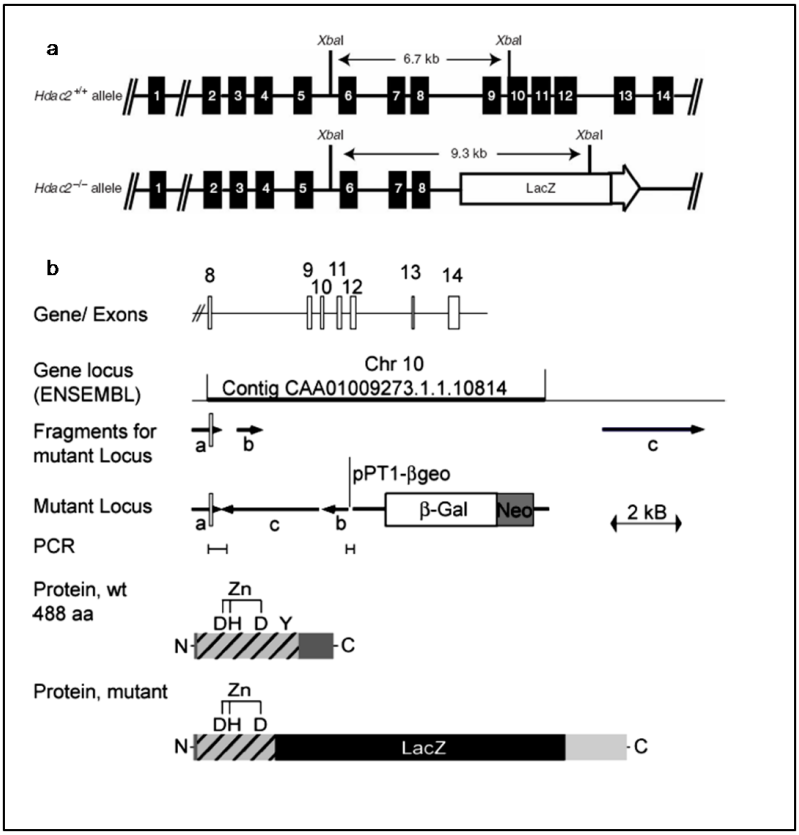

Figure 5.14: HDAC2 gene trap construct

a Schematic depiction of the HDAC2 WT allele and the HDAC2 def allele. The insertion of the pPT1-βgeo vector in intron 8 results in a mutant lacZ fusion protein. **b** Schematic overview of the gene trap construction and depiction of WT and mutant protein. Note the disruption of the zinc-finger binding domain in the deficient protein, inducing a loss of the catalytic domain of HDAC2.

5.2.2 HDAC activity assay from WT and HDAC2 def tissue

To examine whether the overall HDAC activity is diminished in different regions of the adult brain, an HDAC activity assay of WT and HDAC2 def tissue of the OB, HC and CB was performed in collaboration with Sabine Lagger (Max F. Perutz Laboratories, Medical University of Vienna, Institute of Medical Biochemistry, Dr. Bohr-Gasse 9/2, A-1030 Vienna). The HDAC activity, measured as counts per minute (CPM), was reduced in all 3 tested brain regions. In the HC the decrease in HDAC activity was highly significant compared to the OB and CB (**Figure 5.15**). Interestingly, the highest HDAC activity was measured in the cerebellum, where developmental defects could already be detected at postnatal stages, an observation that, with a view to the specific focus on the forebrain, will not be further discussed within this work.

5.2.3 HDAC2 def mice - offspring

HDAC2 def mice were born according to Mendelian rates. Neonatal pups were all monitored and then genotyped at the age of 3 weeks. If pups died during the first postnatal weeks, they were included in the statistical analysis (**Figure 5.16**).

5.2.3.1 Survival rate of HDAC2 def mice

After HDAC2 def mice were born according to Mendelian rates suggesting no severe defects during embryonic development, as will be further explained in the next paragraph, severe defects in the postnatal development shortly after birth lead to the dynamic increase in lethality of HDAC2 def pups compared to WT littermates. The complete knock out (KO) of HDAC2 has a 100 % lethality in the first 2 postnatal days [Montgomery et al., 2007]. The HDAC2 def mice studied here, showed a postnatal lethality of about 70 % compared to WT or heterozygous littermates that have a survival rate of nearly 100 % (**Figure 5.17**).

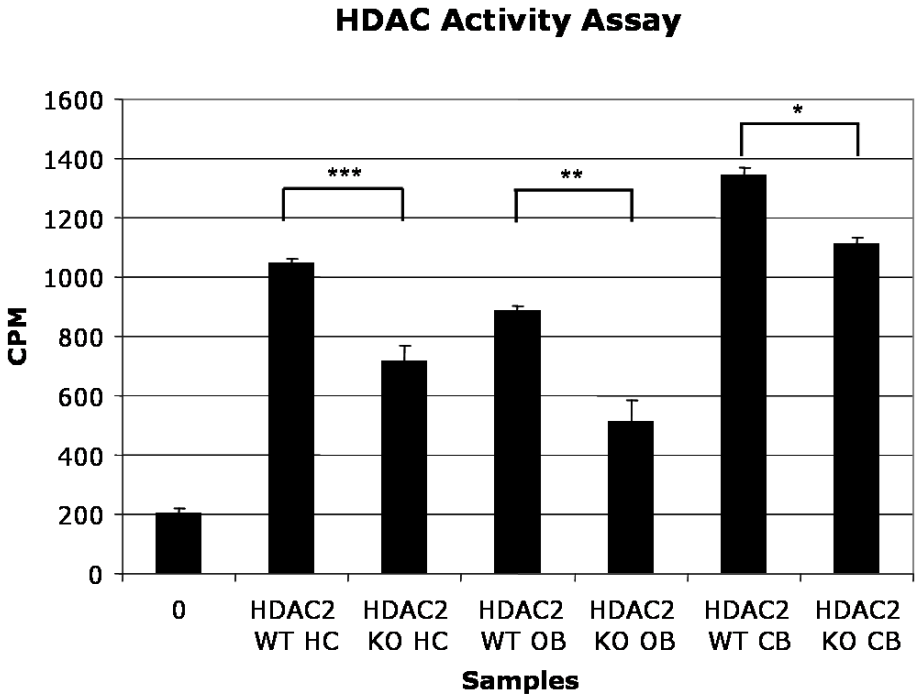

Figure 5.15: HDAC activity assay

Tissue from specific regions of the adult forebrain of WT and HDAC2 def mice was processed and an HDAC activity assay was designed to compare the overall HDAC activity between WT and HDAC2 def mice. CB= cerebellum, CPM= counts per minute, OB= olfactory bulb, HC= hippocampus. SEM=*;**;*** depict p≤0,04 ;0,002 ;0,0001 , respectively.

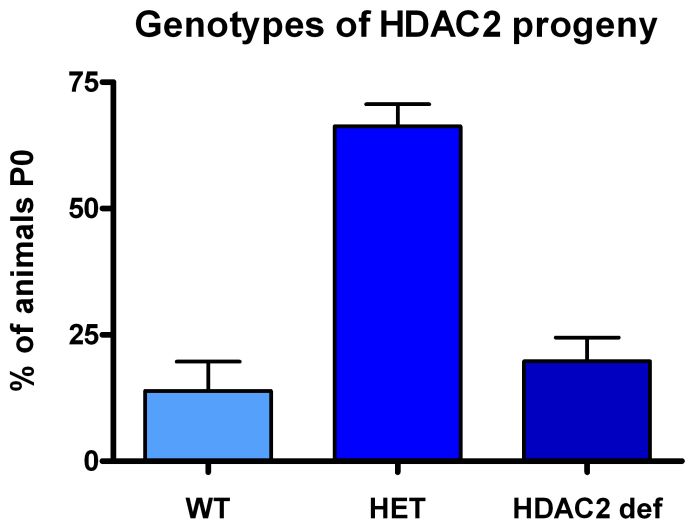

Figure 5.16: Genotypes of HDAC2 progeny

Genotypes of HDAC2 progeny are distributed normally according to Mendelian rates.

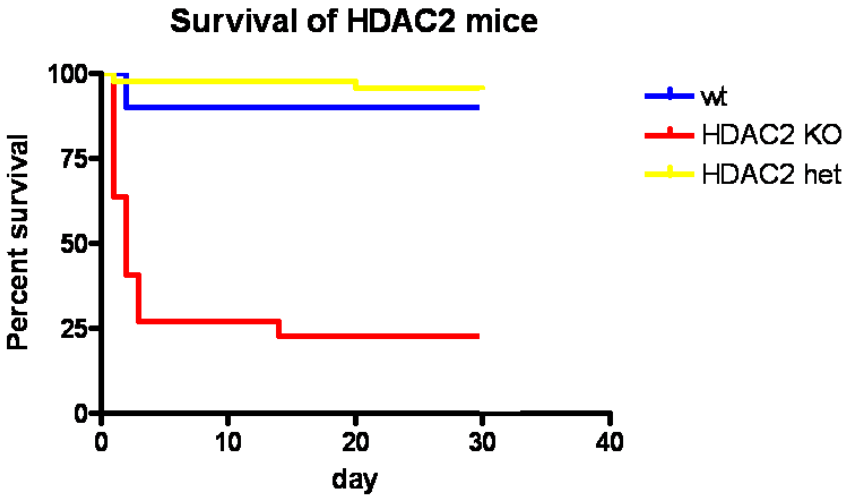

Figure 5.17: Postnatal survival rate of HDAC2 def mice

5.2.4 Embryonic brain development of HDAC2 def mice

Immunostaining was performed on sections of WT and HDAC2 def mice (**Figure 5.18 a,b**) to test the specificity of the HDAC2 antibody that binds to the C-terminal end of the HDAC2 WT protein, which is disrupted in the HDAC2 def mice and replaced by a lacZ fusion protein (**Figure 5.14 b**). Note that immunoreactivity was absent on sections from HDAC2 def brains, confirming the specificity of the antibody. At E14 (midneurogenesis) embryonic neurogenesis occurs completely normal, the newly born neurons labeled by β-IIItubulin (**Figure 5.18 c,d**) form the CP with the different neuronal layers. Therefore radial migration of young neurons to their final destination from the basal to the pial surface is not obviously affected by the loss of the HDAC2 function. This is also consistent with the normal pattern of radial glial cells in the forebrain depicted by an immunostaining with Blbp (brain lipid binding protein) that is expressed in radial glia from early stages on (**Figure 5.18 e,f**). The thickness of the Ctx and of the whole brain is comparable to WT littermates at this stage of development. Along this line, quantifications to examine cell density also showed no difference between HDAC2 def mice and WT littermates (WT= 233±15 DAPI+ cells/0,01 mm^2, n=2; HDAC2 def= 238±8 DAPI+ cells/0,01 mm^2, n=2). The same was true for the neuronal density in the CP (WT= 87±7 NeuN+ cells/0,01 mm^2, n=2; HDAC2 def= 91±7 NeuN+ cells/0,01 mm^2, n=2). To test whether proliferation might be affected in HDAC2 def brains, two different immunostainings were performed using Ki67 (**Figure 5.18 g,h**), a marker for all dividing cells and PH3 (**Figure 5.18 i,j**) labeling only cycling cells in M-phase of mitosis. The number of proliferating cells in total and, in more detail, cells in specific phases of mitosis (WT= 563±12 PH3+ cells/mm^2, n=2; HDAC2 def= 566±22 NeuN+ cells/mm^2, n=2) remained unchanged.

5.2.5 Postnatal brain development of HDAC2 def mice

5.2.5.1 Phenotypic differences in body and organ size

The high postnatal lethality rate points to severe defects in the postnatal development of HDAC2 def mice. Adult mice have a clear growth retardation compared to their WT littermates. This raises the question when this phenotype starts? At

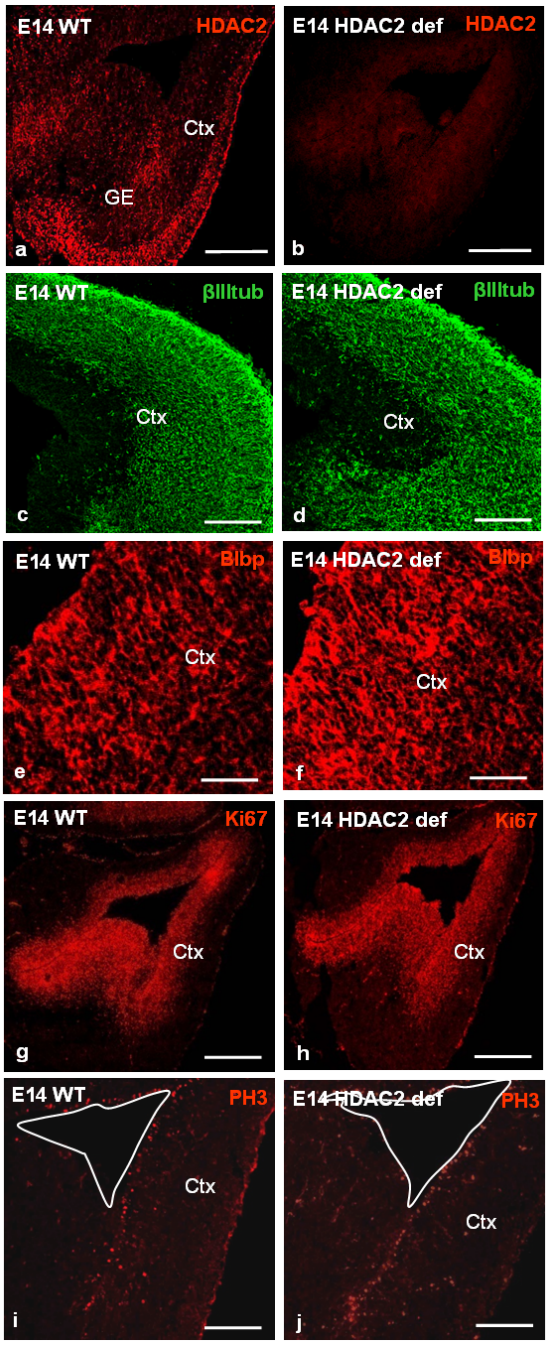

Figure 5.18: Embryonic brain development of HDAC2 def mice

a,b Expression of HDAC2 at E14 on WT brain sections(a) and on HDAC2 def sections (b). Note the absence of detectable WT protein by HDAC2 immunostaining. **c,d** Expression of β-IIItubulin that labels young neurons in the Ctx is comparable between WT and HDAC2 def embryos. **e,f** Blbp expression is not changed in the mutant mice at E14. **g-j** Proliferation examined by an immunostaining with Ki67 (g,h) and PH3 (i,j) is not affected in HDAC2 def embryonic brains. The white line in (i,j) marks the ventricle. Ctx= cortex, GE= ganglionic eminence. Scale bars: a,b,g,h 100 μm; c,d,i,j 50 μm; e,f 20 μm.

P3 the surviving animals showed no obvious difference in body size (**Figure 5.19 a**) while at P21, when postnatal development had progressed, a severe growth retardation became manifest in almost all HDAC2 def mice. They were half of the size and the weight of their WT littermates (**Figure 5.19 b**). Interestingly, not only the body size but also the adult brain of HDAC2 def mice in comparison to WT brains showed the same phenomenon, namely being smaller in size and weight. Other single organs also showed a decrease in weight (≈25%), however, not related to the overall reduction in size and weight [Zimmermann et al., 2007], but rather independent thereof. The cross morphology of HDAC2 def brains was normal examined by sagittal sections of perfused and fixed WT and mutant brains (**Figure 5.19 e,f**).

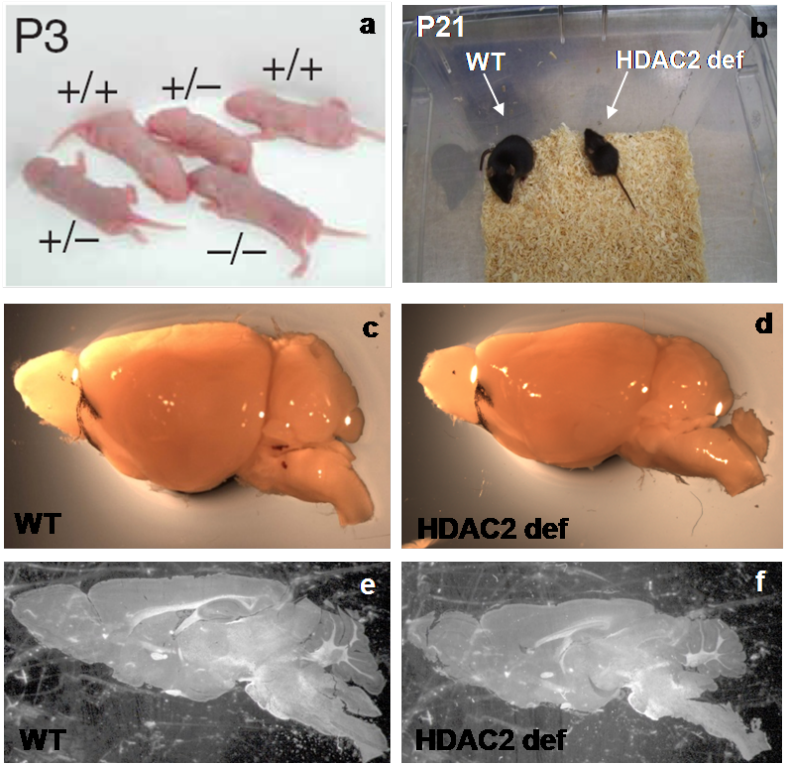

Figure 5.19: Phenotypic differences in body and organ size

a At P3 no difference in body size between the genotypes could be detected. **b** At P21 a severe growth defect of HDAC2 def mice becomes manifest. **c,d** Sideview of a WT (c) and HDAC2 def brain (d). Note the reduced size of the brain in the mutant situation. **e,f** Sagittal section of adult WT (e) and HDAC2 def brain (f). Note the smaller size, but the comparable morphology of the mutant brain. +/+ = WT, +/– = heterozygous mutant, –/– = homozygous mutant.

5.2.5.2 Increased cell death at postnatal stages

While the embryonic development was completely normal in HDAC2 def mice, there must be several defects occuring at early postnatal stages that lead to the growth retardation defect and to the high postnatal lethality. The smaller size of the brain might be a result of apoptosis occuring as previously described in other organs such as the intestine [Zimmermann et al., 2007] in these mice. Therefore, activated caspase 3 (casp3) was checked, a protein that is activated by cleavage in a small time window when cells undergo apoptosis [Riedl and Shi, 2004]. There was a significant increase in the number of activated casp3+ cells throughout the brain (**Figure 5.20 a,b**). Neurogenic regions such as the HC were affected as well as nonneurogenic regions, e.g. the Ctx, while all showing a higher number of dying cells in HDAC2 def mice (**Figure 5.20 c**). Notably the minority of the casp3+ cells have neuronal identity (**Figure 5.20 d**). This could be observed by double stainings of activated caspase 3+ cells with GFAP, a marker for astrocytes (**Figure 5.20 d**) and by then counting the percentage of double-positive cells in WT and HDAC2 def postnatal brains. In the mutant brains the number of neuronal cells that are casp3+ is only $\approx 30\,\%$ compared to $45\,\%$ in WT animals (**Figure 5.20 e**).

5.2.6 Phenotypic changes in the adult brain of HDAC2 def mice

5.2.6.1 Cytoarchitecture of the mutant brain

To examine whether the observed deficits in the postnatal brain development have a direct influence on the morphology and cytoarchitecture of HDAC2 def brains, NeuN-immunostainings in the Ctx were performed (**Figure 5.21 a,b**). No difference regarding the cytoarchitecture was detectable. Equally, the formation of the different layers of the Ctx appeared to be completely normal as shown by the expression of a specific layer marker such as Cux2, which is only expressed in neurons of layer 2/3 (**Figure 5.21 c,d**). After quantifiying NeuN+ cells and DAPI+ cells in the WT and HDAC2 def Ctx no difference in cell number could be observed (**Figure 5.21 e,f**). These observations were in line with the expectations, since no defects in embryonic neurogenesis were detectable.

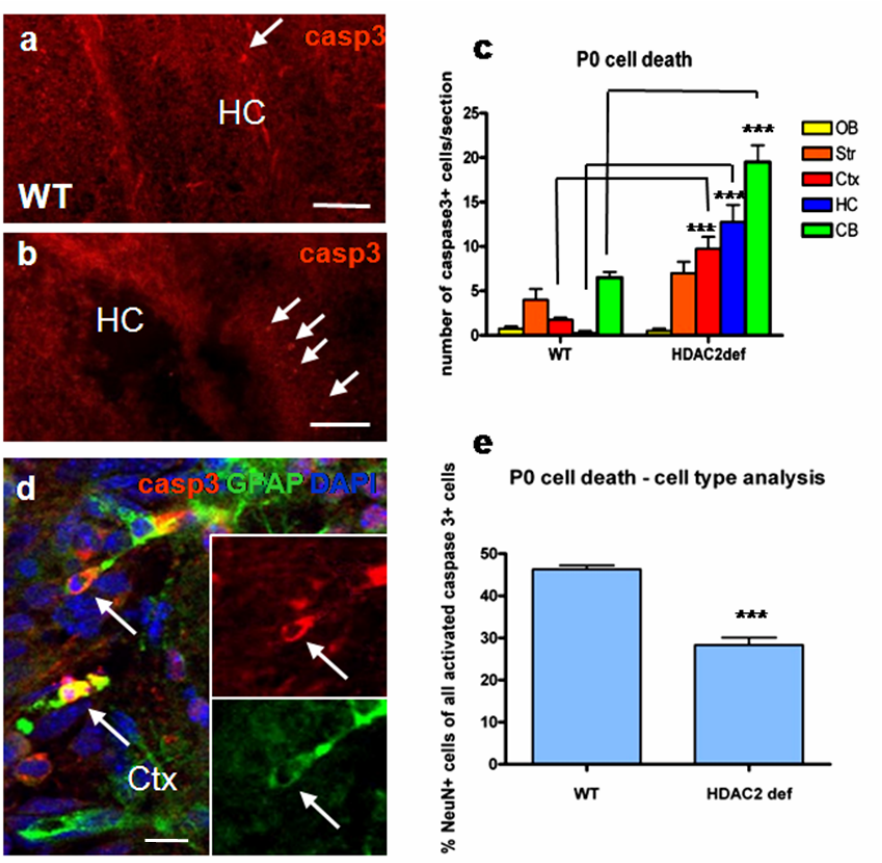

Figure 5.20: Postnatal cell death in HDAC2 def mice

a,b Immunostaining of activated caspase 3 depicts the increase in apoptosis postnatally in HDAC2 def (b) compared to WT brains (a). **c** Histogram shows the widespread cell death allover the mutant brain at P0. **d** Cells undergoing cell death are positive for GFAP in the Ctx. **e** Histogram depicts the percentage of neuronal cells undergoing apoptosis in WT and HDAC2 def mice. Arrows in (a,b) depict casp3+ cells, in (d) a double-positive cell. CB= cerebellum, Ctx= cortex, HC= hippocampus, OB= olfactory bulb, Str= striatum. SEM=*** depict $p \leq 0{,}001$ (Ctx), 0,0007 (HC), 0,0006 (CB) and 0,0008 (Cell type analysis). Scale bars: a,b 50 μm; d 20 μm.

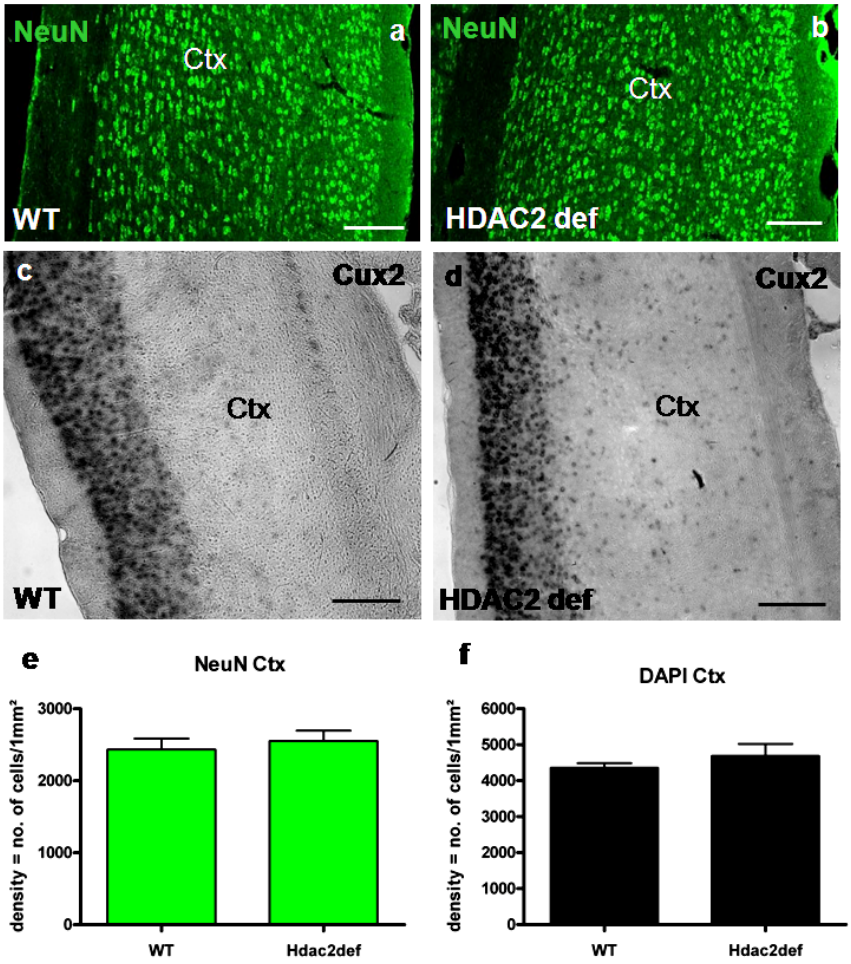

Figure 5.21: Cytoarchitecture of WT and HDAC2 def brains

a,b NeuN immunostaining of WT and HDAC2 def cortices. **c,d** mRNA expression of Cux2 in the upper layers of the Ctx in WT and HDAC2 def brains. **e,f** Histograms show the density of neurons (NeuN+) and the density of all DAPI+ cells in the Ctx. Note that the mutant Ctx is completely normal in terms of neuronal as well as cell density. Ctx= cortex. Scale bars: 50 μm.

5.2.6.2 Increased cell death in adult neurogenic regions

The higher rates of cell death in the postnatal HDAC2 def forebrain were transient in nature and declined to normal levels when gliogenesis around P21 came to an end. Only two regions of adult neurogenesis, the DG and the SEZ/RMS/OB system showed higher levels of apoptosis in the adult mutant brain (**Figure 5.22 a**). The colocalization of casp3 and neuronal markers such as NeuN revealed a prevalence of neurons amongst the dying cells. In the HDAC2 def OB 72% of the activated caspase 3+ cells were NeuN+, whereas in the WT OB only 43% of the dying cells were NeuN+ (**Figure 5.22 b,c**). This points toward the fact that specifically adult generated neurons die in HDAC2 def brains.

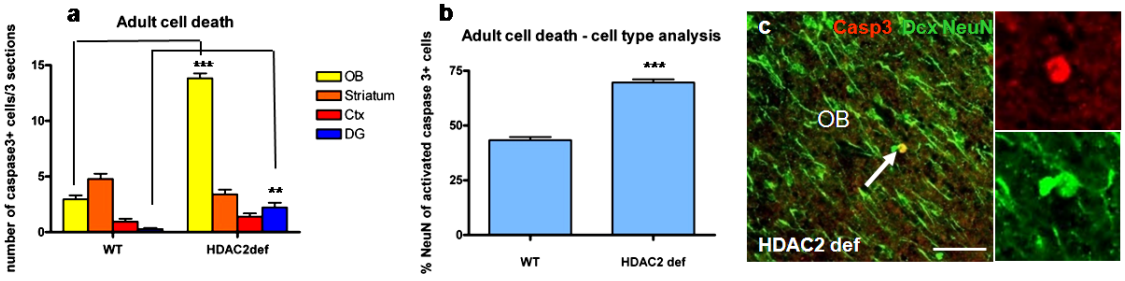

Figure 5.22: Cell death in the adult brain of WT and HDAC2 def mice

a Cell death persists in adult neurogenic regions, the DG and SEZ/RMS/OB system in HDAC2 def brains. **b** The number of neuronal cells (NeuN+) undergoing apoptosis in the OB of HDAC2 def mice is increased. **c** Fluorescent micrograph shows an apoptotic cell that is identified as a neuron by NeuN double staining. OB= olfactory bulb. Arrow depicts a double-positive cell. SEM=**;*** depict p≤0,0011 ;0,0001 (OB) and 0,0007 (Cell type analysis). Scale bar: 20 μm.

5.2.7 The adult neurogenic regions in HDAC2 def mice: DG

5.2.7.1 Expression of Dcx in the DG

In order to examine adult neurogenesis in HDAC2 def mice the expression of different lineage markers, such as Dcx was analyzed. Dcx is expressed in dividing neuroblasts and also in young immature neurons that have previously exited the cell cycle [Abrous et al., 2005]. The immunostaining of Dcx show a remarkable finding in the DG. A prominent loss of Dcx+ cells in HDAC2 def DG (**Figure 5.23**

a,b; **Figure 5.24 a,b**) could also be revealed by the quantification of Dcx+ cells as depicted in **Figure 5.23 c**. The significant decrease concerned the total number of Dcx+ cells in the DG of mutant mice suggesting that mitotic as well as postmitotic Dcx+ cells could be diminished. The higher magnification of single Dcx+ cells also revealed an aberrant morphology in the HDAC2 def DG. The dendrites appeared shorter in length and the dendritic tree was reduced in size. As it was shown by other research groups [Kronenberg et al., 2003], two types of Dcx+ cells are present in the adult DG. The Dcx+ cells that are still cycling show a more horizontal morphology, while Dcx+ postmitotic immature neurons have a characteristic radial morphology. The latter type of Dcx+ cells appeared most affected in the HDAC2 def brains.

5.2.7.2 Proliferation analysis in the HDAC2 def DG

In order to to unravel whether defects in proliferation caused the decrease in Dcx+ cells in adult neurogenesis, the proliferation rates in WT and mutant mice were checked. This was done by giving a short pulse of BrdU 1 hour before the animals were sacrificed as described (Material and Methods 4.3). Consistent with the observations at earlier postnatal stages, a significant increase in the overall number of BrdU+, i.e. fast proliferating cells was observed in the SGZ of HDAC2 def mice compared to WT littermates. BrdU labeled cells were then double-stained for several lineage markers such as GFAP to label adult stem cells and Dcx to detect proliferating neuroblasts. The cells that are only BrdU+ are supposed to be the transit-amplifying precursor cells that are GFAP- and Dcx-. The histogram in **Figure 5.23 d** shows the quantification of this cell type analysis of the BrdU-labeled cells. The relative composition of cell types amongst the observed proliferating cells revealed no difference between the WT and HDAC2 def DG.

5.2.7.3 BrdU label retaining experiment in the DG of HDAC2 def mice

To examine the progeny of the above labeled progenitors, mice were treated with BrdU added to the drinking water for 2 weeks followed by one additional week with normal water to dilute the BrdU in the fast proliferating cells that had already incorporated the DNA-base analogue. This protocol allows to monitor not only the number of newly generated neurons but also the number of stem cells in the mutant DG. If stem cells are diminished this could also lead to a loss of neurons

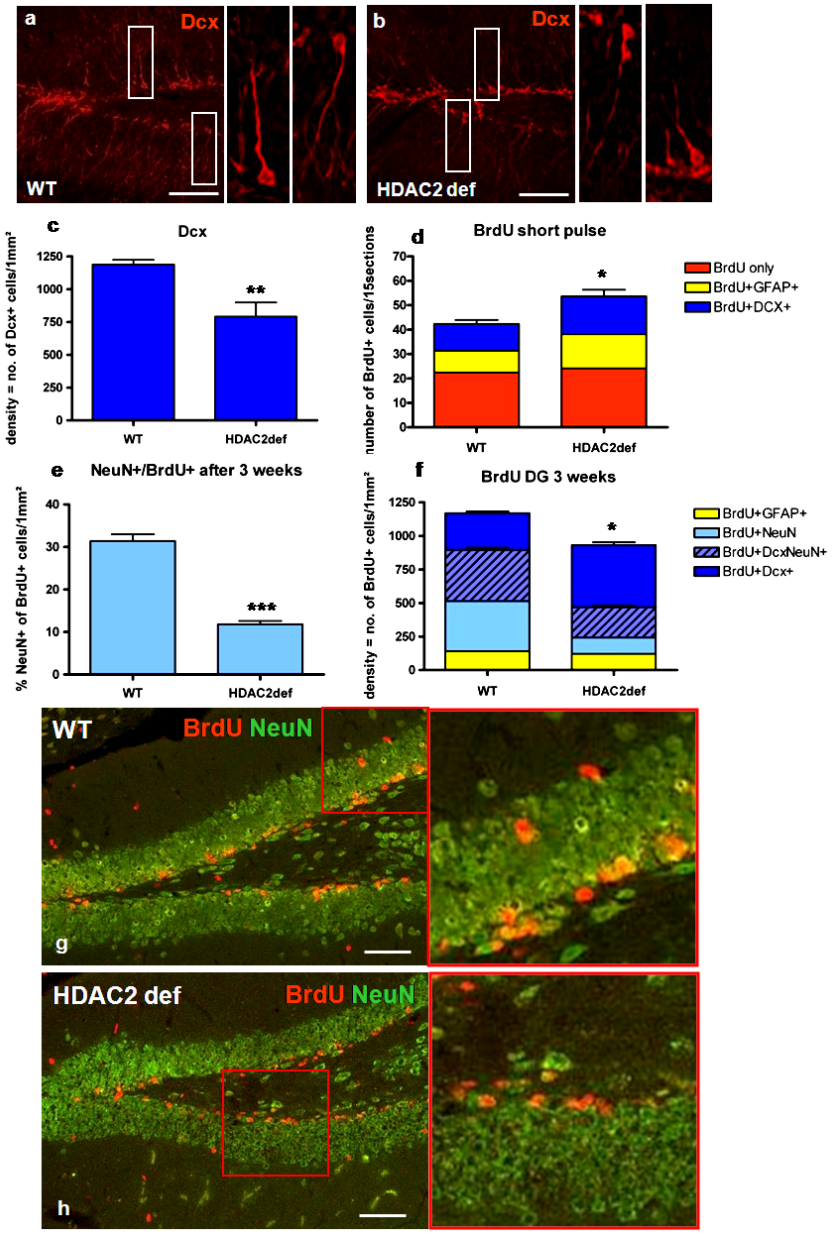

Figure 5.23: Adult neurogenesis in the DG of WT and HDAC2 def mice

a,b Fluorescent micrographs depict the reduced number of Dcx+ cells in the HDAC2 def DG. **c** Statistical analysis underlines the significant decrease in number of Dcx+ neuroblasts and newly generated neurons. **d** A BrdU short pulse analysis shows an increase in fast proliferating cells in the mutant DG. Note that cell type composition remained unchanged. **e-h** BrdU label retaining experiment (2 weeks BrdU/1 week water). The number of newly generated NeuN+ neurons is significantly reduced (e). The number of stem cells (yellow fraction) is not altered in HDAC2 def DG. (f). Fluorescent micrographs in g,h underline the reduced number of newly generated neurons after 3 weeks of BrdU treatment. White and red rectangles depict cells in higher magnification. SEM=*;**;*** depict p≤0,01 ;0,005 ;0,0001 . Scale bars: a,b 50 μm; g,h 20 μm.

at the end of the neurogenic differentiation pathway. As the histograms in **Figure 5.23 e,f** show, the number of BrdU+NeuN+ cells was significantly reduced in the HDAC2 def DG, whereas the stem cell number (BrdU+GFAP+) was not altered. The fraction of BrdU+Dcx+ cells was increased, whereas already the number of BrdU+Dcx+NeuN+ cells starts to decline in the HDAC2 def DG. Therefore the number of maturating neurons declines in the HDAC2 def DG at the time of NeuN upregulation (**Figure 5.23 e,f**). These are very likely the cells that die as observed by casp3 staining.

5.2.7.4 Expression of neuron-specific genes in the HDAC2 def DG

To further determine when neuronal maturation resulted in the initiation of cell death that is then reflected in a reduction of cells positive for Calretinin (Calr), a Ca-binding protein expressed at the time of transition from Dcx to NeuN expression of maturating neurons [Johansson et al., 1999] was examined in the DG of WT and mutant mice. In **Figure 5.24 a-c** the reduction in the number of Calretinin+ neurons in the HDAC2 def DG is depicted via a double-immunostaining with Dcx. In the BrdU label retaining experiment 6 % of BrdU+ cells were Calretinin+ in the WT, whereas only 1 % contained Calretinin in the mutant DG. A more global marker for cells differentiating along the neuronal lineage is NeuroD1, a bHLH transcription factor that has been implicated in the regulation of neuronal differentiation in the DG during development [Miyata et al., 1999]. Also NeuroD1 mRNA was found to be reduced in the HDAC2 def DG shown by *in situ* hybridization (**Figure 5.24 d,e**).

5.2.7.5 Retroviral injection of GFP in the HDAC2 def DG

In order to rule out that neuronal cell death in HDAC2 def mice cannot be explained by a specific sensitivity of HDAC2 def cells to BrdU-labeling [Caldwell et al., 2005] we injected a retrovirus containing green fluorescent protein (GFP) into the DG to trace the progeny of infected precursor cells in the DG [Breunig et al., 2007]. Cells that were dividing at the time point of retroviral injection can incorporate the viral DNA encoding for GFP into their genome and hence inherit it to all their progeny that then continues to express GFP. WT and HDAC2 def animals were sacrificed either 14 days or 21 days after viral injection. Brains were then analyzed

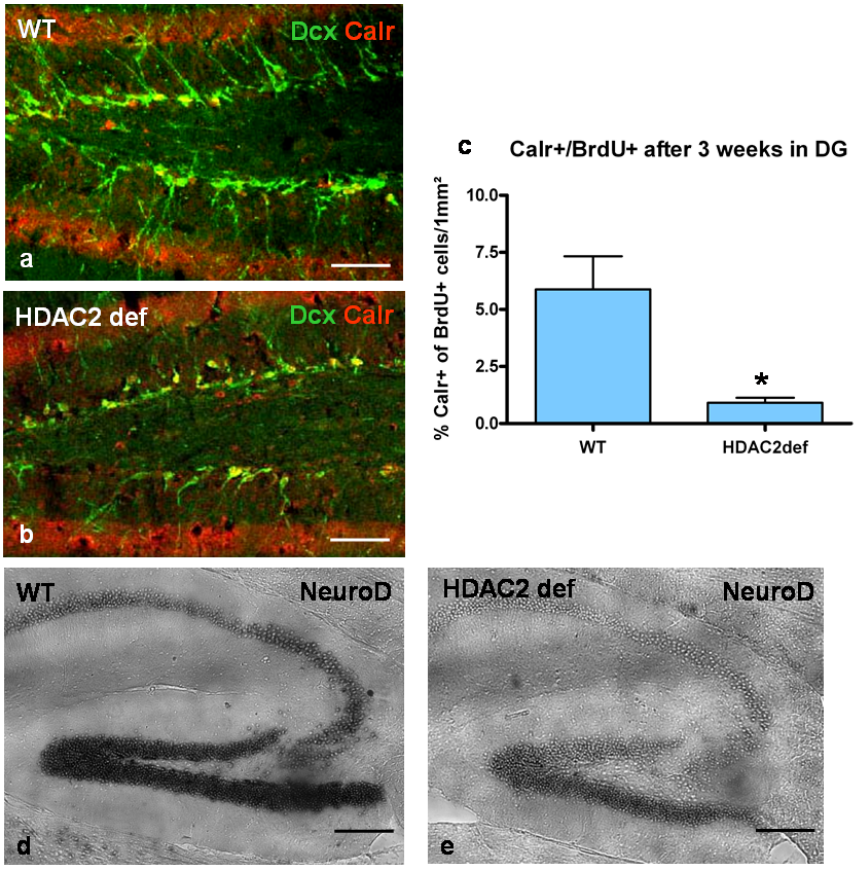

Figure 5.24: Neuronal marker gene expression in the DG

a,b Fluorescent micrographs depict double-staining of Dcx and Calretinin. Note the reduced number of cells positive for both markers in HDAC2 def DG. **c** Histogram shows the quantification of BrdU+Calr+ cells. Note the significant reduction in the mutant DG. **d,e** *in situ* hybridization of NeuroD1 shows an overall reduction of mRNA levels in the hippocampus of HDAC2 def mice. SEM=* depict p≤0,01 . Scale bars: a,b 20 μm; d,e 100 μm.

by immunohistochemical means. After 14 days the proportion of GFP+ cells that express Dcx was slightly although not significantly increased in the HDAC2 def brains (**Figure 5.25 a**). After 21 days, some of the GFP+ cells had differentiated into NeuN+ neurons. These mature neurons were strongly reduced to less than half in number in HDAC2 def DG, consistent with the reduction of BrdU+NeuN+ cells after BrdU labeling (**Figure 5.25 b**). The proportion of GFP+Dcx+ cells was still increased, suggesting a similar effect to the results of the BrdU label retaining experiment after 3 weeks. This experiment fully confirmed the results obtained by the performed BrdU studies, thereby demonstrating that the defect in neuronal differentiation cannot be explained by the concern that HDAC2 def cells might be BrdU sensitive and die after BrdU incorporation.

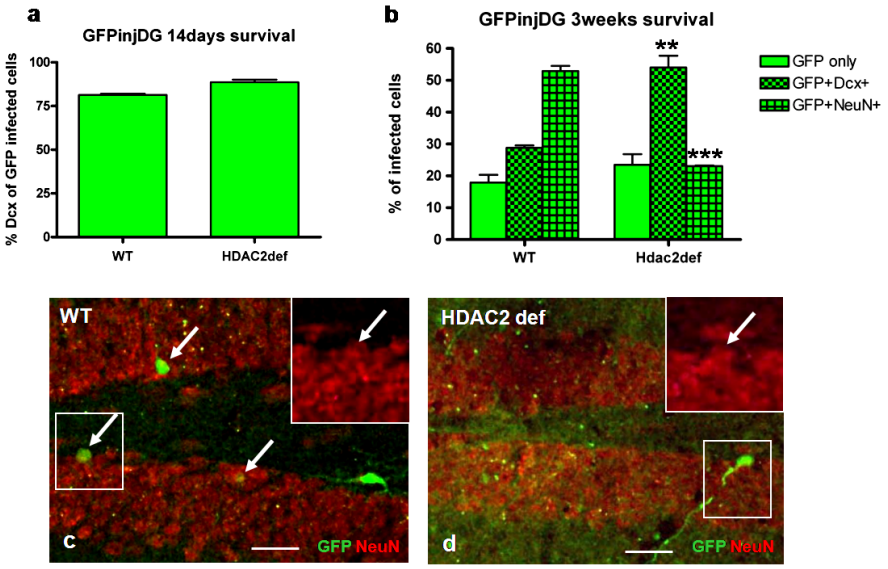

Figure 5.25: Retroviral injection of GFP in the DG of WT and HDAC2 def mice

a Histogram shows GFP+ cells 14 days after retroviral injection. In this experiment only one pair of WT and HDAC2 brains was analyzed, both hemispheres were pooled. **b** Histogram shows the identity of GFP+ cells 21 days after retroviral GFP injection into the DG of WT and HDAC2 def mice. Note the significant increase in Dcx+ cells and the significant decrease in NeuN+ cells amongst GFP+ cells after 21 days in the HDAC2 def mice. **c,d** Micrographs depict GFP+NeuN+ cells 21 days after GFP injection in the WT and HDAC2 def DG. Arrows depict double-positive cells. SEM=**;*** depict $p \leq 0{,}005 ; 0{,}0001$. Scale bars: c,d 20 μm.

5.2.7.6 Upregulation of Sox2 and Prox1 in the mutant DG

The increased proliferation of adult neurogenic precursors in HDAC2 def mice may be due to the down-regulation of genes expressed at more immature stages during neuronal maturation. As many progenitors in the SGZ express Sox2 [Gage, 1998], Sox2+ cells in the HDAC2 def and WT DG were examined. As expected, not only a slight increase in the number of Sox2+ cells was observed but also a persistence of Sox2 in some Dcx+ cells in the HDAC2 def DG, an observation that was rarely seen in the DG of WT littermates (**Figure 5.26 a,b**). Statistics underline the colocalization of Sox2 and Dcx in a significantly higher percentage (**Figure 5.26 e,f**). The transcription factor Prox1 is expressed in young neurons in the DG [Lavado and Oliver, 2007]. Prox1+ neurons appeared to be increased also in the mutant DG as depicted in **Figure 5.26 c,d** as a broader band overlapping with the mature NeuN+ neurons in the HDAC2 def DG compared to the WT DG. Thus, the delay in the downregulation of genes like Sox2 that are expressed in neuronal progenitors may cause conflicting signals during further maturation of newly born cells in HDAC2 def mice.

5.2.8 The adult neurogenic regions in HDAC2 def mice: SEZ

To understand whether the detected phenotype in the DG was also present in the second neurogenic region, the SEZ, adult neurogenesis in the SEZ and OB of HDAC2 def mice and their WT littermates was examined. Same as in the DG the number of Dcx+ cells was also reduced in the OB of HDAC2 def mice. Adult neural stem cells generate neuroblasts at the SEZ that then migrate toward the OB in the RMS. In the OB itself they reach their final destination by radial migration. This pattern was significantly altered in HDAC2 def mice (**Figure 5.27 a,b**), as Dcx+ neuroblasts seem to spread in an unorganized manner in the OB. Similar to the results obtained in the DG the number of BrdU-labeled cells in the SEZ was also increased after a short BrdU pulse (**Figure 5.27 c**). Furthermore, cells that were BrdU+ in the BrdU label retaining protocol were also reduced in number in the HDAC2 def SEZ, again comparable to the DG results (**Figure 5.27 d**). The analysis of BrdU+NeuN+ neurons in the OB also revealed a decrease in the number of mature neurons in the HDAC2 def OB (**Figure 5.27 e-g**). Taken together, the decrease in adult generated neurons was observed to a similar extent in the two regions of adult neurogenesis.

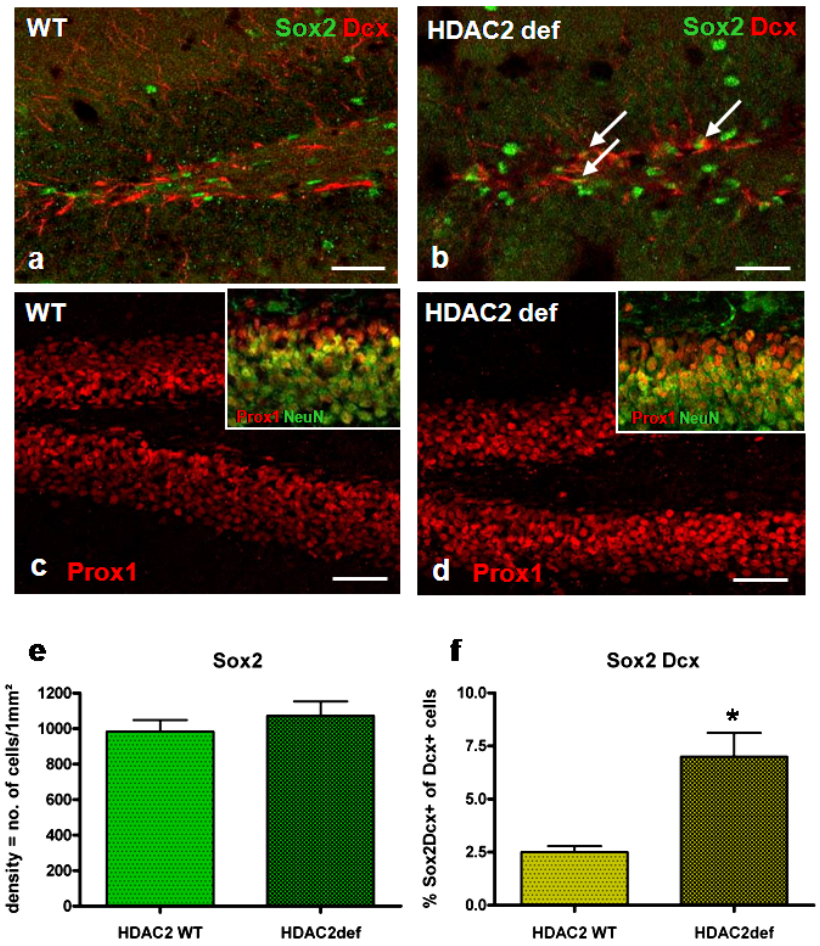

Figure 5.26: Upregulation of Sox2 and Prox1 in the HDAC2 def DG

a,b Double-staining with Sox2 and Dcx shows the increase of Sox2 expressing cells that are still Dcx+ in the HDAC2 def DG. **c,d** Prox1 seems to be upregulated and differently localized in the DG of mutant mice, shown in the inlay by a double-staining with NeuN. **e** Histogram shows the slighty increased number of Sox2+ cells in the HDAC2 def DG. **f** Histogram shows the significant increase in the percentage of Sox2+Dcx+ cells in HDAC2 def DG. Arrows depict double-positive cells. SEM=* depict $p \leq 0{,}02$. Scale bars: a-d 20 μm.

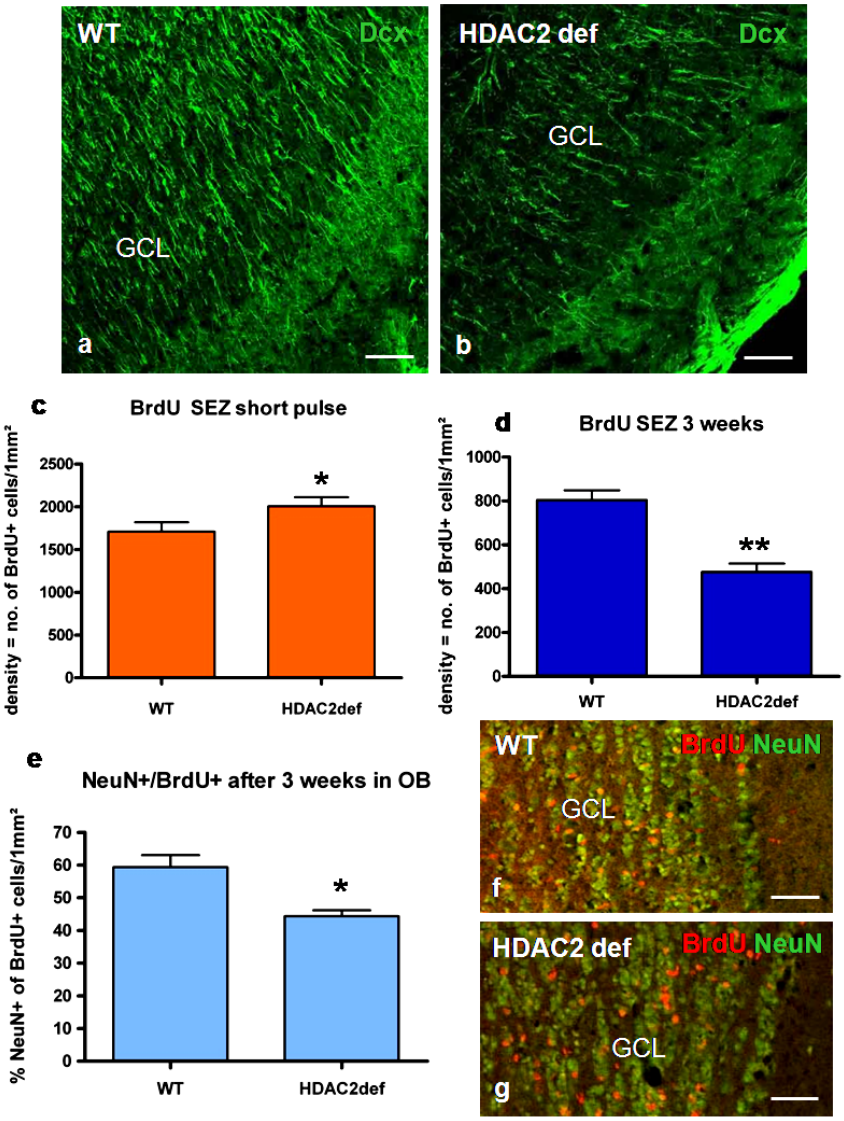

Figure 5.27: Adult neurogenesis in the SEZ/RMS/OB of WT and HDAC2 def mice

a,b Fluorescent micrographs depict Dcx+ neuroblasts in the OB. Note the significant reduction in the mutant mice. **c** BrdU short pulse experiment shows an increase in proliferating neural precursors in the SEZ. **d,e** The quantification of the BrdU label retaining experiment shows a significant reduction in BrdU+ cells in the SEZ (d) as well as BrdU+NeuN+ cells in the OB (e). **f,g** Antibody stainings against BrdU and NeuN depicting the reduced number of newly generated neurons within 3 weeks of BrdU label retaining experiment. GCL= granule cell layer. SEM=*;** depict p≤0,01 ;0,005 . Scale bar: 20 μm.

5.2.8.1 Fluorescence-activated cell sorting (FACS) analysis

To further quantify the proportion of neuroblasts in the SEZ and OB WT and mutant SEZ and OB of 5 mice, each was dissected and cells prepared as described in Materials and Methods. Cells were stained against PSANCAM, a surface protein expressed in neuroblasts. Fluorescent cells positive for PSANCAM were isolated using a FACSAria (BD). Notably, the number of PSANCAM+ cells was reduced in OB tissue of HDAC2 def mice, confirming the reduced number of differentiating neurons in the OB (**Figure 5.28**). By contrast, the number of neuroblasts positive for PSANCAM was increased after sorting cells from the SEZ of HDAC2 def mice (**Figure 5.29**). This finding was also consistent with the increase in proliferating cells at the SEZ in HDAC2 mutant mice after a short pulse of BrdU. Both FACS analysis experiments were performed twice with comparable results. Taken together, these results reflect the observed phenotype *in vivo*, namely that neuronal differentiation is impaired in adult neurogenic regions.

5.2.9 A gliogenic region in HDAC2 def mice: subcortical white matter (SCWM)

5.2.9.1 Proliferation analysis in the HDAC2 def SCWM

Besides the phenotypic changes in the adult neurogenic regions, a prominent increase in cells that have incorporated BrdU within 1 hour before analysis could be observed in the region of the subcortical white matter. This region is located between the Ctx and the HC extending from the caudal edge of the lateral ventricle and ending in the caudal part of the Ctx. It is described to contain gliogenic precursors but it was shown previously, that also some cells may carry neurogenic potential as they express Dcx [Nunes et al., 2003; Takemura, 2005]. In HDAC2 def mice a broad band of BrdU+ cells lining the HC in a sagittal view after a short pulse of BrdU could be detected (**Figure 5.30**). To examine the identity of these proliferating cells, sections were double-stained with Dcx and GFAP. 56 % of BrdU+ cells were Dcx+, and 10 % expressed GFAP (remaining 34 % was only BrdU+) compared to the WT SCWM where 10 % of BrdU+ cells were Dcx+, the remaining 90 % was only BrdU+, pointing to the fact that they were supposedly a mixed population of

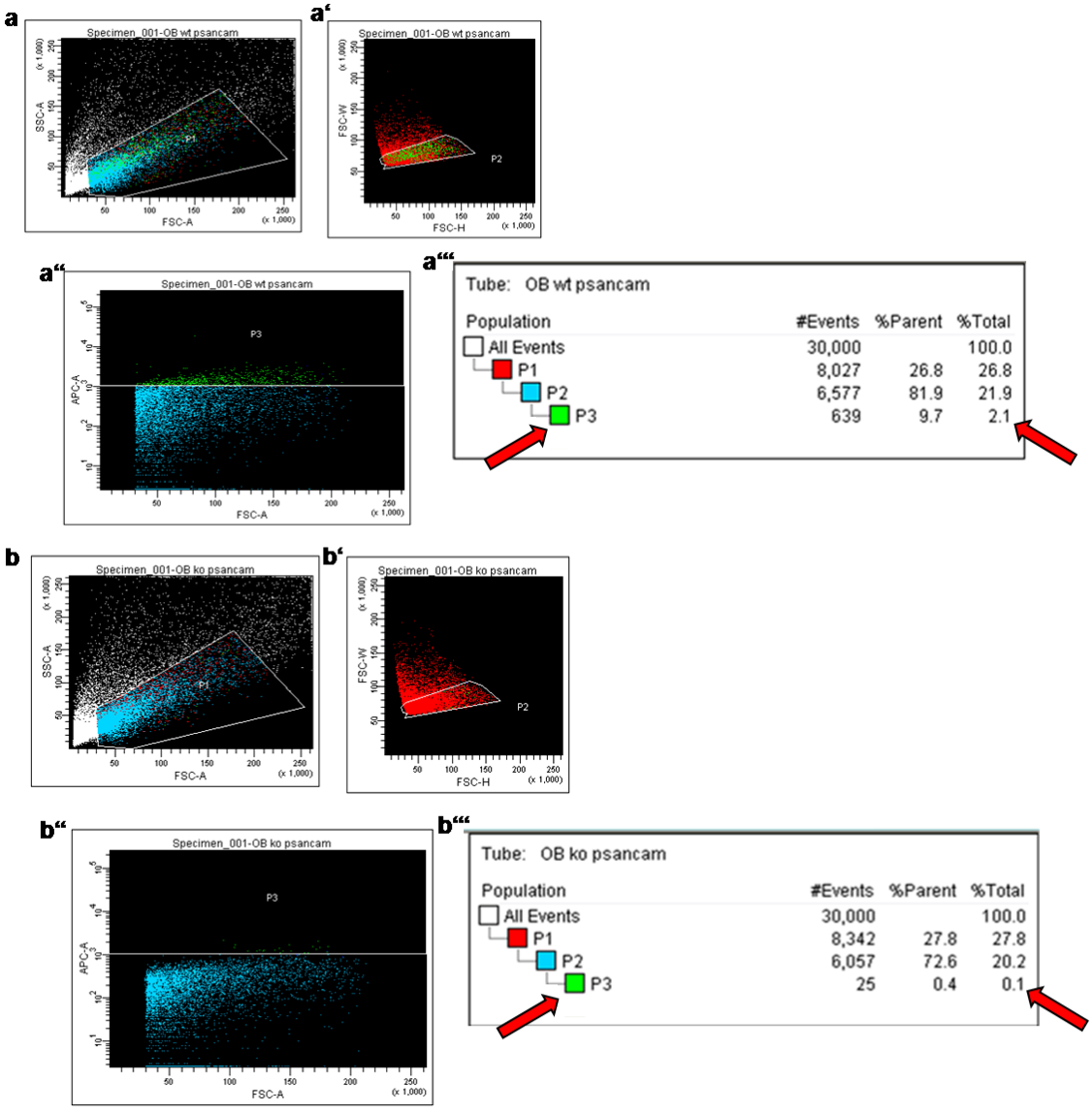

Figure 5.28: FAC sorting with PSANCAM from OB of WT and HDAC2 def mice

a,b FAC sorted cells of WT (a) and mutant OBs (b) were measured according to size (y-axis depicts FSC-A) and granularity (x-axis depicts SSC-A) of individual cells. **a',b'** The predefined cells in **a,b** were measured according to width (y-axis depicts FSC-W) and height (x-axis depicts FSC-H) of individual cells to exclude cell clumps. **a",b"** All chosen PSANCAM+ cells (APC-A on y-axis) were measured according to their size again (x-axis depicts FSC-A). **a"',b"'** Note the reduced percentage of P3 containing predefined PSANCAM+ cells in HDAC2 def OBs. FSC-A= forward scatter all, FSC-H= forward scatter height, FSC-W= forward scatter width, SSC-A= side scatter.

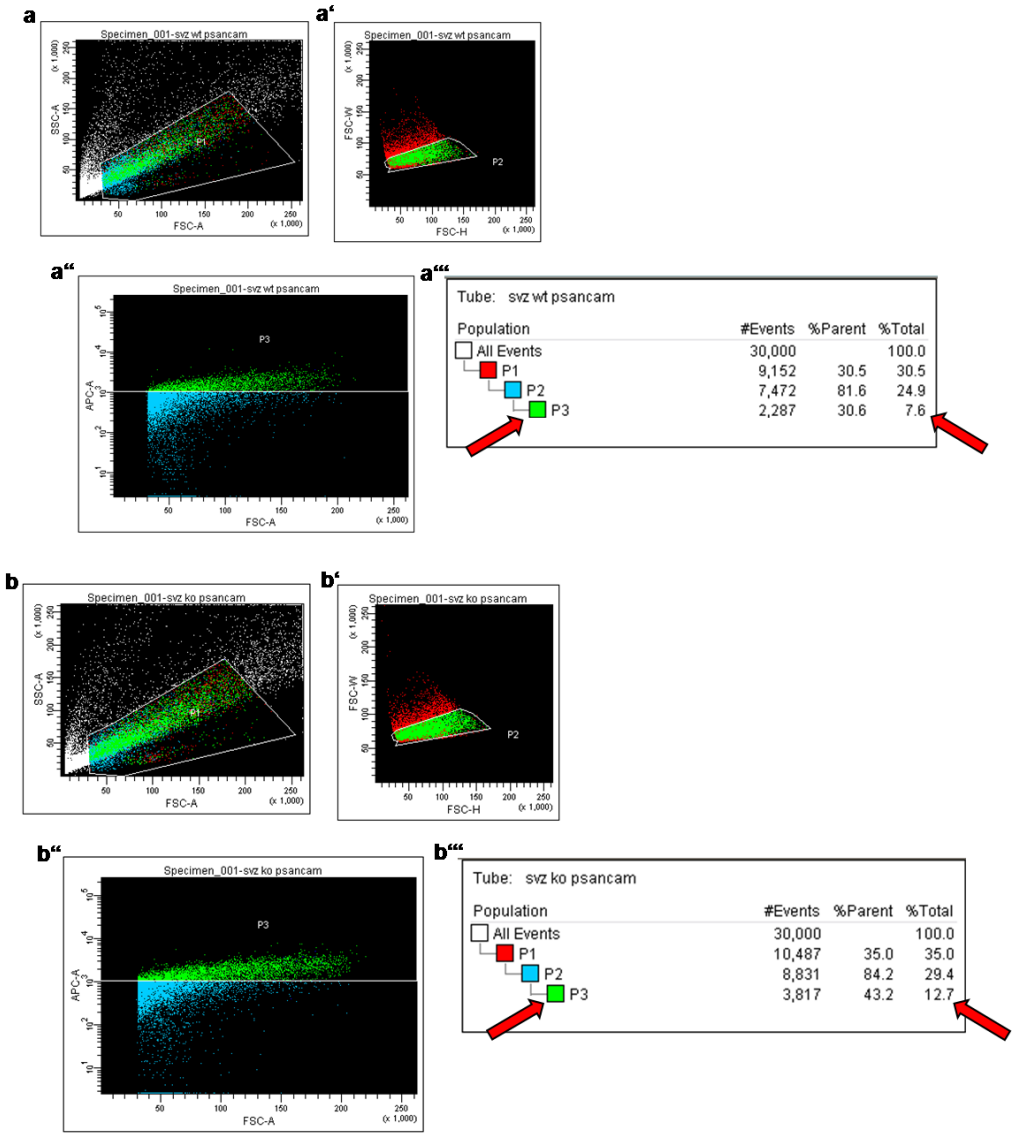

Figure 5.29: FAC sorting with PSANCAM from SEZ of WT and HDAC2 def mice

a,b All FAC sorted cells of WT (a) and mutant SEZs (b) were measured according to size (y-axis depicts FSC-A) and granularity (x-axis depicts SSC-A) of individual cells. **a',b'** The predefined cells in **a,b** were measured according to width (y-axis depicts FSC-W) and height (x-axis depicts FSC-H) of individual cells to exclude cell clumps. **a",b"** All chosen PSANCAM+ cells (APC-A on y-axis) were measured according to their size again (x-axis depicts FSC-A). **a"',b"'** Note the increased percentage of P3 containing predefined PSANCAM+ cells in HDAC2 def SEZs. FSC-A= forward scatter all, FSC-H= forward scatter height, FSC-W= forward scatter width, SSC-A= side scatter.

precursor cells that have either neurogenic or gliogenic potential. This suggests that a loss of the HDAC2 function caused a widespread increase in fast proliferating cells in both neurogenic and non-neurogenic regions of the forebrain.

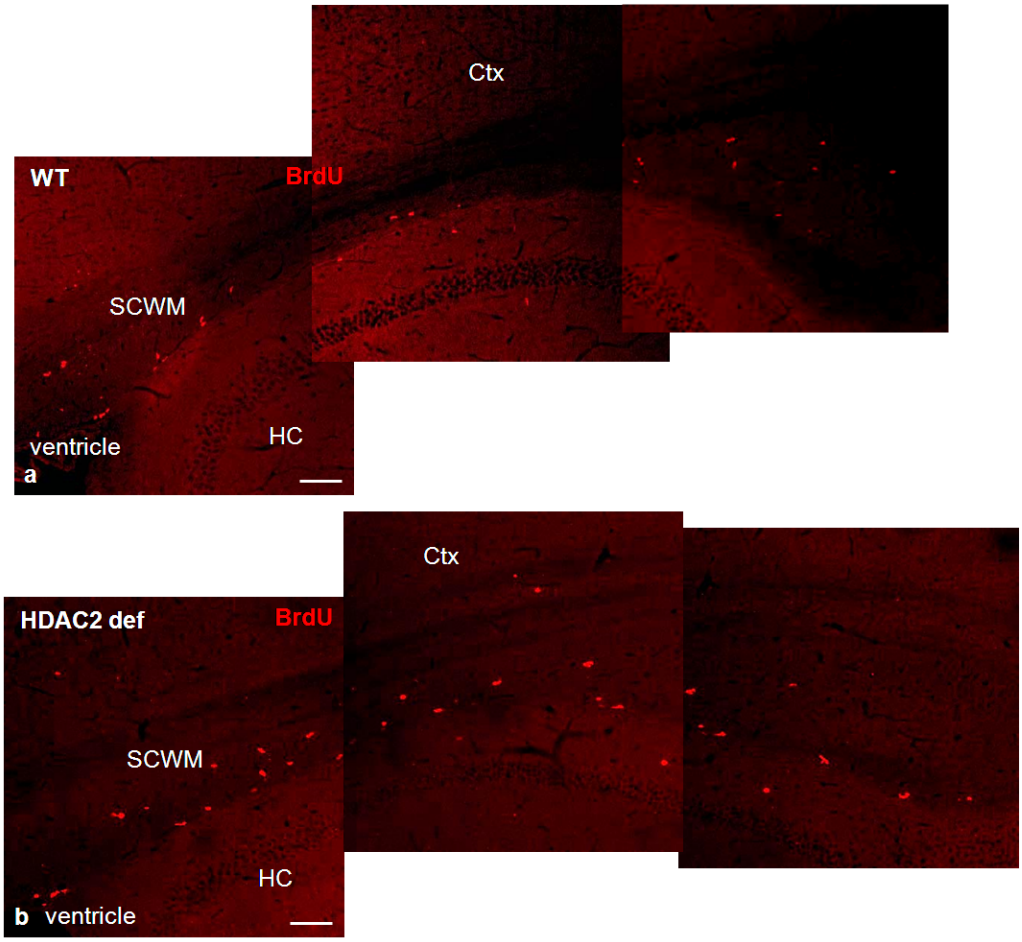

Figure 5.30: BrdU short pulse analysis in the SCWM

a,b Proliferating cells labeled with a short BrdU pulse in the WT (a) and HDAC2 def SCWM (b) shown in a sagittal view. Ctx= cortex, HC= hippocampus, SCWM= subcortical white matter. Anterior is to the left, posterior is to the right side of the panel. Scale bars: a,b 50 μm.

5.2.9.2 Retroviral injection of GFP in the SCWM

To examine the progeny of the cycling cells in the mutant SCWM more directly, we injected the GFP-containing retrovirus in the SCWM of HDAC2 def mice and analyzed the GFP+ cells 14 days after injection. GFP labeled cells could be detected some distance away from the injection site that is located in the center of the panel in

Figure 5.31. GFP+ cells had spread either to the lateral ventricle or to the caudal end of the Ctx. GFP+ cells express to some extent GFAP as shown by costaining. In order to further examine whether GFP+ cells may enter the grey matter (GM) at later stages, mice were analyzed 21 days after GFP injection. However, no GFP+ cells were observed in the GM of the Ctx after 21 days, while GFP+ cells remained restricted to the WM.

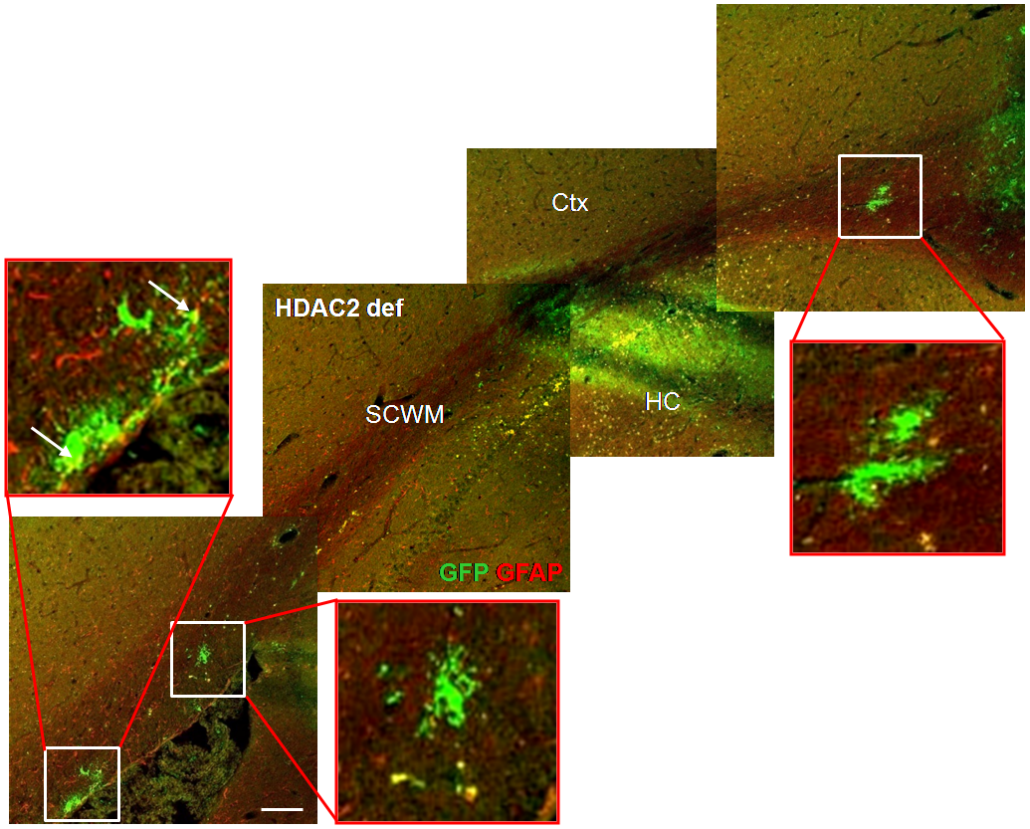

Figure 5.31: GFP injection in the SCWM of HDAC2 def mice

Lineage tracing of proliferating cells in the SCWM. GFP labeled cells can be detected either in the caudal Ctx (right) or at the dorsal wall of the lateral ventricle (left) and partially express GFAP. Ctx= cortex, HC= hippocampus, SCWM= subcortical white matter. Arrows depict double-positive cells. White rectangles show GFP+ cells in higher magnification. Scale bar: 50 μm.

5.2.10 Analysis of the HDAC2 function *in vitro*

5.2.10.1 Expression of HDAC2 in neurosphere cultures

Since the HDAC2 function lacks in all tissues of this HDAC2 gene trap mouse line and hence may exert indirect effects on adult neurogenesis, the neurosphere assay was used to examine the propagation and differentiation of neural stem and progenitor cells and their differentiation properties were isolated under *in vitro* conditions. Embryonic neurosphere cultures were prepared by isolating E14 Ctx and adult neurosphere cultures were done by dissecting the SEZ. The expression of HDAC2 in embryonic neurospheres is mainly present in postmitotic neurons that are β-IIItubulin+ and weakly detectable in GFAP+ astrocytes (**Figure 5.2 b**). In adult neurosphere cultures HDAC2 immunoreactivity was observed more ubiquitously including strongly expressing GFAP+ cells that after 2 hours are probably still proliferating. As it is believed that the neural precursors in neurosphere cultures are not multipotent, slow-dividing stem cells but even more likely fast-dividing, transit-amplifying progenitor cells that also express GFAP [Capela and Temple, 2002; Imura et al., 2003]. This suggests that HDAC2 immunoreactivity is weakly detectable in those cells *in vitro* (**Figure 5.32 a**). After 2 days of differentiation HDAC2 is strongly expressed in young neurons that are β-IIItubulin+ (**Figure 5.32 b**).

5.2.10.2 HDAC2 function in embryonic neurosphere cultures

As our *in vivo* analysis had demonstrated a specific effect of HDAC2 on adult, but not embryonic neurogenesis, we tested whether this difference could be verified in the neurosphere *in vitro* system. Furthermore, the striking difference in HDAC2 expression in embryonic versus adult neurosphere cultures prompted us to examine the neuronal differentiation of HDAC2 def neurosphere cells derived from the embryonic Ctx. Consistent with the *in vivo* results, these cells could differentiate well into mature neurons and no defects were observed in the process formation or neuronal survival after 7 days *in vitro* (DIV) (**Figure 5.33**).

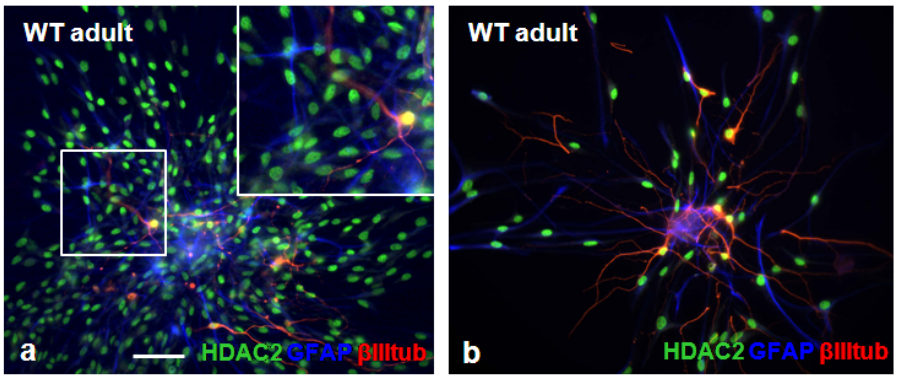

Figure 5.32: HDAC2 expression in neurosphere cultures

a In adult neurospheres already 2 hours after plating HDAC2 immunoreactivity is detectable in almost all cells with the highest immunoreactivity in differentiating neurons that are β-IIItubulin+ and weaker in GFAP+ astrocytes. **b** HDAC2 immunoreactivity in adult neurospheres from the SEZ 2 days after plating. Note that HDAC2 immunoreactivity increases in GFAP+ astrocytes and strong HDAC2 immunoreactivity persists in β-IIItubulin+ neurons. Scale bar: 20 μm.

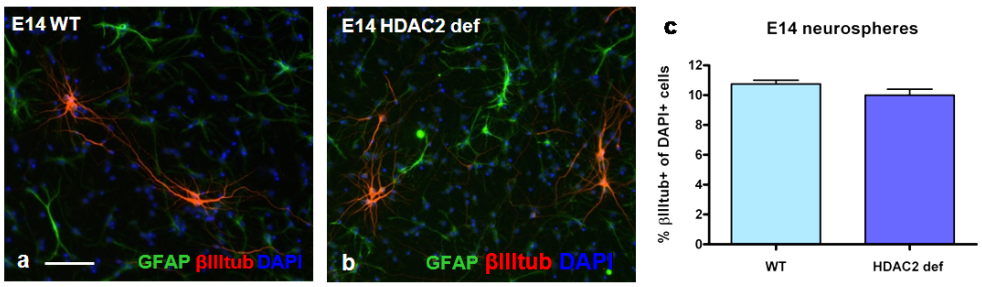

Figure 5.33: WT and HDAC2 def embryonic neurospheres

a,b WT and HDAC2 def cortical embryonic neurosphere cultures. Note the normal differentiation of β-IIItubulin+ neurons in HDAC2 def cultures after 7 days *in vitro*. **c** Histogram depicts the comparable number of β-IIItubulin+ neurons generated after 7 days of differentiation in WT and HDAC2 def neurosphere cultures of the E14 Ctx. Scale bar: 20 μm.

5.2.10.3 HDAC2 function in adult SEZ neurosphere cultures

Consistent with the higher number of progenitors observed in the HDAC2 def SEZ *in vivo*, a significantly increased number of primary neurospheres formed by the HDAC2 def adult SEZ (aSEZ) cells was also observed compared to those derived from the WT SEZ (**Figure 5.34 a**). Further consistent with the *in vivo* results, the number of self-renewing stem cells appeared no different in this assay as the number of secondary neurospheres formed by HDAC2 def or WT neurosphere cells was identical (**Figure 5.34 b**) although these cells showed weak HDAC2 immunoreactivity. In the next step we exposed neurosphere cells to differentiating conditions by plating them onto adhesive substrates and omitting the growth factors EGF and FGF2. At this stage cells were infected with a GFP-containing retroviral vector to identify the cells that were still proliferating at the time of plating and follow their lineage [Hack et al., 2004]. Already after 8 days, neuronal differentiation of HDAC2 def cells was impaired as neurons exhibited fewer and shorter neurites than those derived from WT littermates (**Figure 5.34 c,d**). While the proportion of differentiating neurons amongst the GFP labeled cells was only weakly reduced in the HDAC2 def cultures by 8 DIV with differentiating conditions (**Figure 5.34 e**), it became severely reduced to less than half after 14 days (**Figure 5.34 f**). Thus, neuronal differentiation defects of HDAC2 def cells appear de novo in isolated cells *in vitro*, suggesting that this phenotype is not due to general alterations in the HDAC2 def mice.

5.2.11 Transplantation of WT cells into the HDAC2 def SEZ

While the above results imply a cell-autonomous role of HDAC2 in the adult neurogenic lineage, additional defects in the adult neurogenic niche that might add to the cell-autonomous effects *in vivo* cannot be excluded. We therefore tested whether WT cells could differentiate normally in an HDAC2 def environment by transplanting them into the adult SEZ of HDAC2 def mice (**Figure 5.35 a**). As described previously [Colak et al., 2008], cells were isolated from the SEZ of 6 week old mice that ubiquitously express the fluorescent protein Venus targeted to the plasma membrane [Rhee et al., 2006] and transplanted into the SEZ of 8 week old WT and HDAC2 def littermates. Transplanted cells were detected 7 or 21 days after transplantation and double-stained for neuron-specific antigens, e.g. Dcx or NeuN. For each time point

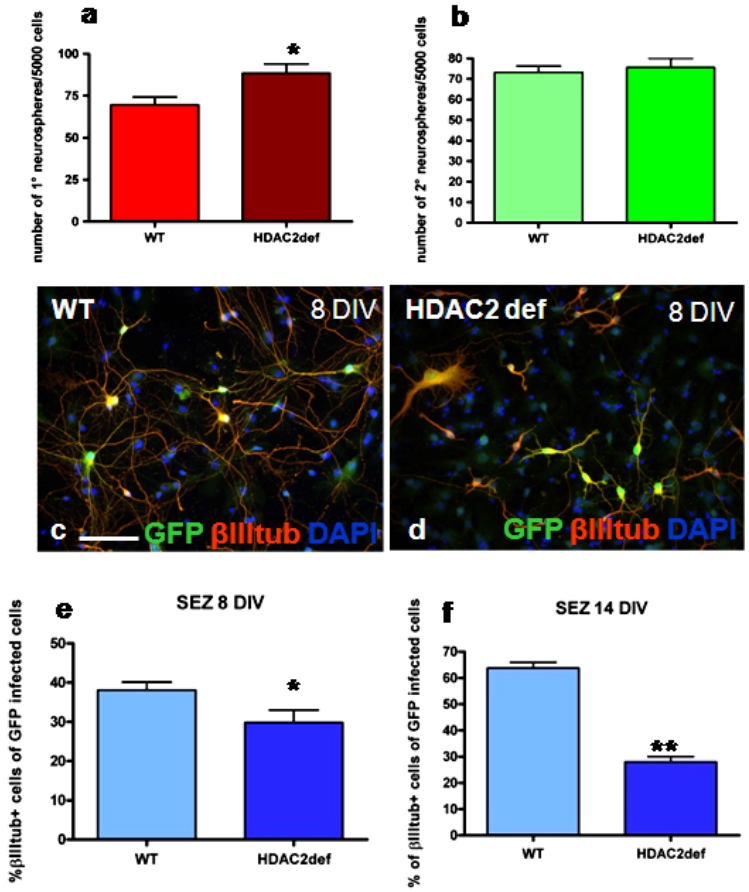

Figure 5.34: WT and HDAC2 def adult SEZ neurospheres

a,b Histograms depict the increase in the number of primary neurosphere forming cells (= proliferating cells) (a), but not self-renewing neurospheres (=stem cells) (b) isolated from HDAC2 def SEZ. **c,d** Fluorescent micrographs show that HDAC2 def cells exhibit shorter processes already after 8 days in differentiationg conditions. **e,f** Histograms depict the slight decrease of neurons generated in HDAC2 def cultures after 8 DIV (e). After 14 DIV upon loss of HDAC2 neurons are reduced to half compared to WT neurons, presumably through cell death. SEM=*;** depict $p \leq 0{,}03$;0,006 . Scale bar: 20 μm.

2 WT and 2 HDAC2 def mice were used for transplantation. Already after 7 days GFP+ cells that are Dcx+ and show a neuroblast morphology (**Figure 5.35 b**) could be observed in the RMS migrating towards the OB. After 21 days a similar proportion of transplanted WT cells had differentiated into mature NeuN-positive neurons in the HDAC2 def environment (**Figure 5.35 c**). Taken together, these experiments imply no major changes in the adult neurogenic niche in the HDAC2 def mice but rather demonstrate a cell-autonomous role for the catalytically active form of HDAC2 in proliferation and neuronal differentiation of adult progenitors.

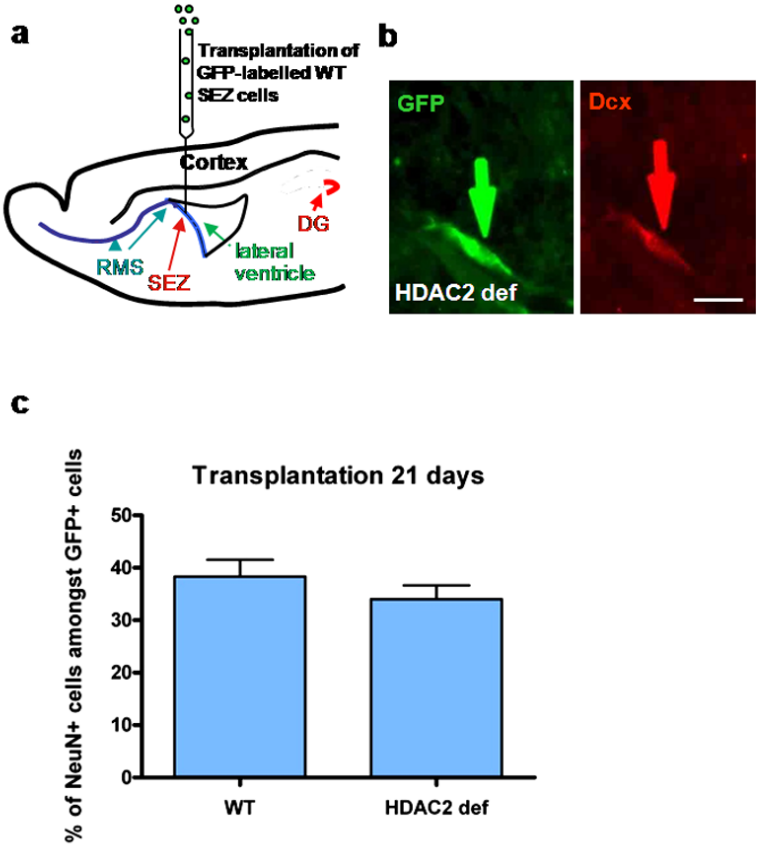

Figure 5.35: Transplantation of WT cells into the HDAC2 def SEZ

a Technique of the transplantation of GFP-labeled WT SEZ cells into the HDAC2 def SEZ. **b** Fluorescent micrographs depict a transplanted cell (GFP+) that expresses Dcx in the RMS and shows normal morphology typical for neuroblasts. **c** Histogram shows the quantification of GFP+ cells after 21 days that were found to be NeuN+ in the HDAC2 def OB. Note the comparable numbers in WT controls and HDAC2 def mice. Arrows depict double-positive cells. Scale bar: 10 μm.

5.2.12 The role of HDAC1 during brain development of HDAC2 def mice

As HDAC1 and HDAC2 are often found in the same repressor complexes but show a complementary protein expression pattern, one possibility could be that HDAC1 compensates for the loss of the HDAC2 function. HDAC1 is expressed at the ventricular zone in neural precursor cells at embryonic stages and starts to be expressed in postmitotic neurons in the CP on mutant sections. However, during postnatal brain development HDAC1 was exclusively expressed in non-neuronal cells given that no protein could be detected in postmitotic NeuN+ neurons (**Figure 5.36 a,b**). This holds true until postnatal development ends at around P21 (**Figure 5.36 c**). Furthermore, no HDAC1 protein could be found in neurogenic regions at postnatal stages, e.g. in the developing HC (**Figure 5.3 b**). At late postnatal stages HDAC1 is expressed in the HC but does not seem to be upregulated in the HDAC2 def DG to compensate for the loss of HDAC2 in adult neurogenic regions (**Figure 5.36 d,h**). By contrast, in HDAC2 def brains HDAC1 was present in NeuN+ neurons from neonatal stages on, here shown at P5 (**Figure 5.36 e,f**). Later on, at the end of postnatal development HDAC1 expression began to decline to normal levels and from there on was observed only in non-neuronal (NeuN-) cells (**Figure 5.36 g**). These findings show that HDAC1 might compensate for the loss of functional HDAC2 protein during brain development as it was upregulated in neurons in HDAC2 def mice, but not in adult neurogenic regions.

5.2.13 Western Blots of HDAC1 and HDAC2 of WT and HDAC2 def brain tissue

To further examine the protein levels of HDAC1 in the WT and the HDAC2 def background, Western Blots were performed to show the protein levels of HDAC1 and HDAC2 in different brain regions. The HDAC2 protein could be detected in tissue lysates from all tested WT brain regions, whereas HDAC2 was not detectable in HDAC2 def brain regions (**Figure 5.37**). HDAC1 as a potent candidate to compensate for the loss of functional HDAC2 protein was found to be reduced also in HDAC2 def tissue lysates compared to WT and normalized to β-actin control (**Figure 5.37**). Thus, in the adult brain there is no upregulation of a closely related

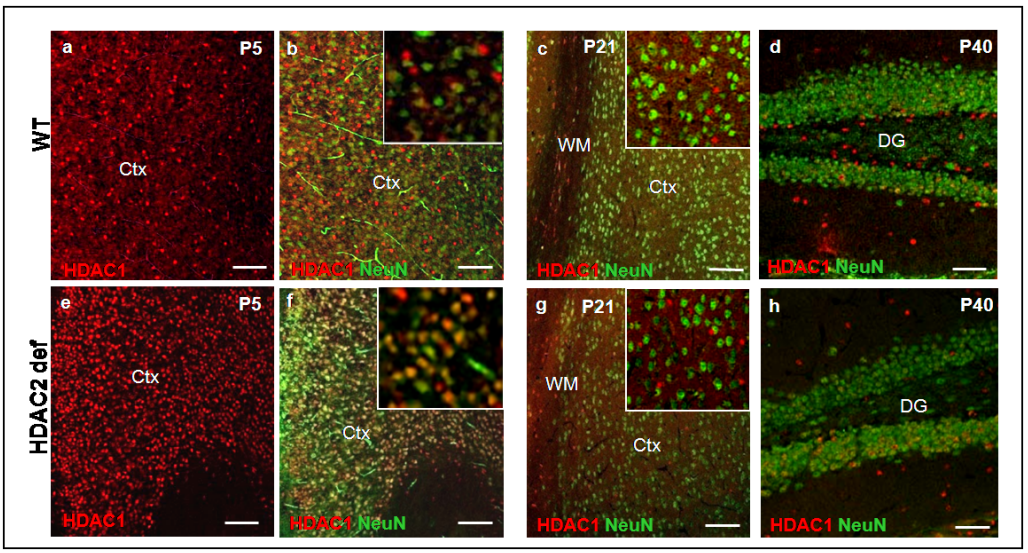

Figure 5.36: HDAC1 immunoreactivity during development in WT and HDAC2 def mice

a,b In WT sections at P5 HDAC1 expression is restricted to non-neuronal cells and shows no overlap with NeuN expression. **c** At P21 it is not detectable in NeuN+ cells. **d** Expression of HDAC1 in zones of neurogenesis at P40 is restricted to non-neuronal cells. **e,f** HDAC1 comes up in NeuN+ neurons in HDAC2 def brains at P5. **g** At the end of postnatal development upregulation of HDAC1 in neurons declines to normal levels again. **h** No upregulation of HDAC1 in neurogenic zones, e.g. the DG at P40. Ctx= cortex, DG= dentate gyrus, WM= white matter. White rectangles show higher magnification. Scale bars: a-g 50 μm.

HDAC family member, HDAC1, in HDAC2 def brain regions.

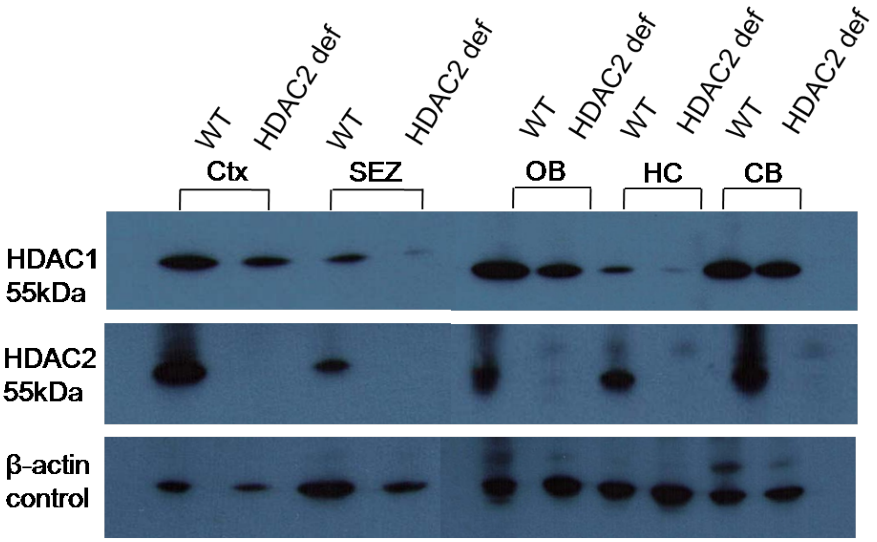

Figure 5.37: HDAC Western Blots

The Western Blots show the HDAC1 protein (upper panel) in all WT brain regions that becomes reduced in HDAC2 def brain regions, e.g. the SEZ, HC as the zones of adult neurogenesis. The HDAC2 protein was completely undetectable in HDAC2 def brain tissue (middle panel). The lower panel shows β-actin control. CB= cerebellum, Ctx= cortex, HC= hippocampus, OB= olfactory bulb, SEZ= subependymal zone.

5.2.14 Microarray analysis of WT and HDAC2 def brain regions

The results of the functional analysis of HDAC2 prompted us to perform a gene expression analysis of WT and HDAC2 def brain tissue from the HC, OB and SEZ by oligonucleotide microarrays. The aim of this detailed examination was to identify candidate genes that are differentially regulated between the two genotypes providing hints which mechanisms might be involved in the above described phenotype of HDAC2 def mice in adult neurogenesis. **Figure 5.38** shows the clustering of the tissue derived from WT and HDAC2 def animals (here labeled with KO). The OB analysis was performed by using tissue from three different WT and HDAC2 def animals. For the HC analysis tissue from 3 WT but only 2 HDAC2 def animals were used excluding one HDAC2 def mouse, given its RNA expression was only half reduced compared to WT, suggesting that this animal was a heterozygous mouse.

For the SEZ only one pair was studied, because all other RNA preparations showed a high variance in regard to quality and thus could not be compared. This had to be taken into account when analyzing and interpreting the data. The clustering was performed on normalized RMA data (see Materials and Methods 4.13.2) and showed a separation of different tissues although not a complete separation of genotypes, which is relevant for the reproducibility and significance of these data (**Figure 5.38**).

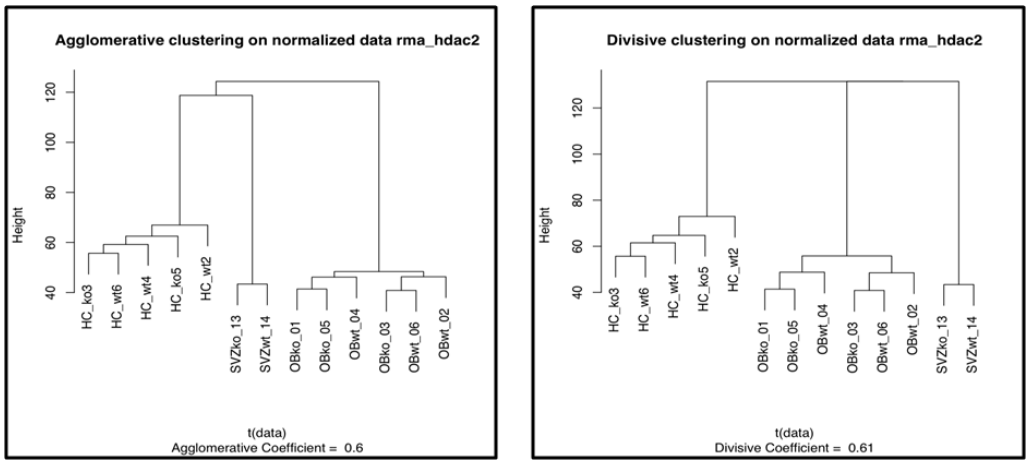

Figure 5.38: Clustering of RMA microarray data

Hierarchical clustering of HDAC2 microarray data. In both types of clustering, agglomerative or divisive, there is a separation of tissue but not genotypes.

However, despite the redundant difference between brain regions, the highest expression differences between genotypes should give some insights into key genes that are differentially expressed in the HDAC2 def neurogenic regions. In order to have an impression of possible genes that are differentially regulated the list of the 55 Best-of-results that were significantly different regulated in WT and HDAC2 def brain regions, either the OB or HC, was analyzed. More genes were found to be upregulated than one would assume from the repressor function of HDAC2 (**Figure 5.39**). One of the most highly regulated gene found amongst them was Protocadherine β 9 (Pcdhb9). Protocadherines are expressed in the central nervous system, where they play a role in synapse formation [Junghans et al., 2008]. Therefore, it might be interesting to study Pcdh9 in more detail in HDAC2 def mice. Moreover, 22 genes were also found to be downregulated in HDAC2 def brain regions (**Figure 5.40**), of which the calcium/-calmodulin-dependent protein kinase IIa (CamKIIa) is the most interesting. It was reported for CamKII that it interacts with Nr2b, a sub-

GeneSymbol	Ratio BO RMA	Ratio HC RMA	Ratio SVZ	Gene Title	Entrez Gene	unclear annotation	Probe Set ID
Fbxo39	1.0	4.5	3.7	F-box protein 39	327959		1443621_at
Pcdhb9	3.0	3.2	1.4	protocadherin beta 9	93880		1422640_at
AK085625	1.4	2.7	1.5	D630048D13 product			1442708_at
Scn2b	1.4	2.4	4.6	sodium channel, voltage-gated, type II, beta	72821		1430648_at
Ddr2	1.8	2.3	1.6	discoidin domain receptor family, member 2	18214		1455688_at
Serpina3g	1.0	2.1	0.9	serine (or cysteine) peptidase inhibitor, clade A, member 3G	20715		1424923_at
Ptgs2	1.1	2.1	1.0	prostaglandin-endoperoxide synthase 2	19225		1417263_at
Six6os1	1.1	1.9	1.8	Six6 opposite strand transcript 1	75801		1431393_at
Tcfl5	1.3	1.8	2.6	transcription factor-like 5 (basic helix-loop-helix)	277353		1456515_s_at
Prokr2	1.2	1.8	1.0	prokineticin receptor 2	246313		1437695_at
Ddo	1.1	1.8	1.0	D-aspartate oxidase	70503		1439096_at
Nts	1.6	1.7	1.2	neurotensin	67405		1422860_at
Pgam2	1.3	1.6	2.5	phosphoglycerate mutase 2	56012		1418373_at
Prss23	1.1	1.6	1.1	protease, serine, 23	76453		1437671_x_at
Ccbe1	1.1	1.6	0.7	collagen and calcium binding EGF domains 1	320924		1437385_at
Pvrl2	1.5	1.5	1.3	poliovirus receptor-related 2	19294		1424456_at
Dynll1	1.6	1.5	2.2	dynein light chain LC8-type 1	56455		1440278_at
Gnb4	1.4	1.5	1.1	guanine nucleotide binding protein (G protein), beta 4	14696		1419470_at
Htr3a	1.6	1.5	1.6	5-hydroxytryptamine (serotonin) receptor 3A	15561		1418268_at
Nov	1.7	1.4	2.5	nephroblastoma overexpressed gene	18133		1426851_a_at
Rbp4	1.6	1.4	0.8	similar to retinol binding protein	100047573	*	1426225_at
A730017C20Rik	1.4	1.4	0.8	RIKEN cDNA A730017C20 gene	225583		1437528_x_at
Ifi27	1.7	1.4	2.1	interferon, alpha-inducible protein 27	76933		1426278_at
Nov	2.0	1.4	3.1	nephroblastoma overexpressed gene	18133		1426852_x_at
Ccny	0.3	1.4	0.6	cyclin Y /// similar to cyclin fold protein 1	100044842	*	1428414_at
Htr2c	1.6	1.3	1.1	5-hydroxytryptamine (serotonin) receptor 2C	15560		1435513_at
Lancl2	1.0	1.3	1.0	similar to testis-specific adriamycin sensitivity protein	100045439	*	1450028_a_at
Ipw	1.6	1.2	1.5	imprinted gene in the Prader-Willi syndrome region	16353		1440557_at
Efcab1	1.8	1.1	1.2	EF hand calcium binding domain 1	66793		1454198_a_at
Tnni3	1.6	1.1	2.8	troponin I, cardiac	21954		1422536_at
3110032G18Rik	2.3	1.0	1.2	RIKEN cDNA 3110032G18 gene	73121		1453192_at

Figure 5.39: Best-of list of all upregulated genes

GeneSymbol	Ratio BO RMA	Ratio HC RMA	Ratio SVZ	Gene Title	Entrez Gene	unclear annotation	Probe Set ID
Scd2	0.7	0.8	1.0	stearoyl-Coenzyme A desaturase 2	20250		1415824_at
Camk2a	0.7	0.8	0.7	calcium/calmodulin-dependent protein kinase II alpha	12322		1452453_a_at
Atg5	0.8	0.8	0.8	autophagy-related 5 (yeast)	11793		1418235_at
Adat2	0.6	0.7	0.9	adenosine deaminase, tRNA-specific 2, TAD2 homolog	66757		1419130_at
Prdx2	0.8	0.7	0.9	peroxiredoxin 2	21672		1430979_a_at
Clta	1.1	0.7	1.3	clathrin, light polypeptide (Lca)	12757		1434540_a_at
Anp32a	2.0	0.7	1.1	acidic nuclear phosphoprotein 32 family, member A	11737		1450407_a_at
Aqp4	0.9	0.7	0.8	aquaporin 4	11829		1425382_a_at
Adi1	0.7	0.6	0.4	acireductone dioxygenase 1	104923		1438758_at
6330527O06Rik	0.7	0.6	0.6	RIKEN cDNA 6330527O06 gene	76161		1423853_at
AI314180	2.0	0.6	1.6	expressed sequence AI314180	230249		1439127_at
A330104H05Rik	1.0	0.6	1.1	RIKEN cDNA A330104H05 gene	77767		1436578_at
Wfs1	1.1	0.6	0.9	Wolfram syndrome 1 homolog (human)	22393		1448411_at
Plp1	0.9	0.5	1.1	proteolipid protein (myelin) 1	18823		1425467_a_at
Apod	1.0	0.5	1.1	apolipoprotein D	11815		1416371_at
Trf	1.0	0.5	1.1	transferrin	22041		1425546_a_at
Mobp	1.0	0.5	1.1	myelin-associated oligodendrocytic basic protein	17433		1450088_a_at
Mbp	0.9	0.5	1.2	myelin basic protein	17196		1451961_a_at
Clic6	1.6	0.4	1.3	chloride intracellular channel 6	209195		1454866_s_at
Ptgds	1.1	0.4	0.9	prostaglandin D2 synthase (brain)	19215		1423860_at
Scn4b	1.1	0.4	1.0	sodium channel, type IV, beta	399548		1434008_at
LOC100044048	2.1	0.3	2.1	X-linked lymphocyte-regulated 4B	100044048	*	1449347_a_at
Hdac2	0.0	0.0	0.0	histone deacetylase 2	15182		1445684_s_at
Hdac2	0.0	0.0	0.0	histone deacetylase 2	15182		1449080_at

Figure 5.40: Best-of list of all downregulated genes

unit of the NMDA receptor expressed in neurons and involved in synaptic plasticity and learning [Zhou et al., 2007]. NMDA receptors are important for the survival of newly generated neurons in the adult brain [Tashiro et al., 2006]. As proof of principle, the two different probe sets of HDAC2 were also found to be downregulated to undetectable levels (Probe set IDs 1445684 and 1449080). Both probe sets bind to the C-terminal end of HDAC2, which is altered in the mutant mice. Moreover, the observed defects in HDAC2 def mice occurred only in a small amount of cells, namely the neuronal progenitors and the newly generated neurons in the tissue examined. Therefore, this microarray analysis was decided not to follow in more detail, but rather to perform a more clear microarray analysis with FAC sorted cells from HDAC2 floxed/floxed mice. This mouse line crossed with an inducible GLASTCreER^{T2}line [Mori et al., 2006] and in addition with a reporter line (ZEG) can be used to specifically delete HDAC2 in adult neural stem cells and their progeny which will be GFP+. Only then can these GFP+ cells that lack HDAC2 in adult neurogenic regions be used for a microarray analysis.

5.3 Functional analysis of Brg1

5.3.1 Brg1 floxed mice - construct

Former studies have suggested that HDAC2-containing complexes and chromatin remodeling complexes recruit each other and act in an orchestratic manner [Narlikar et al., 2002]. After examining the extent of the overlay of Brg1 and HDAC2 expression in the adult brain we wanted to check whether deletion of Brg1 would cause the same phenotype as observed in the HDAC2 def mice. Brg1 floxed/floxed mice were received from Pierre Chambon, Institut de Genetique et de Biologie Moleculaire et Cellulaire, CNRS/INSERM/ULP, College de France, 67404 Illkirch Cedex, CU de Strasbourg [Sumi-Ichinose et al., 1997] generated through the homologous recombination in ES cells using the pSNF2$\beta^{L:LHLa}$ targeting vector. The Brg1 floxed locus and the targeting strategy are shown in **Figure 5.41**. The insertion of the vector leads to the deletion of exons 2 and 3 of the genomic coding sequence. The Brg1 L2 allele can be detected by PCR with the primers TG57 (indicated as P1) and TH185 (indicated as P2) (**Table 4.1**), as described above to identify animals homozygous for the floxed Brg1 allele.

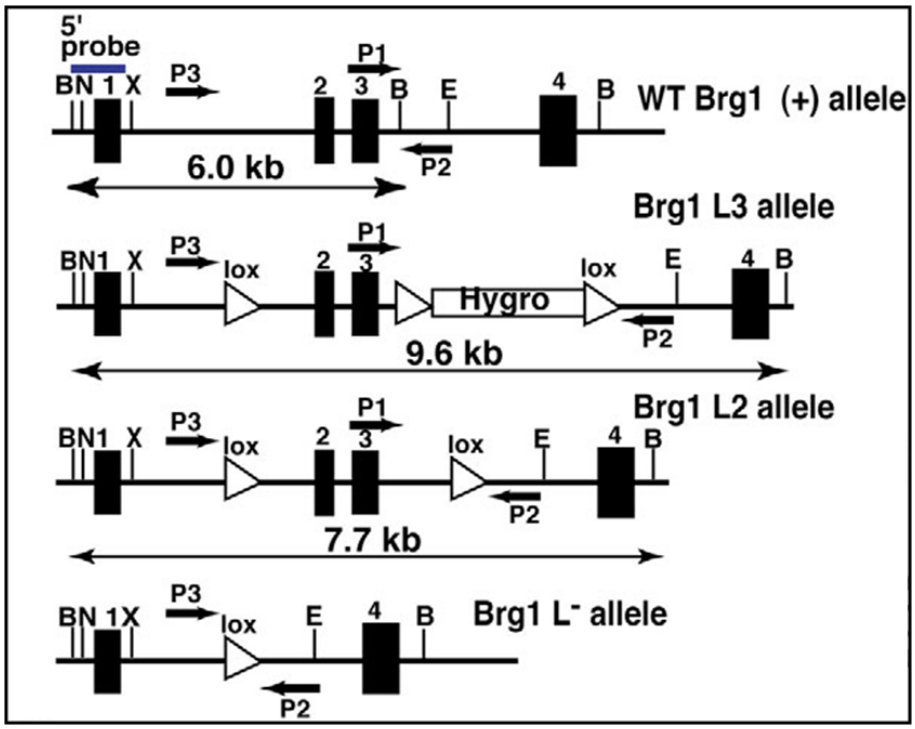

Figure 5.41: Brg1 floxed locus

Targeting strategy of the mouse Brg1 locus to generate mice harboring Brg1 floxed alleles. Partial structure of the Brg1 locus [Brg1 (+) allele]. Exons are indicated by black boxes. The Brg1 L3 allele containing the three loxP sites (lox) and the hygromycin resistance marker (Hygro) is presented. The expected genomic maps after excision of the floxed marker Hygromycin (Brg1 L2 allele) and excision of both the marker and exons 2 and 3 (Brg1 LŰ allele) are shown. The arrows indicate the PCR primer location (P1-P3). The location of the Southern Blot 5'-probe [Sumi-Ichinose et al., 1997] is shown. The size of DNA segments obtained after BamHI restriction digest and detection with the 5'-probe are indicated. B, BamHI; E, EcoRV; N, NheI; X, XbaI. Graph taken from Kumar Indra, A et al. 2005.

5.3.2 Brg1 deletion during embryonic neurogenesis

The floxed Brg1 mouse line was crossed with the Emx1Cre mouse line [Guo et al., 2000] to delete Brg1 specifically in the developing Ctx. In this Emx1Cre transgenic line Cre is driven by the Emx1 promoter which is only active after E 9.5 [Guo et al., 2000] exclusively in the developing Ctx. Brg1 loxP sites will be detected by Cre and the flanked region will be cut out. This leads to a loss of the Brg1 protein in all cells where Cre is active and also in their progeny as this is an irreversible event. The principle of using the CreloxP-system is illustrated in **Figure 5.42**. The embryonic analysis of Brg1 knockout offsprings was performed by Sebastian Maas, a bachelor student supervised by me. **Figure 5.43** shows that the Brg1 protein was lost in the mutant Ctx at E14, 4 days after recombination has started, whereas the Brg1 protein in the GE was still detectable. Brg1 KO embryos showed a completely disorganized Ctx. Morphologically the Ctx was smaller and extended in length. Cortical layers were not formed at all, since migration was also highly affected, which means that the migrating neurons were diffusely distributed allover the Ctx. Proliferating cells showed no spatial restriction to the VZ either. β-IIItubulin immunoreactivity depicts the neurons and reveals the disorganized structure of the Ctx lacking Brg1 (**Figure 5.43**).

5.3.3 Brg1 deletion in adult neural stem cells

In order to focus the analysis on the deletion of Brg1 selectively in adult neural stem cells, the inducible GLASTCreER^{T2} mouse line [Mori et al., 2006] was used. This inducible Cre line causes ablation of Brg1 protein after the induction with tamoxifen (see Materials and Methods, 4.2.) specifically in cells expressing the glutamate-aspartate transporter (GLAST). The inducible form of a Cre-loxP system used here functions in the way that Cre is fused to an estrogen receptor 2 which localizes the translated protein Cre in the cytoplasm leading to no recombination of floxed alleles. After the tamoxifen injection, the tamoxifen binds to the receptor as a ligand and this results in a translocation of the complex into the nucleus, where Cre recognizes the loxP-sites and recombines the DNA. As CreER^{T2} is only expressed in GLAST+ cells in this mouse line [Mori et al., 2006] recombination only occurs in GLAST expressing astrocytes in the adult brain [Rothstein et al., 1994; Storck et al., 1992; Ninkovic and Gotz, 2007]. Moreover, as GLAST was also shown to be expressed

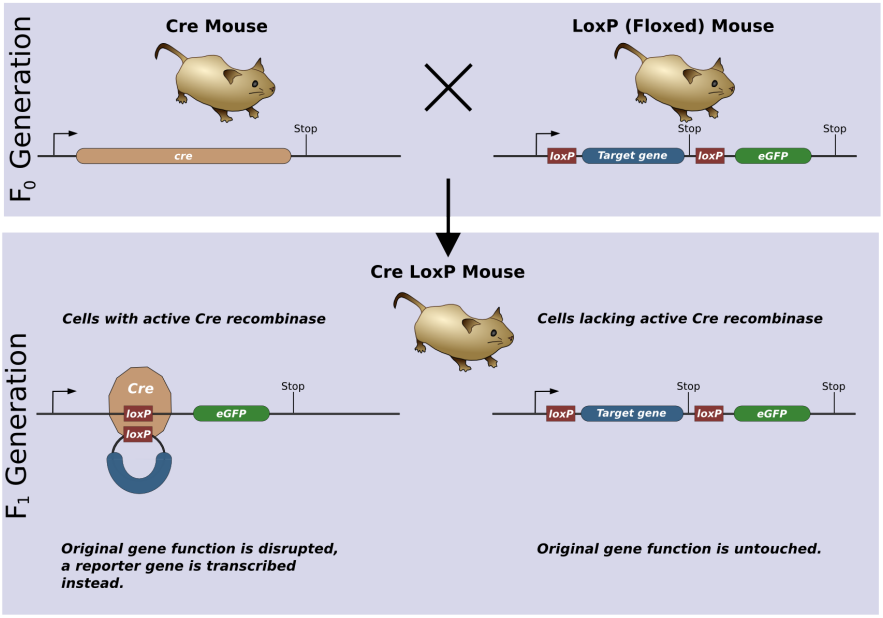

Figure 5.42: creLoxP system

Illustration of the CreLoxP-system. A mouse line in which Cre is driven by a specific promoter is crossed to a transgenic mouse in which a target gene is flanked by loxP sites. This crossing leads to the deletion of the floxed gene in all cells with active Cre recombinase.

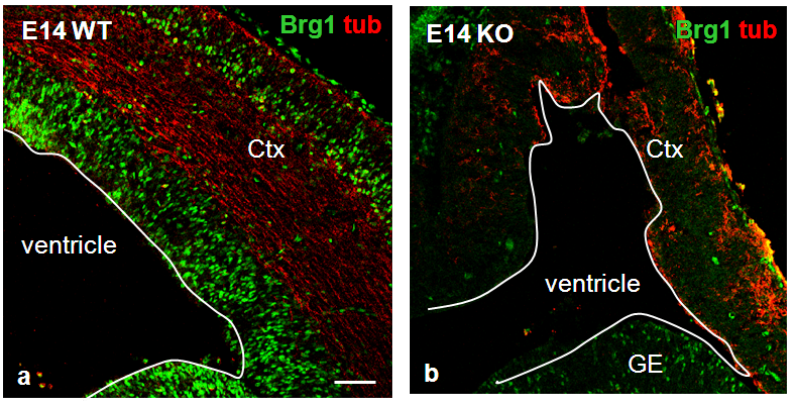

Figure 5.43: Phenotype during embryonic neurogenesis

a,b Fluorescent micrographs depict Brg1 expression double-stained with β-IIItubulin in WT (a) and in Brg1 KO (b) sections of E14 brains. Note the ablation of the Brg1 protein in the KO Ctx which is highly affected during brain development, while the protein is still detectable in the GE. Ctx=cortex, GE=ganglionic eminence. Scale bar: 20 μm.

in adult neural stem cells at the SEZ as they were shown to be astroglial-like cells [Jackson and Alvarez-Buylla, 2008], Brg1 will also be deleted in neural stem cells. In order to monitor the recombined cells, Brg1 floxed/floxed mice were crossed with a double reporter mouse line called Z/EG in which the lacZ protein is expressed without Cre-mediated excision and eGFP is expressed after recombination [Novak et al., 2000]. According to the literature Brg1 is known to play an important role in the embryonic brain in stem cell maintenance and later on in glial differentiation [Matsumoto et al., 2006]. To examine the Brg1 function in the adult brain and especially its role in neural stem cells and their differentiation the following mice were analyzed: Mice that were Brg1 floxed/floxed//GLASTCreER^{T2}//ZEG+ were used as experimental mice and Brg1 wt/wt//GLASTCreER^{T2}//ZEG+ and Brg1 floxed/wt//GLASTCreER^{T2}//ZEG+ mice as the appropriate controls since the heterozygous mice did not display a phenotype.

5.3.3.1 Analysis of Brg1 floxed mice 6 days after tamoxifen induction

Mice of comparable age (10 weeks) were induced twice a day for 5 days with an intra peritoneal (IP) injection of tamoxifen. The applied dosis of tamoxifen each day was 2 μg and therefore the total amount of applied tamoxifen 10 μg. This was shown to be the optimal induction method [Mori et al., 2006]. To this point, only one pair of Brg1 WT and Brg1 floxed mice could be analyzed. To monitor whether the Brg1 protein was already lost 6 days after tamoxifen treatment, Brg1 immunoreactivity was examined as shown in **Figure 5.44**. The Brg1 protein was still detectable in GFP+ recombined cells in the WT Ctx as well as in GFP+ cells at the SEZ. In the mutant situation the Brg1 protein is still present in some GFP+ cells at the SEZ, showing that Brg1 protein is not completely deleted. Moreover, BrdU was applied 1 hour before sacrificing the animals to monitor cells in the S-phase in the adult neurogenic regions. This preliminary data revealed a decrease in BrdU+ cells along the ventricle and in the RMS (**Figure 5.45**). Furthermore, GFP+ cells also seem to be reduced. This might be due to a reduction in the recombination rate in Brg1 floxed mice or to a specific decrease of recombined cells after Brg1 deletion. However, these findings have to be confirmed with further experiments to exclude artefacts of BrdU-labeling or tamoxifen induction.

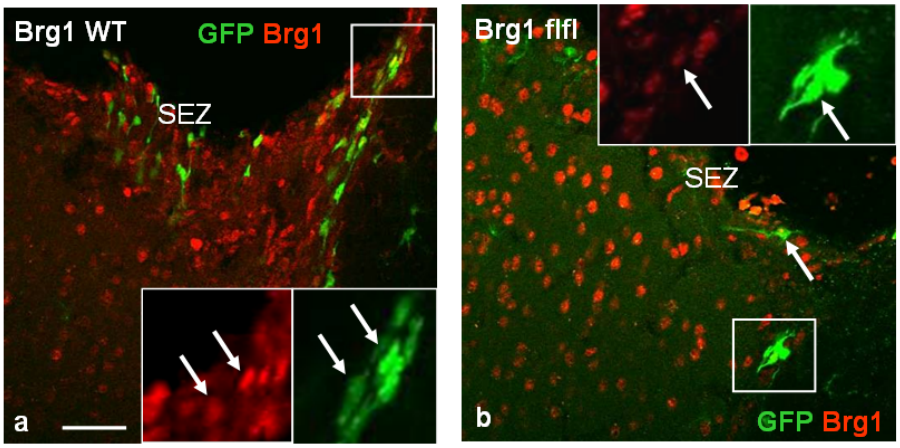

Figure 5.44: Brg1 protein detection in some recombined cells 6 days after tamoxifen induction

a,b The Brg1 protein is still detectable in some GFP+ recombined cells 6 days after tamoxifen induction. Arrows depict double-positive cells. SEZ= subependymal zone. White rectangles depict the region shown as insert in higher magnification. Scale bar: 20 μm.

5.3.3.2 Analysis of Brg1 floxed mice after 14 days of tamoxifen induction

The next time point analyzed was 14 days after the end of tamoxifen induction. First of all, it was checked whether the Brg1 protein had vanished in GFP recombined cells, because this is a crucial event for the interpretation of the data. If the Brg1 protein can still be detected, the recombination efficiency may be too low or the half life of the protein may be too long. As Brg1 is ubiquitously expressed including neural stem cells and postmitotic astrocytes, it might be assumed that it is in most of the recombined cells in the control situation. **Figure 5.46** shows Brg1 immunoreactivity in many GFP+ cells in the control whereas no Brg1-immunoreactive GFP+ cells were detectable in homozygous Brg1 floxed mice. Thus, two weeks after tamoxifen treatment Brg1 protein had fully disappeared.

Since the downregulation of Brg1 was proved 14 days after recombination, WT and mutant brains were stained for GFP to monitor cells that lack Brg1, and Dcx to label neuroblasts. At the WT SEZ many of the GFP+ cells are Dcx+, meaning that these cells differentiated into neuroblasts within 14 days after tamoxifen induction (**Figure 5.47 a**). In homozygous Brg1 floxed mice less GFP+ cells are Dcx+ and they seem to spread in an uncoordinated fashion, in such a way that GFP+ cells are found in the WM, which suggests that they migrate out of the RMS into the

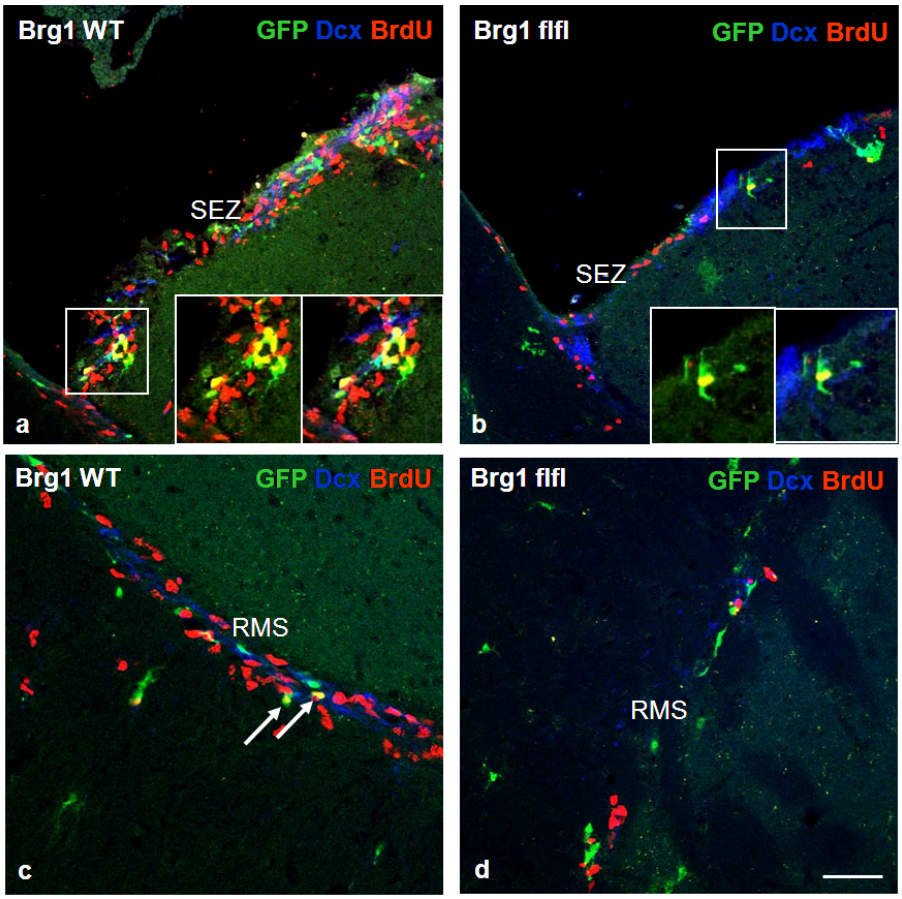

Figure 5.45: Brg1 floxed mice analyzed 6 days after tamoxifen induction

a,b The deletion of the Brg1 protein results in a decrease of BrdU positive cells amongst the recombined cells after 6 days. Roughly half of the GFP+ cells express Dcx, hardly any double-positive cell was found in the mutant. **c,d** In the RMS GFP+ cells were mainly BrdU+ in the WT compared to mutant. RMS= rostral migratory stream, SEZ= subependymal zone. Scale bar: 20 μm.

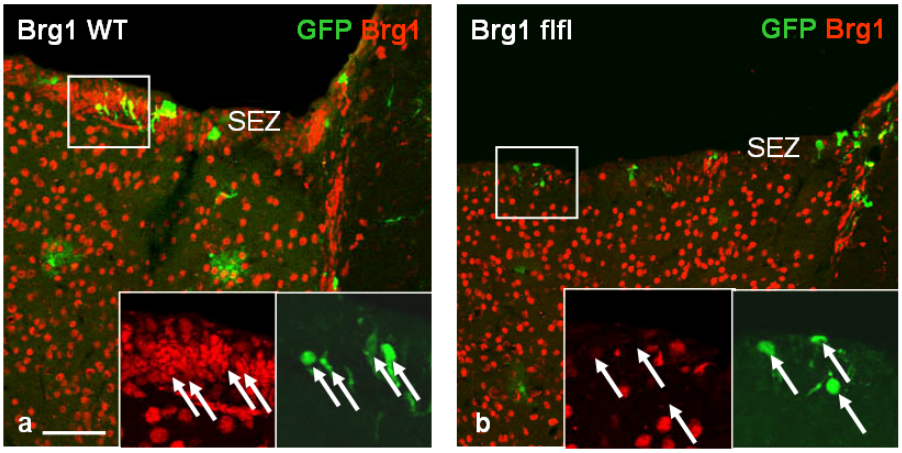

Figure 5.46: Brg1 protein is gone 14 days after tamoxifen induction

a,b The Brg1 protein is undetectable in Brg1 floxed mice 14 days after tamoxifen induction, whereas in Brg1 WT mice most of the GFP recombined cells express Brg1 protein. SEZ= subependymal zone. Arrows depict double-positive cells. White rectangles depict the region shown as insert in higher magnification. Scale bar: 20 μm.

WM (**Figure 5.47 b**). Further along the RMS where Dcx+ neuroblasts enter the OB GFP+ cells migrate radially toward the GCL and GL (**Figure 5.47 c,e,f**). In the homozygous Brg1 floxed mice GFP+ cells have an altered morphology and few of them are Dcx+, suggesting that they lose their neuronal identity (**Figure 5.47 d,g**).

Since the morphology of the Brg1 $^{-/-}$ cells was reminiscent of glial cells, the identity of the GFP+ cells in the mutant brains was examined by staining for glial markers. In the mutant, GFP+ cells express NG2, a marker for oligodendrocyte precursors. This colocalization is virtually never observed in the control mice (**Figure 5.48 a,b**). These data support the hypothesis of a switch from neuronal to glial cell fate due to the lack of Brg1. The quantification of Dcx+ cells at the SEZ in two pairs of WT and Brg1 floxed animals show a slight reduction of neuroblasts already after 14 days (**Figure 5.48 c**), while the percentage of Dcx+ cells amongst GFP+ cells counted was significantly reduced in the OB. These data suggest a change from neuronal to an NG2 glial fate as a result of the loss of the Brg1 protein.

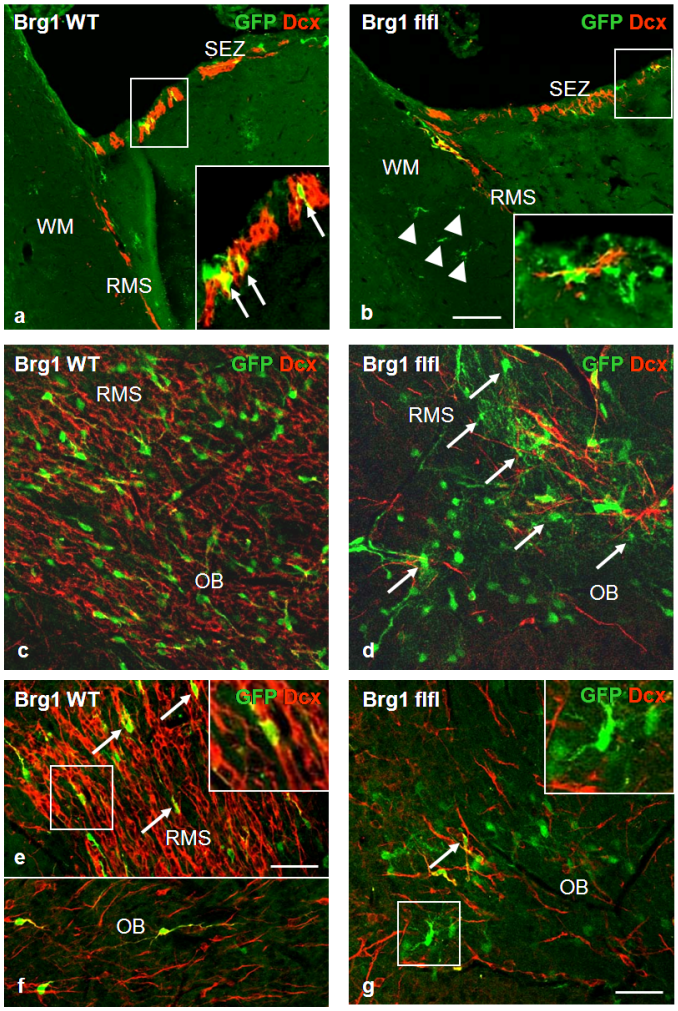

Figure 5.47: Analysis of Brg1 floxed mice 14 days after tamoxifen induction - Dcx expression

a,b In the control animals GFP+ cells mainly expressed Dcx at the SEZ (a), which was not the case in the Brg1 floxed mice. Note the migration of GFP+ cells into the WM indicated by white triangles and the reduced overlay of GFP and Dcx upon Brg1 deletion. **c,d** In the RMS many GFP+ cells coexpress Dcx in the WT brains (c), whereas in the Brg1 floxed mice GFP+ lose their neuronal identity and are mainly Dcx-. Note the change in the morphological shape of Brg1 deleted cells (d). **e-g** Higher magnification of GFP+ cells in the RMS entering the OB shows the colocalization of GFP+ cells with Dcx in WT brains and also in the outer layers of the OB (f). In Brg1 floxed mice GFP+ cells are mainly Dcx-. Note some GFP+ cells expressing Dcx, but they look unhealthy. OB= olfactory bulb, RMS= rostral migratory stream, SEZ= subependymal zone, WM= white matter. Arrows in a depict double-positive cells. Arrows in d depict cells with altered morphology. Arrows in e and f depict double-positive cells. White triangles depict GFP+ cells in the WM. White rectangles depict the region shown as insert in higher magnification. Scale bars: a,b 50 μm; c,d,f,g 20 μm; e 10 μm.

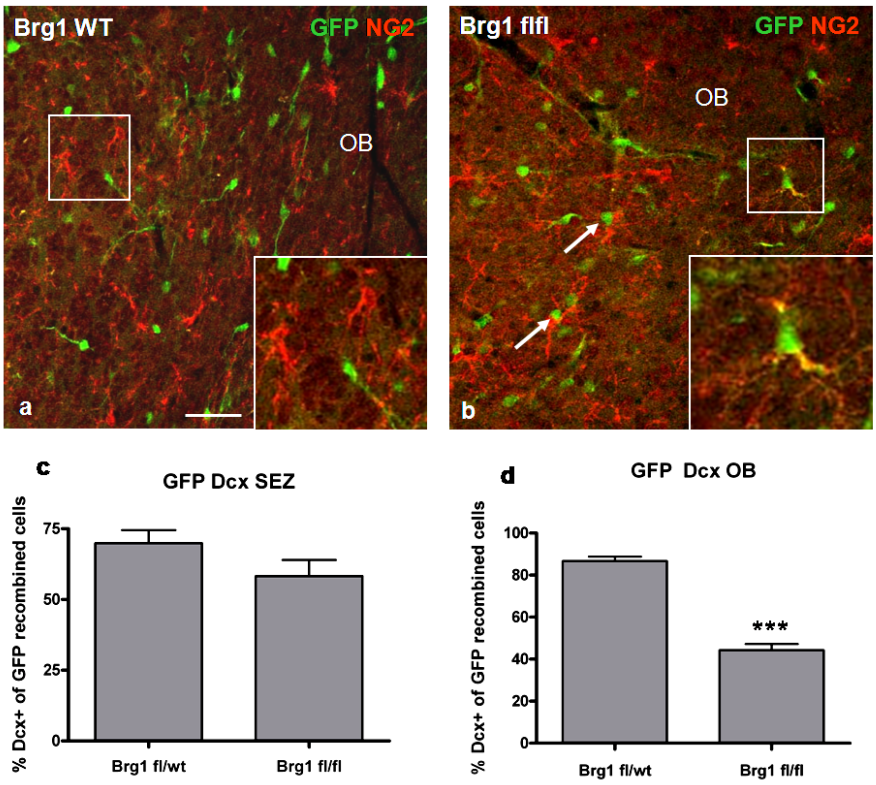

Figure 5.48: Analysis of Brg1 floxed mice 14 days after tamoxifen induction - NG2 expression and quantifications

a,b GFP+ cells normally do not express glial markers, e.g. NG2 in the WT (a). GFP+ cells in the mutant often double-stained for NG2, indicative of a switch to a glial fate (b). **c** Histogram depicts the percentage of Dcx+ cells out of recombined cells in the WT and Brg1 homozygous SEZ. Note the slight reduction of Dcx+ cells already at the SEZ in homozygous Brg1 mice 14 days after tamoxifen induction. **d** Histogram shows the percentage of Dcx+ cells amongst GFP recombined cells counted in the OB of WT and Brg1 homozygous mice (n=2). Note the significant reduction of Dcx+ cells in the mutant. OB= olfactory bulb. Arrows depict double-positive cells. White rectangles depict the region shown as insert in higher magnification. SEM=*** depicts $p \leq 0{,}001$. Scale bar: 20 μm.

5.3.3.3 Analysis of Brg1 floxed mice 28 days after tamoxifen induction

To examine whether the phenotype is progressive, mice were analyzed 28 days after tamoxifen induction. The main question was whether Brg1 deficient cells integrate into the normal circuitry of the OB or whether they disappear, presumably undergoing cell death. To understand this, the results from the analysis in Brg1 WT and floxed mice 14 days after tamoxifen induction were compared with the Dcx-immunoreactivity amongst all GFP+ cells analyzed after 28 days. **Figure 5.49 a,b** shows that GFP-recombined cells at the SEZ were fewer in number in WT and Brg1 floxed animals compared to the observed findings 14 days after tamoxifen induction although most of them were still Dcx+ in the WT. GFP+ cells in the Brg1 mutant animals were still found to spread out of the RMS into the WM. As a possible consequence of this, very few GFP+ cells were observed to migrate toward the OB in Brg1 floxed mice and the majority of them were Dcx-negative (**Figure 5.49 c,d**). In the WT situation GFP+ cells migrate radially to the outer layers of the OB where they become integrated into the circuitry. Some of these GFP+ cells are still Dcx+, whereas in the mutants 4 weeks post recombination almost no cells were seen in the GCL. GFP+ cells were only found in the OB close to the RMS (**Figure 5.49 e,f**). Additionally several immunostainings were performed with anitbodies directed against antigens characteristic for mature neurons and glia. In the WT OB many GFP+ cells were already NeuN-immunoreactive, suggesting that they were mature neurons. Homozygous Brg1 floxed mice did not display the ability to give rise to NeuN+ neurons 4 weeks after Brg1 ablation. The preliminary analysis of GFAP- and S100β-immunostainings showed no aberrant astroglial identity of GFP+ cells in homozygous Brg1 floxed mice.

The observed data in the analysis 14 days after Brg1 protein ablation revealed that GFP+ cells were able to migrate to the OB but already start to express oligodendrocyte progenitor markers while entering the OB. Two weeks later GFP+ cells could still be detected as immunoreactive for NG2 in the mutant OB (**Figure 5.50 a,b**), although GFP+ cells also expressing Olig2 were rarely present. The histograms in **Figure 5.50 c,d** depict the significant decrease in the percentage of recombined cells reaching the OB in homozygous Brg1 floxed mice that were Dcx+, whereas the percentage of GFP+ Dcx+ cells at the SEZ was comparable. The percentage of Dcx+ cells amongst all GFP+ cells compared to two weeks before remained unchanged, but due to the overall decrease in GFP cell number, the Dcx+ cell number

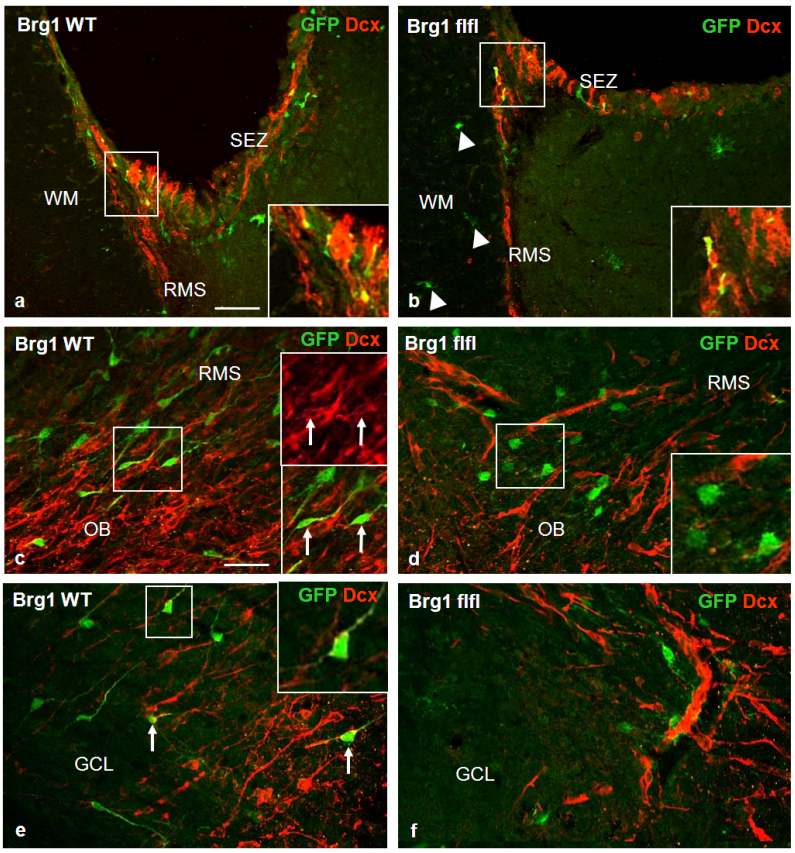

Figure 5.49: Analysis of Brg1 floxed mice 28 days after tamoxifen induction

a,b At the SEZ GFP+ recombined cells were fewer in number compared to 14 days after tamoxifen treatment. Some cells still expressed Dcx in both Brg1 WT and floxed mice. In Brg1 floxed mice green cells still spread out of the RMS into the WM. **c,d** In the WT OB many GFP+ cells are Dcx-immunoreactive, whereas in the Brg1 floxed mice fewer cells reach the OB out of which only a minority show Dcx-immunostaining. **e,f** In the outer layers of the OB, the GL, many GFP+ recombined cells were found in WT mice but almost no cells were found at this position in homozygous Brg1 floxed mice. GCL= granule cell layer, OB= olfactory bulb, RMS= rostral migratory stream, SEZ= subependymal zone. WM=white matter. Arrows depict double-positive cells. Arrowheads depict GFP+ cells in the WM. White rectangles depict the region shown as insert in higher magnification. Scale bar: a,b 20 μm; c-f 10 μm.

continued to further decline. These data suggest that GFP+ cells change their cell fate to a glial fate 14 days after Brg1 protein loss but then fail to differentiate further into mature oligodendrocytes and eventually die.

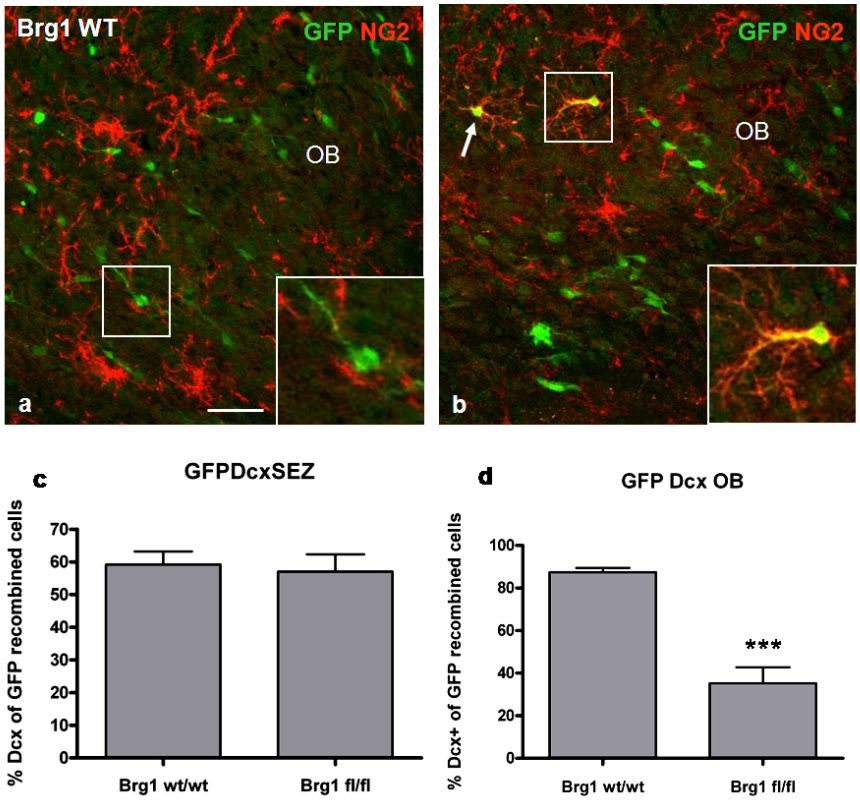

Figure 5.50: Analysis of Brg1 floxed mice 28 days after tamoxifen induction - NG2 expression and quantifications

a,b GFP+ cells normally do not show immunoreactivity for glial markers, e.g. NG2 in the WT OB (a). In the OB of homozygous Brg1 floxed mice GFP+ cells were found to double-stain for NG2 (b). **c** Histogram depicts the percentage of Dcx+ cells out of GFP+ cells in the WT and Brg1 homozygous SEZ. Note the comparable percentage of Dcx+ cells 28 days after Brg1 deletion. **d** Histogram shows the percentage of Dcx+ cells amongst GFP recombined cells counted in the OB of WT and homozygous Brg1 mice. Note the significant reduction of Dcx+ cells in the mutant. OB= olfactory bulb. Arrow depicts a double-positive cell. White rectangles depict higher magnification. SEM=*** depicts $p \leq 0{,}001$. Scale bar: 20 μm.

5.3.4 Brg1 deletion in adult neurosphere cultures

5.3.4.1 Expression of Brg1 in adult neurosphere cultures

In line with the expression of Brg1 in embryonic neurosphere cultures (see 4.1.2.) Brg1 immunoreactivity was also detected in many cells in adult neurospheres derived from SEZ of WT mice already 2 hours after plating. When cells had differentiated for 7 days Brg1 immunoreactivity was still present in almost all cells, including postmitotic neurons labeled with β-IIItubulin (**Figure 5.51**).

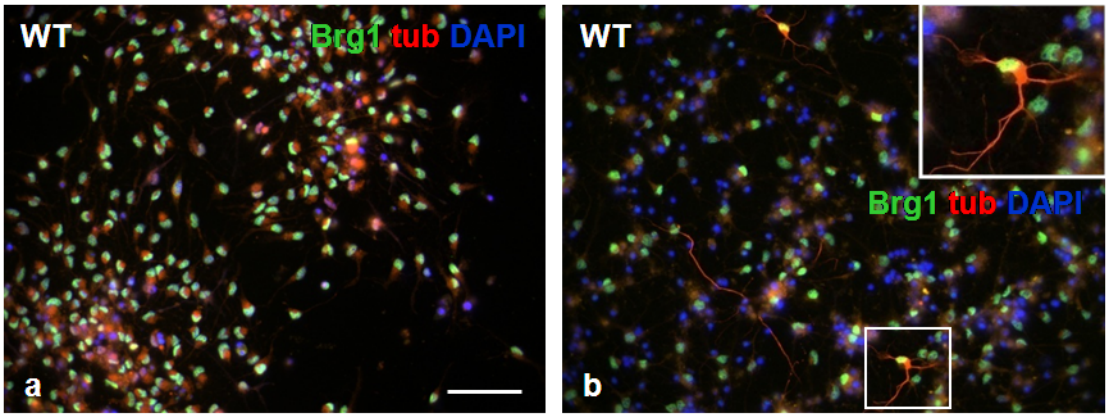

Figure 5.51: Brg1 expression in adult neurospheres

a Brg1 immunoreactivity 2 hours after plating of adult SEZ neurosphere cells, where most of the cells are Brg1+. Note the background staining in red. **b** After 7 DIV the Brg1 protein is detectable in β-IIItubulin+ neurons. White rectangle depicts the region shown in higher magnification in the insert. Scale bar: 20 μm.

5.3.4.2 Adult neurosphere cultures from Brg1 floxed mice

After the ablation of Brg1 protein *in vivo* the consequences of the Brg1 protein loss were analyzed *in vitro* to examine whether Brg1 is required already in the stem cells or at later stages during differentiation. Therefore neurosphere cultures from adult homozygous Brg1 floxed mice were performed. These cultures were comparable to those derived from WT mice. Cultures were infected with a retrovirus CreIRESGFP expressing Cre in all infected cells that also express GFP behind the IRES sequence (see Materials and Methods 4.11.). All cells that then appear GFP-labeled in the cultures lack the Brg1 protein. After the infection of neurospheres

from adult homozygous Brg1 floxed mice in the proliferative state in the floating medium, the number and size of neurospheres was reduced 7 days in the proliferation medium after infection (**Figure 5.52**). Moreover, after the third passage the growth of the spheres decreased almost to zero.

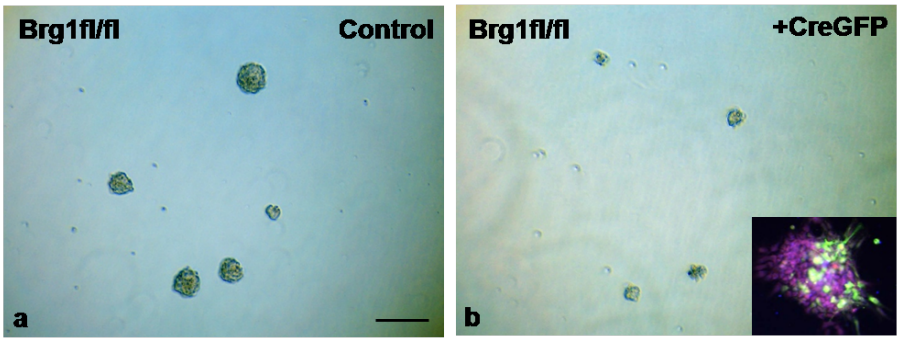

Figure 5.52: Adult neurospheres from SEZ of Brg1 floxed mice

a Adult neurospheres derived from Brg1 floxed mice in culture. Note the size and number of neurospheres in the control cultures. **b** The same cultures analyzed 7 days after infection with a CreGFP retrovirus 2 hours after splitting. Note the reduced size and number of neurospheres. The small panel shows the fluorescent staining of a CreIRESGFP infected neurosphere. GFP+ cells are shown in green, DAPI in blue and β-IIItubulin in red. Scale bar: 20 μm.

5.3.4.3 Differentiation analysis of Brg1 floxed neurospheres

After observing a proliferation defect in Brg1 KO cultures, the differentiation of neurospheres derived from homozygous Brg1 floxed mice was analyzed. The control cultures were not infected and only fixed and stained with antibodies directed against GFAP and β-IIItubulin 7 days after differentiation (**Figure 5.53 a**). When the cells were infected in the proliferation phase in the floating medium followed by differentiation for 7 days, the cells appeared improperly differentiated and β-IIItubulin+ neurons could only rarely be observed (**Figure 5.53 b**). When cells were infected 2 hours after plating GFP+ cells showed a different morphology after 7 DIV, they displayed now a more oligodendrocytic shape (**Figure 5.53 c,d**). GFP+ neurons labeled by β-IIItubulin immunostaining were rarely observed after Brg1 deletion.

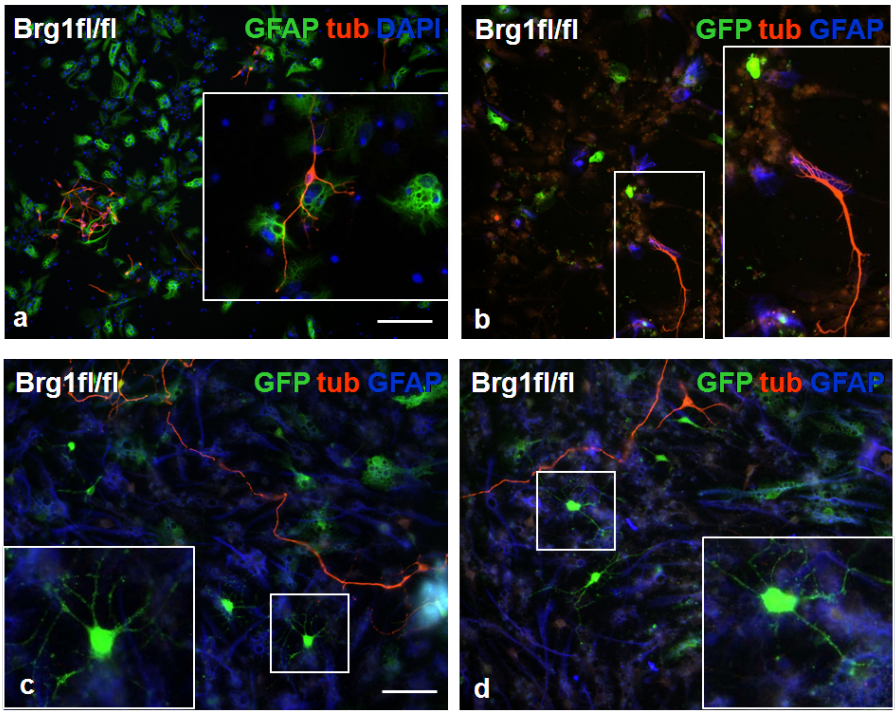

Figure 5.53: Differentiation of adult Brg1 floxed neurospheres

a Brg1 floxed neurospheres used as controls were not infected. After 7 days of differentiation neurons show a normal maturation state. **b** Neurospheres infected during the proliferation phase and analyzed 7 days later. Differentiation seems to be impaired in these cultures. Only a few β-IIItubulin+ cells can be found. **c,d** Cells were infected 2 hours after plating and analyzed 7 days after differentiation. GFP+ cells show an oligendrocytic morphology depicted in small panels with high magnification. Only a few GFP+ cells also express β-IIItubulin. White rectangles depict higher magnifications. Scale bars: a,b 20 μm; c,d 10 μm.

To summarize the results of the functional analysis of the Brg1 protein *in vivo* and *in vitro* it appears that Brg1 plays a crucial role in the maintenance of stem cell fate as the number of neurospheres was drastically reduced after Brg1 deletion. During differentiation Brg1 is also required for a normal neuronal differentiation. Without Brg1, cells switched to a NG2 glia fate.

6 Discussion

The role of epigenetic factors involved in specific regulatory mechanisms such as neuronal differentiation has become increasingly important over the last few years. Chromatin modifications have been characterized and the principal functions of different modification forms such as methylation, acetylation and phosphorylation have, in the mean time, become well understood. However, little is known about specific functions of single HDACs in the nervous system. HDACs are members of a small enzyme family that have the capacity to act as transcriptional repressors, often recruited in complexes such as Sin3 or NuRD. HDACs are described as ubiquitously expressed in certain tissues, e.g. the brain. In order to describe the function of HDACs, studies were conducted in which the catalytic domain of almost all HDACs was inhibited in order to interrupt their activity. This was achieved by HDAC inhibitors such as trichostatin A (TSA), which counteracts predominantly class II HDACs but was also shown to interfere with class I HDACs [Finnin et al., 1999]. While the application of broad-range HDAC inhibitors reflected strong effects with regard to neuronal degeneration and survival [Morrison et al., 2007], it is important to understand the specific functions of individual HDACs in different cellular contexts.

The expression profile and functional analysis of HDAC2 and Brg1 in the developing and adult mouse brain was presented in this work. For HDAC2 a specific expression of HDAC2 in postmitotic neurons and glia at different stages of the brain development and in the adult was observed. Thereby a rather intriguing difference in its expression in adult, but not embryonic progenitor cells was discovered. Based on this, the function of HDAC2 in a gene trap mouse mutant lacking the catalytic domain of HDAC2 was analyzed [Trivedi et al., 2007]. The lack of the functional HDAC2 protein resulted in an aberrant increase in apoptotic cells in most regions of the postnatal brain, while it is redundant in all regions in the adult brain with the exception of those regions where neurogenesis persists. Dying cells in the adult HDAC2 def brain were identified to be mainly adult generated neurons. Moreover, neuronal progenitors were found to be increased in adult neurogenic regions in the HDAC2 def brains. While the initial steps of neuronal progenitors toward neuronal differentiation were accomplished, further maturation was not possible in the absence of the functional HDAC2 protein.

Besides certain chromatin modifications, the remodeling of chromatin was shown to be sufficient for an optimal transcriptional access of DNA. An almost complete overlap with HDAC2 in the adult brain for Brg1 as the ATPase subunit of the most common chromatin remodeling complex SWI/SNF was observed. During development, however, Brg1 as opposed to HDAC2 is already present in progenitor cells and remains expressed in adult neural stem cells. To ablate the Brg1 protein only in adult neural stem cells and to analyze the consequences of its loss in its progeny, the Brg1 floxed mice crossed with an inducible Cre-mouse line (GLASTCreER^{T2}) and a reporter line (Z/EG) were used. Preliminary data derived from the analysis of mice lacking the Brg1 protein in adult neural stem cells points toward a specific role at different stages along the differentiation pathway of neurons. The deletion of Brg1 in adult neural stem cells results in a reduced number of progenitor cells. Later, the progeny migrating to the OB change their cell fate from neuronal to glial, more specifically to NG2 glia. Therefore, these data suggest that Brg1 acts as a crucial factor in the development of a cell toward a neuronal phenotype.

Despite their coexpression, these results highlight the specific roles of a single HDAC, namely HDAC2, and the ATPase subunit of a chromatin remodeling complex SWI/SNF, namely Brg1, in the central nervous system, especially in adult neurogenic regions.

6.1 HDAC2 expression profile

In order to examine the function of a single class I HDAC, I analyzed the specificity of the cellular expression of HDAC2. Already in the analysis of RNA expression it became obvious that HDAC2 was not expressed ubiquitously but rather in a very specific manner. It was found to be enriched in neurogenic and gliogenic precursor populations, highly expressed in postmitotic neurons, but low in astrocytic-enriched cultures (**Figure 5.1 b**). Immunostainings of HDAC2 in E14 neurosphere cultures could only partially confirm the observed RNA expression profile given that HDAC2 protein was very weakly expressed in GFAP+ astrocytes containing the stem cells in these cultures. Consistent with the RNA expression levels, the immunoreactivity of HDAC2 was high in β-IIItubulin+ postmitotic neurons (**Figure 5.2 b**). Furthermore, constant levels of HDAC2 immunoreactivity *in vivo* could be observed in postmitotic neurons in the developing as well as in the adult brain. A rather intriguing difference in the appearance of the HDAC2 protein was found in neu-

ronal precursor cells in the adult neurogenic regions (**Figure 5.10**), where it was expressed at high levels compared to embryonic neurogenic precursors in which it was virtually absent (**Figure 5.5**). This discrepancy of HDAC2 protein presence in adult, but not embryonic neurogenic precursors raised the question of whether HDAC2 carries a specific function in adult neurogenesis. As HDAC2 together with its highly related family member HDAC1 is often found to be part of the same transcriptional repressor complexes [de Ruijter et al., 2003], I performed the same expression analysis for HDAC1. As already described for HDAC2, the RNA expression levels of HDAC1 appeared high in neurons but low in progenitor populations (**Figure 5.1 a**). However, immunostainings for HDAC1 in E14 neurosphere cultures also revealed an expression in GFAP+ astrocytes as well as in many β-IIItubulin+ neurons (**Figure 5.2 a**). Already at embryonic stages this was found to be notably different *in vivo*. HDAC1 was weakly expressed in postmitotic neurons, although highly expressed in neural progenitor cells at the VZ (**Figure 5.3 a**). During postnatal development this difference in expression became more pronounced. HDAC1 was then only expressed in a scattered pattern typical for glial cells whilst completely absent in neuronal cells (**Figure 5.3 d,f**). In the adult brain HDAC1 was detected in GFAP+ as well as in CC1+ cells suggesting that astrocytes as well as oligodendrocytes contain the HDAC1 protein (**Figure 5.3**). Taken together, HDAC1 and HDAC2 were never found to be expressed in the same cell in the adult nervous system *in vivo* except in the WM where both proteins were expressed in glial cells (**Figure 5.9 a,b**). This complementary appearance in a very specific pattern of two individual class I HDACs suggests that HDAC1 and 2 might repress each other. Furthermore, with regard to the data presented here the coexistence of HDAC1 and 2 in the repressor complexes (Sin3, NuRD or CoREST) [Ayer, 1999; Zhang et al., 1999] in the brain is rather unlikely at least with respect to the protein expression analyzed here and remains to be proven.

6.2 HDAC2 - functional analysis

6.2.1 Phenotypical description of HDAC2 def mice

Given the specific expression patterns of HDAC1 and HDAC2 and the difference in the presence of the HDAC2 protein in adult, but not embryonic progenitor cells, a

gene trap mouse line deficient of the HDAC2 function was analyzed. This mouse line was already used in a former study concerning heart diseases, showing that HDAC2 def mice are prone to attenuated cardiac hypertrophy associated with an increased expression of Inpp5f, a gene encoding inositol polyphosphate-5-phosphatase f. This results in a constitutive activation of glycogen synthase kinase 3β (Gsk3β) via inactivation of the Pi3K-Akt-Gsk3β pathway [Trivedi et al., 2007]. Trivedi et al. (2007) identified an important function of HDAC2 in the regulation of cardiac hypertrophy over a well-known molecule Gsk3β, which is also a key regulatory molecule in the canonical Wnt signaling pathway [Lange et al., 2006]. Several studies in the past showed that predominantly the canonical Wnt signaling pathway plays important roles in the nervous system. It was revealed to be crucial for stem cell proliferation and expansion [Chenn and Walsh, 2002] as well as for the inhibition of neural differentiation [Haegele et al., 2003], in particular, the inhibition of Gsk3β promoted polarization and axon formation in hippocampal neurons [Yoshimura et al., 2005]. This interaction of HDAC2 and Gsk3β might also be a reason for the observed phenotype in the adult neurogenic regions in HDAC2 def mice in the sence that HDAC2 would suppress Pi3K-Akt-Gsk3β pathway and hence promote neuronal differentiation.

Trivedi et al. (2007) demonstrated that HDAC2 def mice not only display this heart phenotype. They also refer to a high postnatal lethality and a severe growth retardation of HDAC2 def pups similar to the observations presented here. While HDAC2 def mice were born according to Mendelian rates (**Figure 5.16**), a postnatal lethality rate of about 70 % compared to wildtype littermates between postnatal day 0 and 2 (P0-P2) (**Figure 5.17**) could be observed. A full genetic deletion (KO) of HDAC2 [Montgomery et al., 2007] is also described to exhibit a postnatal lethality rate of 100 % within the first 24 hours after birth due to cyanosis reflecting cardiac defects upon the complete loss of HDAC2. The fully penetrant lethality of these HDAC2-null mice contrasts with the phenotype observed in HDAC2 def mice. This raises the question if a hypomorphic allele can still have residual functionality. After LacZ insertion several phenotypes could be observed due to alternative splicing within the mutant locus [Voss et al., 1998]. This could be the reason for having sufficient levels of HDAC2 for viability and for the penetrance of the phenotype in HDAC2 def mice. Different genetic backgrounds of the mice tested in the two studies might also contribute to the different phenotypes. While HDAC2$^{-/-}$ mice have a mixed background of 129, C57BL/6/, CD1 [Montgomery et al., 2007] while HDAC2 def mice are on clean C57BL/6 background only [Zimmermann et al., 2007]. Several

experiments such as co-immunoprecipitation for HDAC2 and Sin3B have ruled out the possibility that a hypomorphic allele is responsible for the survival of HDAC2 def mice. Without a functional catalytic domain HDAC2 is not able to perform its normal catalytic function [Zimmermann et al., 2007].
However, an HDAC activity assay performed on brain regions of WT and HDAC2 def littermate mice showed a significant reduction in the overall HDAC activity in various brain regions (**Figure 5.15**), indicating that the fusion protein present in HDAC2 def mice leads to an overall decrease of HDAC activity most prominent in the HC. The growth retardation of HDAC2 def mice develops in the first weeks after birth. Compared to WT no obvious difference in body size could be detected at P3. At P21, however, HDAC2 def mice were severely affected in body size and weight (**Figure 5.19**). These findings were also reported by Zimmermann et al. (2007). Despite the early postnatal lethality the embryonic brain of HDAC2 def mice developed normally. Neurogenesis from E10-E18 occurred completely normal, as revealed by β-IIItubulin immunostaining at E14 and E18 (**Figure 5.18**). Along these lines, other aspects such as radial glia formation, shown by the Blbp-immunoreactivity (**Figure 5.18 e,f**), and proliferation (**Figure 5.18 g-j**) remained unchanged. The lack of an obvious brain phenotype during early development is consistent with its specific expression in postmitotic neurons during embryonic stages. With regard to the embryonic development, no obvious defects could be observed in HDAC2$^{-/-}$ mice either [Montgomery et al., 2007]. Moreover, embryonic neurosphere cultures from E14 WT and HDAC2 def embryos showed no defects in neuronal differentiation at all (**Figure 5.33**). However, it was recently reported that HDACs control neurogenesis in embryonic brain cultures derived either from the Ctx or GE respectively [Shaked et al., 2008]. These researchers inhibited all HDACs with TSA and were able to show a reduction in neurogenesis in the GE and a modest increase of neurogenesis in the Ctx. They then suggested a mechanistical interaction between HDACs and Bmp2/4 signaling pathway in radial glia cells, in which HDACs inhibit Bmp2 leading to a reduction in neurogenesis in the GE and an opposite function in the Ctx. These data strongly propose a function of HDACs in embryonic neurogenesis. Nevertheless, which HDAC is the most important to reveal this interaction with Bmps remains to be shown. Taken together, HDAC2 def mice as well as HDAC2$^{-/-}$ show phenotypic defects from early postnatal stages on, whereas HDAC2 seems to play no major role during the embryonic development. In the absence thereof other closely related HDACs such as HDAC1 might assume a compensatory role, as will be discussed below.

6.2.2 The role of HDAC2 in postnatal brain development

Having analyzed to this point the postnatal lethality and the observed growth retardation of HDAC2 def mice during the early postnatal days, this raised the first question of whether only the whole body was affected or if, in addition to this, also single organs became reduced in size compared to WT. Zimmermann et al. (2007) examined the size and weight of several organs, such as the testis and brain. They were found to have the predicted normalized ratio of the body size between WT and HDAC2 def mice. To determine the cause of the decreased brain size immunostainings for activated caspase 3 (casp3), a protein that is only activated in a small time window when cells undergo apoptosis [Riedl and Shi, 2004] were performed. Already at early postnatal stages (P0) there was a widespread increase in cell death in most regions of the HDAC2 def brains observed compared to WT (**Figure 5.20 a-c**). A colocalization analysis of casp3 and cell-type specific markers revealed a prevalence of non-neuronal cells dying at this developmental stage (**Figure 5.20 d,e**). During early postnatal stages gliogenesis takes place while neurogenesis is completed. The SEZ at neonatal stages gives rise to astrocytes and oligodendrocytes that migrate to the neocortex, the subcortical white matter (SCWM) and the deep gray matter [Kakita and Goldman, 1999]. These glial progenitors divide asynchronously giving rise to mixed clones of astrocytes and oligodendrocytes or both types of glia [Zerlin et al., 2004]. HDAC2 was found to be expressed in either GFAP+ and/or Ki67+ cells at P0 in proliferating zones such as the white matter (**Figure 5.7 b**). As the majority of the casp3+ cells are glial cells, postnatal gliogenesis could be affected in HDAC2 def mice thereby causing the smaller brain size that is already very obvious 1-2 weeks after birth [Trivedi et al., 2007]. Importantly, 70 % of postnatal lethality occurring in the first 2 days are not due to brain defects but more likely due to defects in other organs such as the described heart defect in HDAC2 def mice [Trivedi et al., 2007]. Pups analyzed in these first two days after birth include the ones that are sure to die. Therefore, it could be that mice that survive and are deficient of HDAC2 probably display a milder effect in postnatal brain development and adult neurogenesis than the ones that died already. As previously discussed, mice that survived and studied at adult stages can have sufficient levels of HDAC2 to survive and they show a penetrance in the strength of phenotypic changes like growth retardation or an increase in apoptosis. The further discussed defects in adult neurogenesis would probably be also more severe in mice fully lacking HDAC2. Therefore,

a future perspective will be to analyze HDAC2 floxed mice with regard to adult neurogenesis. This analysis is already underway with the first data obtained clearly pointing to a severe defect in neuronal differentiation of newly generated neurons in the adult brain.

6.2.2.1 Compensatory function of HDAC1 during embryonic and postnatal development in HDAC2 def mice

After having observed the complementary expression of HDAC1 and HDAC2, it was examined whether HDAC1 might compensate the loss of HDAC2 protein during embryonic and postnatal development. Already at early postnatal stages HDAC1 protein was found to be upregulated in NeuN+ postmitotic neurons, whilst it was not found in the WT (**Figure 5.36**). This upregulation of HDAC1 in NeuN+ cells could be observed until brain development was nearly completed (P21). Afterward HDAC1 declined to normal levels and normal localization. In fact, no defects in the embryonic development could be observed. It may well be that HDAC1 can take over the function of HDAC2, since they reveal a high sequence identity and are often found to be part of the same repressor complexes [de Ruijter et al., 2003]. Postnatally HDAC2 cannot fully be rescued by HDAC1. Otherwise no such defects as the increase in cell death would occur in HDAC2 def mice. The upregulation of HDAC1 upon the absence of HDAC2 may be also explained by a repression of HDAC1 gene by HDAC2 and vice versa. In the adult brain, HDAC1 is expressed only in glia cells, where HDAC2 is normally not expressed except in the white matter, where both proteins were found in glia cells. In the regions of adult neurogenesis HDAC1 is not upregulated in HDAC2 def mice, because it might be fully absent in these cells. This was also confirmed by the Western Blot analysis performed on tissue of different brain regions from WT and HDAC2 def littermates (**Figure 5.37**). Taken together, after the brain development is completed it seems to be that HDAC1 is not compensating HDAC2 in postmitotic neurons, where HDAC2 is predominantly expressed. This can be due to the fact that either HDAC1 is not present in those cells at all or the function of HDAC2 in postmitotic neurons is redundant because its function is more important in processes leading eventually to a functional neuron. Another possibility might be that the repressor complexes where HDAC1 and 2 can be recruited to recruit only HDAC2 in postmitotic neurons, but this remains to be shown. Moreover, HDAC2 may act on the protein level of

specific key regulators in adult neurogenesis accomplished by the presence of the different repressor complexes, while HDAC1 does not seem to play a role in adult neurogenesis in contrast to its importance in embryonic neurogenesis.

6.2.3 Apoptosis in the adult brain of HDAC2 def mice

The increase in apoptosis was not only limited to early postnatal stages. A higher number of cells undergoing cell death in the adult neurogenic regions of the brain, the HC and the OB, could also be observed. While cell death was very low in WT and mutant mice in non-neurogenic regions such as the Ctx, there was a significant increase in casp3+ cells in the mutant versus WT OB. In the HDAC2 def HC casp3+ cells were only slightly increased (**Figure 5.22 a**). The generation of newly born cells in the HC ranges from 1000-3000 cells per day, while in the SEZ/RMS/OB system 30.000 cells are generated each day [Alvarez-Buylla et al., 2001; Cameron and McKay, 2001]. Therefore, the turnover in the OB is obviously much higher than in the HC. It was previously shown that there are two modes of adding new and replacing old neurons in the existing network in the OB. Interneurons arriving newly in the GL were constantly added and increased over time whereas the proportion of newly generated neurons reaches a plateau in the GCL. This was also shown to be the case in the DG [Ninkovic et al., 2007]. This leads to the conclusion that the addition of newly generated neurons to the preexisting network is rather differently regulated in the GL compared to the GCL and DG. However, hardly any casp3+ cells were found in the WT HC. In the HDAC2 def HC a higher number of casp3+ cells could be found, but less than in the OB, where the difference between WT and HDAC2 def mice was striking. With the latter, cells that undergo apoptosis in the adult brain specifically in the neurogenic areas were mainly neuronal cells that could be identified by neuronal markers, such as Dcx or NeuN (**Figure 5.22 b,c**).

Zimmermann et al. (2007) isolated mouse embryonic fibroblasts (MEF) from E13.5 embryos to examine cell growth. They also observed an increase in apoptosis in HDAC2 def MEFs, while cell growth and proliferation remained unchanged. In general little is known about HDACs playing a role in apoptosis. It is known that HDAC2 interacts with p53, a tumor suppressor which is also involved in apoptosis [Luo et al., 2000; Juan et al., 2000]. p53 activity is modulated by post-translational modifications including acetylation. Deacetylation leads to p53 re-

pression and thereby to a downregulation of p53-dependent gene activation and consequently to the induction of programmed cell death. Interestingly this interaction with p53 has been shown for HDAC1, 2 and 3 respectively [Juan et al., 2000]. Huang et al. (2005) found out a specific functional significance for HDAC2 in HeLa cells inducing apoptosis associated with an increase in p21 expression independent of p53 [Huang et al., 2005]. They could also show that HDAC1 and HDAC2 were differentially expressed in cervical dysplasias and carcinoma, namely that HDAC2 is upregulated in colonic polyps and cancer cells which was not the case for HDAC1. Several studies linked to neurodegeneration argue indirectly for a role of class II HDACs in apoptotic regulation. It has been revealed for HDAC5 that it can induce cell death in cultured neurons [Linseman et al., 2003], whereas a splice variant of HDAC9 called HDAC-related protein (HDRP) promotes the survival of neurons [Morrison et al., 2006]. Recently a neuroprotective function was shown for HDAC4. Mice lacking HDAC4 have elevated cyclin-dependant kinase-1 (CDK1) activity and display cerebellar abnormalities including a progressive loss of Purkinje neurons postnatally, suggesting that HDAC4 neuroprotective function is mediated by its function in preventing cell-cycle progression [Majdzadeh et al., 2008]. Furthermore, most of the studies connecting HDACs with apoptosis were carried out with HDAC inhibitor treatment in several contexts. Regarding neurogenesis it has been shown by Salminen et al. (1998) that after HDAC inhibitor treatment excessive histone acetylation induces a stress response and apoptotic cell death in neurons [Salminen et al., 1998]. As the commonly used HDAC inhibitors block all HDAC proteins efficiently, it is not clear whether the promotion or reduction of neuronal cell death may be context-dependent and influenced substantially by the relative levels of pro- and anti-apoptotic HDAC proteins in the specific cell type. Taken together, the data reported here suggest an important function of HDAC2 preventing apoptosis in neuronal cells in the adult brain, more specifically in adult generated neurons.

6.2.4 The adult brain of HDAC2 def mice

Apart from the increase in apoptosis resulting in the reduced growth of the HDAC2 def brain, the overall brain morphology and cytoarchitecture appeared normal, except for the CB (**Figure 5.19 e,f**), which shows aberrations in the formation of the different lobi and a reduced thickness of the outer cell layer. These phenotypic changes of the CB remains to be further studied in the future on the molecular level.

In contrast, the six layers in the Ctx were clearly visible by NeuN-immunostaining (**Figure 5.21 a,b**) and, furthermore, Cux2, a transcription factor only expressed in the upper layers 2 and 3 was present at normal levels, taking into consideration that the brain and therefore also the Ctx are smaller (**Figure 5.21 c,d**). In addition to this the cell density as well as the neuronal density was unchanged either during embryonic and postnatal brain development or in the adult Ctx (**Figure 5.21 e,f**). The normal cytoarchitecture of adult HDAC2 def brains further supports the notion that embryonic neurogenesis is not affected.

6.2.5 The role of HDAC2 in adult neurogenic regions

6.2.5.1 The subgranular zone of the DG

Besides the increase in apoptotic cells in the adult neurogenic regions of HDAC2 def mice an obvious reduction of Dcx+ cells in the DG (**Figure 5.23 a-c**) was observed. As previously described, Dcx is expressed in neuroblasts that are still dividing and in immature neurons that have exited the cell cycle and have become postmitotic. Several studies have shown the existence of two types of Dcx+ cells in the SGZ [Kronenberg et al., 2003] and other research has described even three types [Seri et al., 2004]. These different types are categorized as Type D cells and are identified as the intermediate precursors in the generation of new granule neurons in the DG [Seri et al., 2001]. The three subtypes differ in their morphology as well as in their maturation state, either being neuroblasts or immature neurons. The higher magnification of Dcx+ cells in the HDAC2 def DG showed an aberrant morphology of those Dcx+ cells having a radial process with a reduced dendritic tree. These cells are classified as D3 cells, which have the certain characteristics of immature granule neurons. Furthermore, specifically these D3-cells seem to be diminished in the HDAC2 def mice due to their affected maturation shown in the aberrant morphology in HDAC2 def mice.

The reduction of Dcx+ cells in the mutant DG raises the question of how and when this reduction occurs. In order to examine a proliferation defect in the mutant DG, HDAC2 def mice were analyzed after a short pulse of BrdU 1 hour before the animals were sacrificed. In HDAC2 def mice a significant increase of cycling cells was detectable. The composition of the different cycling subtypes, namely the three

different precursor cell types existing in the adult neurogenic regions, Type B, C and A cells [Abrous et al., 2005], was not changed at all (**Figure 5.23 d**). An increased number of multipotent stem cells might possibly be conducive to higher numbers of fast dividing progenitors in HDAC2 def mice. To examine this and to further understand the composition of the progeny of these progenitors labeled with a short pulse of BrdU, a BrdU label retaining experiment (BrdU for 2 weeks in drinking water followed by one week with only water) was performed. The number of multipotent stem cells (BrdU+GFAP+) remained unaffected while the number of newly generated NeuN+ neurons labeled with this BrdU protocol was strongly decreased in the absence of catalytically active HDAC2 in the DG. This decrease in the number of BrdU+NeuN+ cells leads to the overall decrease of BrdU+ cells after 3 weeks of BrdU application (**Figure 5.23 e-h**). The number of BrdU+ cells containing Dcx, but not yet NeuN was even increased in HDAC2 def DG, whereas the proportion of BrdU+Dcx+NeuN+ cells was already reduced in number, suggesting a defect in neuronal differentiation at the transition from an immature Dcx+ cell into a more mature NeuN+ neuron [Kempermann et al., 2004]. Moreover, these cells are probably the cells undergoing apoptosis in the HDAC2 def mice. A similar effect of increasing proliferation of neural precursors was observed for sirtuin 1 (Sirt1), a NAD+ dependent HDAC. Redox alterations were shown to be critical and to affect the self-renewal capacity of neural precursor cells mediated by Sirt1. Under reducing conditions Sirt1 is repressed which leads to an increase in the proliferation of neuronal progenitors but is then followed by an enhancement of the neuronal differentiation by upregulation of Mash1 [Prozorovski et al., 2008]. To obtain more evidence for the specific block in neuronal maturation other markers expressed at the transition from a Dcx+ neuroblast to a mature NeuN+ neuron were analyzed. Calretinin, a Ca-binding protein and NeuroD1, a transcription factor thought to regulate neuronal differentiation in *Xenopus laevis* [Lee et al., 1995] by promoting premature cell cycle exit and differentiation in neural precursor cells are expressed at the time of transition from Dcx to NeuN expression [Kempermann et al., 2004]. In the mouse HC NeuroD was highly expressed in developing neurons supporting its role as a neuronal differentiation factor [Miyata et al., 1999; Chae et al., 2004]. NeuroD as well as Calretinin expression were strongly reduced in the HDAC2 def DG, (**Figure 5.24**). Taken together, neuronal differentiation factors are reduced in HDAC2 def DG resulting in the decrease of generating new mature neurons in the mutant brain. In order to demonstrate that the defect in neuronal differentiation and maturation cannot be explained by the concern that HDAC2 def cells may be

more sensitive to BrdU than WT cells, retroviral injections of GFP into the DG of WT and HDAC2 def mice were performed. The same results as for the BrdU label retaining experiment were obtained, namely a significant reduction in the number of GFP+NeuN+ cells 3 weeks after viral injection in the HDAC2 def DG (**Figure 5.26 a,b**). Given the increase in proliferation in HDAC2 def mice, the effects may be due to the upregulation of factors that have the capacity to maintain progenitors in a proliferating state and failed to become downregulated in the absence of functional HDAC2. Such factors could be Sox2 and Prox1. Sox2 is expressed in many progenitor cells including neural stem cells and thereby demonstrated to be sufficient for the multipotency and self-renewal of these cells [Gage, 1998; Ellis et al., 2004]. The expression of Sox2 in WT compared to HDAC2 def mice points to an increase in Sox2+ cells in the SGZ of the mutant mice that seem to colocalize with Dcx in a respective percentage of cells. This colocalization was rarely observed in the WT situation. Prox1 is also a transcription factor exclusively expressed in immature young granule neurons in the DG. The loss of the HDAC2 function also resulted in an increase in the number of Prox1+ cells that are not yet NeuN+ (**Figure 5.26**). The upregulation of those factors specifically expressed in proliferating cells or in immature neurons could explain the phenotype where progenitor cells by the loss of HDAC2 fail to downregulate factors such as Sox2, thereby prolonging the proliferation of the respective cells in HDAC2 def mice. Moreover, the aberrant upregulation of cell cycle-related proteins has been implicated as a mechanism underlying neuronal cell death in a variety of experimental paradigms [Copani et al., 2001].

6.2.5.2 The subependymal zone - rostral migratory stream - OB system

The observations in the second neurogenic region, the SEZ, were comparable to the findings in the DG. Multipotent stem cells located in the subependymal zone of the lateral ventricle give rise to transit-amplifying precursors that then generate neuroblasts that migrate along the rostral migratory stream to reach the OB [Zhao et al., 2008]. These young neuroblasts expressing Dcx differentiate into NeuN+ neurons in the OB to become integrated into the neuronal circuitry. In the OB of HDAC2 def mice a reduction of Dcx+ cells as compared to the DG (**Figure 5.27 a,b**) could also be observed. More fast proliferating cells could be found after a short pulse of BrdU (**Figure 5.27 c**) at the SEZ followed by a significant reduction in the number of newly generated neurons after 3 weeks of BrdU label retaining experiment

in the OB (**Figure 5.27 e-g**). As an independent approach to quantify neuroblasts in the OB FACS to sort PSANCAM+ cells was used. It was shown that Dcx and PSANCAM are expressed in the same cells, namely the neuroblasts [Seri et al., 2004]. The percentage of PSANCAM+ cells sorted from tissue of the SEZ of WT and HDAC2 def mice was slightly increased, supporting the fact that the number of proliferating neuroblasts is increased in HDAC2 def mice (**Figure 5.29**). In contrast to this, the number of PSANCAM+ cells is reduced while sorting cells from tissue of WT and HDAC2 def OBs, which suggests the fact that newly generated neurons are diminished when reaching the OB in HDAC2 def mice (**Figure 5.28**). These data demonstrate that proliferation is increased while neuronal differentiation is impaired in the HDAC2 def OB neurogenic system.

Since the HDAC2 function is lacking in all tissues of the HDAC2 def mice and hence may exert indirect effects on adult neurogenesis, the neurosphere assay was used to examine the propagation and differentiation of neural progenitor cells and their differentiation properties isolated under *in vitro* conditions. Consistent with the increase in proliferation *in vivo*, the formation of primary neurospheres from adult SEZ (aSEZ) was slightly increased whereas the secondary neurosphere formation was not changed in HDAC2 def neurosphere cultures (**Figure 5.34 a,b**). Already after 8 days of differentiation, neuronal maturation was affected, meaning in particular that cells were able to express neuronal markers such as β-IIItubulin but failed to form a neuronal network because their neurite outgrowth was severely affected. Once more, this suggests an important function of HDAC2 in neuronal maturation (**Figure 5.34 c,d**). While the number of neurons in HDAC2 def SEZ neurosphere cultures in differentiation medium was only slightly decreased after 8 DIV, the number of newly generated neurons was strongly reduced after 14 DIV compared to the number of WT neurons (**Figure 5.34 e,f**). These data point toward the fact that under isolated conditions in an *in vitro* system HDAC2 is important for neuronal differentiation and maturation. This reflects that the HDAC2 function is mediated via cell-autonomous mechanisms that are present also in isolated neurosphere cells *in vitro*. The treatment of aSEZ neurospheres with general HDAC inhibitors (valproic acid (VPA) or TSA) resulted in an increase of neuronal differentiation [Siebzehnrubl et al., 2007], suggesting that other HDACs rather than HDAC2 reveal this function in aSEZ neurospheres. In order to address the question of whether HDAC2 acts in a cell-autonomous manner in adult neurogenesis, we therefore tested the HDAC2 function *in vivo* by transplanting WT derived SEZ cells into the mutant SEZ. Since adult

neurogenic niches secrete several factors that could influence the cell-autonomous effect *in vivo* the differentiation capability of the transplanted cells was monitored. 3 weeks after transplantation a similar number of NeuN+ neurons reaching the OB in the WT compared to the HDAC2 def mice (**Figure 5.35**). Taken together, these experiments imply no major changes in the adult neurogenic niche of HDAC2 def mice, but rather demonstrate a cell-autonomous role for the catalytically active form of HDAC2 in neuronal differentiation of adult generated neurons. In the following possible explanations for the defects described in HDAC2 def mice shall be described.

6.2.5.3 REST as a key regulator of neuronal genes

As REST (RE1 silencing transcription factor, also known as NRSF) mediates active repression via recruitment of HDACs by its corepressors mSIN3 and COREST [Ballas et al., 2001], it appears to be a good candidate to act together with HDAC2 in the context of adult neurogenesis. REST is expressed in neural progenitor cells as well as in non-neuronal cells to repress neuronal differentiation. REST binds to the RE1 binding sites and there are two classes of genes described to be repressed by REST [Ballas et al., 2005]. Class I are neuronal genes downregulated in neural progenitor cells . Class II are neuronal genes that are repressed while REST binds to the RE1 binding site. Additionally, the two repressor complexes Sin3 and CoREST bind to methylated CpG islands known to be highly concentrated in heterochromatic regions [Bird, 2002; Craig, 2005]. Upon differentiation into cortical neurons, both repressor complexes bind to the promoters thereby preventing high transcription rates to regulate these genes. As REST is described to be absent in postmitotic neurons, it is likely that HDAC1 interacts in this play with REST. The group of Ballas et al. could only identify HDAC1 as an interaction partner with REST by CHIP experiments on several promoters of neuronal genes, such as BDNF or calbindin. Moreover, given that HDAC2 is also expressed in progenitor cells during postnatal brain development, HDAC2 could also be involved in the repression of neuronal genes in progenitor cells together with REST. Later, in the adult brain, HDAC2 is maintained in postmitotic neurons but its function to repress neuronal genes there is no longer required. On the other hand, in adult neurogenic regions HDAC2 seems to repress a set of genes in neuronal progenitor cells possibly sufficient for stem cell maintenance as it was shown for Sox2. Another recent study has reported a REST mediated pathway over a microRNA miR-124a repressing non-neuronal mR-

NAs in neuronal cells, while REST is absent and cannot repress this micro RNA itself. In non-neuronal cells REST represses the activity of miR-124a and neuronal genes thereby preventing neuronal differentiation [Conaco et al., 2006]. The study of Hsieh et al. (2004) is in line with the assumption that REST functions in concert with two transcriptional repressor complexes known to contain also HDAC2. They were able to show an induction of neuronal differentiation of adult hippocampal neural progenitors after HDAC inhibitor treatment. This is contradictory to the results observed in the HDAC2 def mice, suggesting that using broad range inhibitors for HDACs results in the loss of a variety of derepressed genes that display functions in a variety of different mechanisms.

6.2.5.4 Implications of HDAC inhibitor treatment in the context of lineage decision

Other studies on HDAC inhibitor treatment refer to oligodendrocyte progenitor cells (OPC) by affecting the timing of their differentiation. Histone deacetylation is known to be essential during a specific temporal window of development, and this was dependent on the activity of HDACs [Shen et al., 2005] by repressing genes inhibiting differentiation in OPCs. In line with these observations another study described the necessity of HDAC activity for oligodendrocyte lineage progression. By blocking HDAC activity using TSA in cultures derived from neonatal rat cortices the progression of oligodendrocyte progenitors into mature oligodendrocytes was prevented [Marin-Husstege et al., 2002] while no increase in astrocyte or neuronal differentiation was observed. Using TSA to treat embryonic mouse neural stem cells an increase of neuronal differentiation was observed while astrocyte differentiation was decreased [Balasubramaniyan et al., 2006]. By contrast, the inhibition of HDAC activity with VPA induced the neuronal differentiation of adult hippocampal progenitors. Moreover, VPA inhibited astrocyte and oligodendrocyte differentiation, respectively [Hsieh et al., 2004]. In another study VPA was reported to promote differentiation and cell death of neuroblastoma cells which were shown to have neuronal precursor characteristics [Stockhausen et al., 2005]. In the study of Lyssiotis et al. (2007) a genome-wide expression analysis after inhibiting HDAC activity in OPCs was reported, in which the reactivation of Sox2 and several other genes responsible for maintaining the neural stem cell state leads to developmental plasticity in these progenitor cells also capable of having neuronal differentiation potential [Lyssiotis

et al., 2007]. These observations are well in agreement with our results of an increase in proliferation in the adult neurogenic regions and the upregulation of Sox2 in HDAC2 def mice.
Most of the studies reporting the role of HDAC inhibitors cannot explain specific functions of single HDACs. Furthermore, all studies reported here showed HDAC inhibitor treatment in different cell culture systems at different developmental stages of neural progenitors, so that a comparison is not possible. However, studies inhibiting all HDACs could give hints about the involvement of specific mechanisms and offer a direction that future studies can follow. This should be done by defining specific functions of single HDACs along the lines of what this work revealed for HDAC2 in adult neurogenesis.

6.2.5.5 Specific functions for single class I HDACs

A study in zebrafish addressed the role of HDAC1 in two independent aspects. First, it was reported that in HDAC1 mutant zebrafish hindbrain the specification of oligodendrocytes fails to occur, while the persistence of neural progenitors in the mutant hindbrain VZ, which express Pax6a and Sox2, is independent of HDAC1 activity [Cunliffe, 2004]. Interestingly, HDAC1 expression is restricted to glial cells in which Sox2 is also expressed. This implies that HDAC1 does not suppress Sox2, although they are often coexpressed. Moreover, according to the data shown here, HDAC2 seems to repress Sox2 in neuronal progenitors allowing them to differentiate further, while HDAC1 cannot and is therefore not upregulated in the adult neurogenic regions in the HDAC2 def mice. Another group described HDAC1 as a necessary component for the switch from proliferation to neuronal differentiation in the zebrafish retina by antagonizing the Wnt and Notch/Hes pathway to promote cell-cycle exit and neurogenesis in the zebrafish retina [Yamaguchi et al., 2005]. In more detail, their data support the possibility that aberrant activation of Wnt signaling causes hyperproliferation in HDAC1 mutant retinas. Overexpression experiments further show that HDAC1 suppresses cell cycle progression and promotes the cell cycle exit of retinal progenitor cells. They further suggest that this suppression of Wnt signaling is achieved by the repression of genes that normally are activated by Wnt signaling such as cyclinD1. Several pharmacological components that inhibit HDAC activity, such as TSA or butyrate also cause cell cycle arrest at both G1 and G2 phases [Yoshida and Beppu, 1988]. Indeed, this function provides the basis for using HDAC

inhibitors to treat cancer. What is the molecular basis behind these cell cycle effects induced by HDAC inhibitors? The G1-arrest phenotype may be caused by the repression of key cell cycle regulating genes such as p21 by HDACs. The effects on G2/M may be a result of the role of HDACs in providing deacetylated histones to be deposited during the replication processes [Kouzarides, 1999]. This suggests a possible role for HDAC2 in the regulation of cell cycle, because the loss of HDAC2 also causes a hyperproliferation in adult neuronal progenitors.

6.2.5.6 Differentiation and maturation of newly generated neurons in the adult brain

As new neurons are continuously generated and integrated into existing neuronal circuits in the DG or the OB [Zhao et al., 2008], the hypothesis is that the survival or death of newly generated neurons is information-dependent. Because neurons receive their information primarily through their input synaptic activity, it was shown that the survival of new neurons is regulated by a specific NMDA-type glutamate receptor during a short, critical period soon after neuronal birth. This suggests that the survival of new neurons and their integration in preexisting neuronal circuits is information- and cell-type specific [Tashiro et al., 2006]. The synaptic integration is regulated not only by information- and cell specificity but also by their activation catalyzed by γ-aminobutyric acid (GABA), a major neurotransmitter in the adult brain. During embryonic neurogenesis, until the first postnatal week GABA induces depolarization resulting in an excitatory function [Ben-Ari, 2002]. In the adult brain, when newly born neurons mature, a conversion from GABA-induced depolarization into hyperpolarization occurs and this turns out to be essential for the establishment of functional GABAergic and glutamatergic synapses of newly generated neurons such as in the GCL of the DG [Ge et al., 2006]. The sequential expression of the Na^+-K^+-$2Cl^-$ transporter NKCC1 (a Cl^- importer) and the K^+-coupled Cl^- transporter KCC2 (a Cl^- exporter) is believed to underlie the conversion from depolarization to hyperpolarization by GABA during neuronal maturation in the brain [Ben-Ari, 2002; Owens and Kriegstein, 2002; Payne et al., 2003]. After shRNA treatment against NKCC1, newly generated GCL neurons exhibited significant defects in their dendritic arborization as shown by a reduction of the dendritic complexity. This suggests a GABA-induced depolarization as well as a reduction of the dendritic development of newborn neurons in adult neurogenic regions [Ge et al.,

2006], while in mature neurons GABA carries mainly inhibitory functions during the synaptic transmission. Given that the dendritic complexity in the HDAC2 def DG is affected in line with the neuronal maturation, it is likely that newborn neurons are not able to transduce local information needed for a proper integration into the preexisting neuronal network. This can have several causes. One might be that the depolarization/hyperproliferation shift mediated by the transporters NKCC1 and KCC2 does not occur correctly in HDAC2 def mice. This calls for further examination in the future.

Thus, the function of HDAC2 is crucial for the proper specification and subsequent survival of adult generated neurons, thereby revealing remarkable differences in the molecular mechanisms governing neuronal maturation in the embryonic and adult brain. The classification of neural stem cells and the differentiation toward the neuronal lineage in the adult brain is summarized in the diagram in **Figure 6.1** with respect to the observed phenotypic changes in the HDAC2 def mice. HDAC2 is necessary for regulating proliferation and differentiation of adult neurogenic progenitors. In the absence of HDAC2 proliferation genes are not repressed anymore and cells cannot differentiate properly to eventually undergo cell death.

6.2.6 The role of HDAC2 in non-neurogenic regions in the adult brain

We also observed prominent differences in the subcortical white matter (SCWM) of HDAC2 def mice (10 weeks old) with a significant increase of cells that incorporated BrdU after 1 hour short pulse, suggesting that these are cycling cells described to have gliogenic potential [Takemura, 2005; Nunes et al., 2003]. Double-staining with Dcx and GFAP displayed that the majority of these cells were Dcx+ (56 %) compared to 10 % in the WT and hence may be neuroblasts as Dcx encodes a microtubule-associated protein expressed in migrating neuroblasts [Abrous et al., 2005]. Proliferating cells in this region are described to have glial rather than neuronal potential [Nunes et al., 2003] and some of the BrdU+ cells in the SCWM also express glial markers such as GFAP and Olig2. In order to trace these proliferating Dcx-expressing cells and to examine whether they have the capacity to migrate toward the SCWM or other regions such as the Ctx, we injected GFP retrovirus in the region of the SCWM. After 14 days GFP+ cells could be detected at the edge

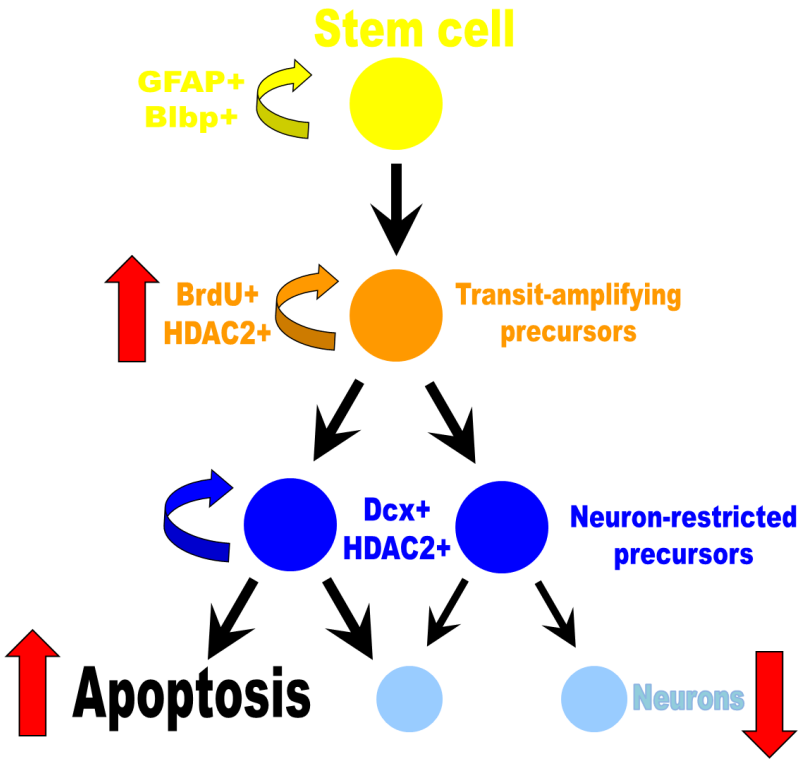

Figure 6.1: Summary of the phenotypic changes in HDAC2 def mice

Multipotent stem cells (GFAP+, Blbp+) give rise to transit-amplifying precursors (BrdU+) that generate neuroblasts (Dcx+) which then generate neurons. HDAC2 is expressed in all cell types except multipotent stem cells. Fast dividing cells are increased in HDAC2 def mice and the pool of adult generated postmitotic cells is depleted while cells undergo apoptosis.

of the lateral ventricle and at the caudal end of the SCWM, suggesting a migratory capacity rostrally and caudally. However, the cells remained in the SCWM. GFP+ cells that were found at the ventricle expressed to some extent GFAP (**Figure 5.31**). GFP+ cells did not label for other cell-type specific antigens such as Olig2 or Dcx. After a longer survival period of GFP injection (21 days) no GFP+ cells could be monitored in the GM of the Ctx. Instead, GFP+ cells remained in the WM. This suggests that besides the fact that they are able to migrate they do not have the neurogenic potential to generate new neurons entering the GM of the Ctx. In contrast to this it was recently shown that transplanted oligodendrocyte precursors (NG2+) from the neonatal rat Ctx into the corpus callosum (CC) of pups (same age) have under normal conditions the potential to generate only oligodendrocytes. After treatment with VPA these oligodendrocyte precursors can now also generate neurons [Liu et al., 2007]. The reprogramming of these specified precursor cells is due to the loss of epigenetic memory after HDAC inhibition, because global histone acetylation is detected in precursor cells during the early stages of brain development [Shen et al., 2005]. Taken together, the studies in the SCWM of HDAC2 def mice show another non-neurogenic region where proliferation is increased, but these cells does not seem to have neurogenic potential. The function of these proliferating cells has to be addressed in further studies.

6.3 Brg1 expression profile

Brg1 as a key molecule in the chromatin remodeling complex SWI/SNF showed a very specific expression pattern during the different stages of brain development. The comparison of the HDAC2 and Brg1 proteins was highly interesting especially when a high colocalization at different stages of neurogenesis became apparent. During embryonic neurogenesis Brg1 was already detectable in neural precursor cells on the mRNA level (**Figure 5.1 c**) as well as on the protein level at E14 (**Figure 5.2 c**). Brg1 was also present in differentiated cells, such as β-IIItubulin+ neurons at this age (**Figure 5.2 d**). Later, at the end of embryonic neurogenesis at E18, Brg1 immunoreactivity was present in postmitotic neurons in the cortical plate and low levels remained at the VZ similar to HDAC2 at this stage (**Figure 5.13**). Another research group also described Brg1 protein upregulation after E13 in the mouse embryonic VZ and also in postmitotic neurons [Matsumoto et al., 2006]. In contrast

to the absence of HDAC2 immunoreactivity in adult neural stem cells, Brg1 was also present in these cells in the SGZ of the DG and in the SEZ (**Figure 5.12 a,b**). Besides this difference the overlap of HDAC2 and Brg1 was very remarkable in the adult brain (**Figure 5.11**). Given the very specific colocalization of a protein that is part of the main transcriptional repressor complexes existing in the mammalian system and a protein function as an ATPase-subunit in the most prominent chromatin remodeling complex it could be shown that these complexes can be recruited to act in an orchestratic manner and coordinate with each other and with the transcription machinery to create specific regulation of specific genes [Narlikar et al., 2002]. Despite this similar expression pattern, the observed phenotypes were rather different.

6.4 Brg1 - functional analysis

6.4.1 Ablation of Brg1 protein in adult neural stem cells

In order to address the function of Brg1 in adult neural stem cells, the Brg1 protein was ablated by using an inducible GLASTCreER^{T2} line to specifically delete the protein in GLAST expressing astrocytes that are described to contain the multipotent stem cells in the adult neurogenic regions [Ninkovic and Gotz, 2007; Jackson and Alvarez-Buylla, 2008]. Supported by previous studies it became clear that Brg1 holds an important function in embryonic neural stem cells as reported by Matsumoto et al. (2006). The researchers claimed that stem cell maintenance is mediated by Brg1 and later during differentiation it seemed to be important for glial differentiation rather than neuronal differentiation. The two temporal as well as spatial independent roles of Brg1 were also well described by Lessard et al. (2007). They reported that a switch in the subunit composition of Brg1-containing complexes may promote neural stem cell self-renewal/proliferation. The specialized function of Brg1 in neural stem cells was likely mediated through its interaction with the progenitor-specific subunits of the SWI/SNF chromatin remodeling complexes. The transition from proliferative to neurogenic divisions required the exchange of these subunits specific for stem cell maintenance and thereby promoting neuronal differentiation. Therefore two different, very specific Brg1 containing complexes appeared at two distinguishable time points in embryonic neurogenesis [Lessard et al., 2007] and it

is believed that Brg1 is required for neuronal differentiation [Seo et al., 2005b]. An antagonist of Brg1 function with regard to neuronal differentiation was shown to be Geminin, a novel coiled-coil protein which was previously characterized to play a role in maintenance of genome integrity through regulation of DNA replication licensing [Seo and Kroll, 2006]. Geminin was found to be highly expressed in embryonic neuronal progenitor cells where it blocks the association of Brg1 with proneural genes, such as Neurogenin or NeuroD [Seo et al., 2005b]. In differentiating neurons Gem levels diminish and allow Brg1 to promote neuronal differentiation [Seo et al., 2005a]. However, the function of Brg1 containing complexes and the interaction with other regulatory proteins in adult neurogenesis was so far unknown.
By analyzing Brg1 floxed mice crossed with GLASTCreER^{T2} and a reporter line (Z/EG) to follow the recombined cells after tamoxifen induction in the adult brain at 3 different survival times an important phenotype in neuronal differentiation could be detected. The Brg1 protein was not completely disappeared 6 days after tamoxifen induction (**Figure 5.44**), but after 14 days Brg1 protein was no longer detectable in GFP+ recombined cells (**Figure 5.46**). GFP+ Dcx+ cells were slightly reduced at the SEZ in Brg1 floxed mice suggesting a reduction in the number of newly generated neuroblasts 14 days after tamoxifen induction. GFP+ cells entering the RMS to migrate to the OB seemed to disperse and migrate into other areas, such as the nearby white matter or the striatum (**Figure 5.47 b**). The few recombined cells that managed to reach the OB were often not neuronal as they did not contain Dcx but started to express glial markers such as NG2 (**Figure 5.48 a,b**) and also showed a clear change in cell morphology as the cells positive for GFP had a branched process formation characteristic for oligodendrocyte progenitors (**Figure 5.47 c-g**). The quantification of GFP+Dcx+ cells in the OB reflected a significant reduction in Brg1 floxed mice from $\approx$ 85 % to 40% suggesting the possibility that Brg1 is important for neuronal differentiation in the adult SEZ/RMS/OB system (**Figure 5.48 c,d**). The DG remains to be examined in the future to compare the observed effects after Brg1 deletion in both neurogenic areas.

The third time point analyzed 28 days after tamoxifen application confirmed the observations made already after 14 days. Moreover, the observed change in Brg1 floxed mice became more prominent as very few cells reached the OB and none of the GFP+ cells migrated toward the GL of the OB to become integrated in the neuronal circuitry (**Figure 5.49**). Furthermore, the expression of glial markers such as NG2 was also more prominent in the longer survival analysis than after 14 days

(**Figure 5.50 a,b**).

In order to study adult neural stem cells derived from the SEZ of Brg1 floxed mice were infected with a Cre-containing retrovirus to delete Brg1 in all dividing cells in the floating state. The control cultures were not infected at all. The number and size of neurospheres were reduced in cultures where Cre led to the ablation of Brg1 protein (**Figure 5.52**). This observation was completely consistent with the findings that Lessard et al. (2007) reported. Their *in vitro* analysis was done with embryonic neurospheres from WT and Brg1 floxed mice crossed with a nestinCre mouse line to specifically delete Brg1 protein in cells expressing nestin starting at E10.5. When they analyzed the number and size of the neurospheres, both were significantly reduced in Brg1-deficient cultures compared to WT cultures [Lessard et al., 2007] after 7 days, suggesting a crucial role for Brg1 in stem cell maintenance and a potent function in embryonic neurogenic precursors as well as in adult neurogenic precursors. As Brg1 was found to be expressed in almost all cells in adult neural stem cell cultures it may also play a role in neuronal differentiation *in vitro* as it was shown *in vivo*. Cells were infected with a Cre-containing retrovirus 2 hours after plating. After 7 days of differentiation there was a significant change from neuronal to more oligodendrocytic differentiation (**Figure 5.53**). Taken together, Brg1 seems to be important for neural stem cell maintenance and neuronal differentiation both *in vitro* and *in vivo*. When Brg1 was deleted cells were not able to proliferate in a normal frequence. During neuronal differentiation a switch from the neurogenic to the gliogenic pathway occurred. Besides the importance of Brg1 containing complexes with specific subunit presence in either neural stem cells or more differentiated neurons [Lessard et al., 2007], so far little is known about the function of Brg1 in a complex mechanism such as adult neurogenesis. This study shed some light on the importance of Brg1 in this regard but further examinations will be carried out to address the functions more precisely.

6.5 HDAC2 and Brg1 - comparison

When linking the function of HDAC2 to that of Brg1 it appears that Brg1 plays several important roles in neurogenesis both in embryonic stages as well as in adulthood. The two proteins can act together on the same genes [Narlikar et al., 2002] and it was shown for HDAC2 as well as for Brg1 that they are recruited to REST-mediated

repression. Brg1 activity increases the stability of REST-RE1 interactions with chromatin [Ooi et al., 2006]. Moreover, Brg1 can affect transcription in both a positive and a negative manner, while the negative effect is achieved conjointly with HDACs [Sif et al., 2001]. Along these lines, Brg1 also revealed to interact with the proneural bHLH proteins Neurogenin and NeuroD and mediates their transcriptional activities for neurogenesis in *Xenopus laevis* [Seo et al., 2005b]. Various sequence-specific transcription factors are regulated by the SWI/SNF complex together with HATs or HDACs to either activate or repress transcription and presumably also proneural bHLH transcription factors [Kadam and Emerson, 2003]. This possibly offers the best explanation for the switch from neuronal to glial cell fate after the deletion of Brg1. Furthermore, it was demonstrated that Brg1 also interacts with Pax6 [Yang et al., 2006], a potent regulator of neurogenesis, which is conducive to the neuronal differentiation into adult TH+ glomerular neurons [Brill et al., 2008]. Therefore, it is likely that Pax6 can only fully achieve its potent function by interaction with Brg1. Not only HDACs alone are recruited by SWI/SNF complexes but, most prominently, also the mammalian repressor complex mSin3 containing HDAC2 as a subunit [Xu et al., 2006] then acting together in an orchestratic manner. In the CNS, HDAC2 and Brg1 show an overlapping expression pattern in almost all cells except the multipotent stem cells, which suggests that functions regarding neuronal differentiation can be achieved conjointly, whereas the function of Brg1 in stem cell maintenance might possibly be addressed together with other HDACs. This is also reflected in the mutants for either HDAC2 or Brg1 analyzed in this study, given that both mutants show a neuronal differentiation phenotype. In the HDAC2 def mice the defect in neuronal maturation leads to apoptosis, whereas after Brg1 deletion, a switch from neuronal to NG2-glial cell fate occurs. Hence, it might be interesting to understand the causes of Brg1 and HDAC2 loss in adult neural stem cell differentiation and, on the other hand, to examine the function of each protein in a mutant background of the other. Moreover, the interaction of Brg1 and also HDAC2 with important neurogenic regulators such as Pax6 is a highly interesting study that should be designed in the future.

This study identified for the first time a specific role of two epigenetic factors in the CNS, namely HDAC2 and Brg1. HDAC2 steers the regulation of neuronal maturation in the adult, but not the embryonic brain. Conversely, Brg1 regulates neural stem cell maintenance and neuronal cell fate in both embryonic and adult neurogenesis in which both proteins might act together. Thus, the functions of HDAC2

and Brg1 reveal the specificity by which epigenetic mechanisms affect key features in adult neurogenesis and therefore regulate the final maturation and integration of new neurons into preexisting neuronal networks in the adult brain.

Acknowledgments

First of all, I want to thank Magdalena Götz for her incredible enthusiasm that could leave no doubt about the choice of working in Science being the best ever for your professional life. A big thank you also for the many helpful and inspiring discussions, her time-consuming corrections of my thesis, the financial patronisation but, even more importantly, her 'personal' support over the past 4 years.....and everything else I might have forgotten to mention at this point.

I should like to say thank you to Leda Dimou for her friendship, the helpful discussions we had and last, but not least for her proofreading of the manuscript.

A special thank you to Simone Bauer, Tatjana Simon-Ebert, Andrea Steiner-Mezzadri, Gabriele Jäger, Timucin Öztürk for their phantastic technical support. Many thanks to the lab members, especially Dilek Colak and Inmaculada Rite for lending me a helping hand and providing their experience with stereotactical injections and transplantation experiments. I should also like to thank Pratibha Tripathi for supporting me with her assistance and experience in FACS and RNA preparation for microarray. In this respect, a big thank you also to Martin Irmler for the microarray analysis. Thank you to all other lab members for the exchange of experience, discussions and a pleasant working environment.

I am grateful to Martin Göttlicher, Wolfgang Wurst for a fruitful collaboration. A special thank you also to Carmen Spiller and Alexander Nuber for their incredible support in anything connected to 'mouse stuff', as wells as Sabine Lagger for a perfect collaboration.

A special thanks to Sebastian Maas, the best Bachelor student on this planet.

Another special thanks to Matthias Schimmelpfennig for his support in mastering the text editing program Latex.

I want to thank Natalie Zink for believing in me and her help in proofreading the manuscript.

And last, but not least a warm Thank You to my family, in particular to my mother. She is always there for me...

Curriculum Vitae

PERSONAL DATA

Name	Jawerka, Melanie
Address	SPRINGERSTR. 17, 81477 MÜNCHEN, GERMANY
Telephone	+49 (0)163- 2573824
Fax	
E-mail	melanie.jawerka@helmholtz-muenchen.de
Nationality	German
Date of birth	19.07.1974

EDUCATION AND ACADEMIC CAREER

July 2004	Doctoral thesis with the Institute of Stem Cell Research at Helmholtz Zentrum Munich, Ingolstädter Str. 1, 85764 Neuherberg Topic: The role of epigenetic regulatory mechanisms in adult neurogenesis; Supervising tutor: Prof. Dr. M. Götz
June 2004	Diploma in Biology
September 2003	Diploma thesis on the topic: Characterization of factors of glial development in the embryonic CNS of *Drosophila melanogaster*; Supervising tutor: Prof. Dr. G. Technau; Institute of Genetics, Johannes-Gutenberg-University, Mainz
April 1998	Study of Biology aimed at Diploma, Johannes-Gutenberg-University, Mainz
January 1997	Voluntary social gap year with German Red Cross in Bad Homburg; Training as Emergency Medical Technician (EMT) with state exam on 1997/07/11
April 1995	Study of Sports Science aimed at Master's degree, Johann-Wolfgang-Goethe-University, Frankfurt/Main
September 1994 – November 1994	Internship at county hospital in Bad Homburg, nursing department
May 1994	University Entrance Qualification (Abitur), Christian-Wirth-Schule, Usingen

PUBLICATIONS

Brill, M. S., Snapyan, M., Wohlfrom, H., Ninkovic, J., Jawerka, M., Mastick, G., Saghatelyan, A., Ashery-Padan, R., Berninger, B., Götz, M. J Neurosci 2008 Jun*18*;28(25):6439-52. A Dlx2- and Pax6-dependent transcriptional code for periglomerular neuron specification in the adult olfactory bulb.

PRESENTATIONS

Poster presentation "Annual Meeting 2005 of the German Society for Cell Biology (DGZ)", Heidelberg, 2005

Poster presentation "Chromatin mediated biological decisions", Marburg, 2006

Poster presentation "4th ISSCR Annual Meeting", Toronto, 2006

Oral presentation "2nd UK Stem Cell Meeting: Epigenetics and Differentiation", London, 2007

Poster presentation "EMBO Conference on Chromatin and Epigenetics", Heidelberg, 2007

Oral presentation "FASEB Summer Research Conference: Histone deacetylases", Colorado, 2007

Oral presentation "EMBO Workshop: Can Epigenetics influence reprogramming & metastatic progression?" in Bad Staffelstein, 2008

LANGUAGE SKILLS

Mother tongue	GERMAN
Other languages	ENGLISCH: EXCELLENT
	ITALIAN: BASIC KNOWLEDGE
	SPANISH: BASIC KNOWLEDGE

EDV SKILLS

MS Office	Word, Excel, PowerPoint
Image processing	Adobe Photoshop CS2, Adobe Illustrator
Data evaluation	GraphPadPrism 4.0

COURSE-RELATED ACTIVITIES

November 2000 – March 2003	Allago AG, Temporary employee with 20 semester hours in the Service Center

HOBBIES

Athletics, Fitness, Snowboard, Mountainbike, Travelling, Readings, Music, Art

Bibliography

D. N. Abrous, M. Koehl, and M. Le Moal. Adult neurogenesis: from precursors to network and physiology. *Physiol Rev*, 85(2):523–69, 2005.

A. Alvarez-Buylla and D. A. Lim. For the long run: maintaining germinal niches in the adult brain. *Neuron*, 41(5):683–6, 2004.

A. Alvarez-Buylla, M. Theelen, and F. Nottebohm. Proliferation "hot spots" in adult avian ventricular zone reveal radial cell division. *Neuron*, 5(1):101–9, 1990.

A. Alvarez-Buylla, J. M. Garcia-Verdugo, and A. D. Tramontin. A unified hypothesis on the lineage of neural stem cells. *Nat Rev Neurosci*, 2(4):287–93, 2001.

A. Alvarez-Buylla, B. Seri, and F. Doetsch. Identification of neural stem cells in the adult vertebrate brain. *Brain Res Bull*, 57(6):751–8, 2002.

T. E. Anthony, C. Klein, G. Fishell, and N. Heintz. Radial glia serve as neuronal progenitors in all regions of the central nervous system. *Neuron*, 41(6):881–90, 2004.

D. E. Ayer. Histone deacetylases: transcriptional repression with siners and nurds. *Trends Cell Biol*, 9(5):193–8, 1999.

V. Balasubramaniyan, E. Boddeke, R. Bakels, B. Kust, S. Kooistra, A. Veneman, and S. Copray. Effects of histone deacetylation inhibition on neuronal differentiation of embryonic mouse neural stem cells. *Neuroscience*, 143(4):939–51, 2006.

N. Ballas, E. Battaglioli, F. Atouf, M. E. Andres, J. Chenoweth, M. E. Anderson, C. Burger, M. Moniwa, J. R. Davie, W. J. Bowers, H. J. Federoff, D. W. Rose, M. G. Rosenfeld, P. Brehm, and G. Mandel. Regulation of neuronal traits by a novel transcriptional complex. *Neuron*, 31(3):353–65, 2001.

N. Ballas, C. Grunseich, D. D. Lu, J. C. Speh, and G. Mandel. Rest and its corepressors mediate plasticity of neuronal gene chromatin throughout neurogenesis. *Cell*, 121(4):645–57, 2005.

Y. Ben-Ari. Excitatory actions of gaba during development: the nature of the nurture. *Nat Rev Neurosci*, 3(9):728–39, 2002.

A. Bird. Dna methylation patterns and epigenetic memory. *Genes Dev*, 16(1):6–21, 2002.

B. M. Bolstad, R. A. Irizarry, M. Astrand, and T. P. Speed. A comparison of normalization methods for high density oligonucleotide array data based on variance and bias. *Bioinformatics*, 19(2):185–93, 2003.

J. J. Breunig, J. I. Arellano, J. D. Macklis, and P. Rakic. Everything that glitters isn't gold: a critical review of postnatal neural precursor analyses. *Cell Stem Cell*, 1(6):612–27, 2007.

M. S. Brill, M. Snapyan, H. Wohlfrom, J. Ninkovic, M. Jawerka, G. S. Mastick, R. Ashery-Padan, A. Saghatelyan, B. Berninger, and M. Gotz. A dlx2- and pax6-dependent transcriptional code for periglomerular neuron specification in the adult olfactory bulb. *J Neurosci*, 28(25):6439–52, 2008.

J. J. Buggy, M. L. Sideris, P. Mak, D. D. Lorimer, B. McIntosh, and J. M. Clark. Cloning and characterization of a novel human histone deacetylase, hdac8. *Biochem J*, 350 Pt 1:199–205, 2000.

S. Bultman, T. Gebuhr, D. Yee, C. La Mantia, J. Nicholson, A. Gilliam, F. Randazzo, D. Metzger, P. Chambon, G. Crabtree, and T. Magnuson. A brg1 null mutation in the mouse reveals functional differences among mammalian swi/snf complexes. *Mol Cell*, 6(6):1287–95, 2000.

M. A. Caldwell, X. He, and C. N. Svendsen. 5-bromo-2'-deoxyuridine is selectively toxic to neuronal precursors in vitro. *Eur J Neurosci*, 22(11):2965–70, 2005.

H. A. Cameron and R. D. McKay. Adult neurogenesis produces a large pool of new granule cells in the dentate gyrus. *J Comp Neurol*, 435(4):406–17, 2001.

H. A. Cameron, C. S. Woolley, B. S. McEwen, and E. Gould. Differentiation of newly born neurons and glia in the dentate gyrus of the adult rat. *Neuroscience*, 56(2):337–44, 1993.

K. Campbell and M. Gotz. Radial glia: multi-purpose cells for vertebrate brain development. *Trends Neurosci*, 25(5):235–8, 2002.

L. Cao, X. Jiao, D. S. Zuzga, Y. Liu, D. M. Fong, D. Young, and M. J. During. Vegf links hippocampal activity with neurogenesis, learning and memory. *Nat Genet*, 36(8):827–35, 2004.

A. Capela and S. Temple. Lex/ssea-1 is expressed by adult mouse cns stem cells, identifying them as nonependymal. *Neuron*, 35(5):865–75, 2002.

A. Carleton, L. T. Petreanu, R. Lansford, A. Alvarez-Buylla, and P. M. Lledo. Becoming a new neuron in the adult olfactory bulb. *Nat Neurosci*, 6(5):507–18, 2003.

J. H. Chae, G. H. Stein, and J. E. Lee. Neurod: the predicted and the surprising. *Mol Cells*, 18(3):271–88, 2004.

A. Chenn and C. A. Walsh. Regulation of cerebral cortical size by control of cell cycle exit in neural precursors. *Science*, 297(5580):365–9, 2002.

D. Colak, T. Mori, M. S. Brill, A. Pfeifer, S. Falk, C. Deng, R. Monteiro, C. Mummery, L. Sommer, and M. Gotz. Adult neurogenesis requires smad4-mediated bone morphogenic protein signaling in stem cells. *J Neurosci*, 28(2):434–46, 2008.

C. Conaco, S. Otto, J. J. Han, and G. Mandel. Reciprocal actions of rest and a microrna promote neuronal identity. *Proc Natl Acad Sci U S A*, 103(7):2422–7, 2006.

A. Copani, D. Uberti, M. A. Sortino, V. Bruno, F. Nicoletti, and M. Memo. Activation of cell-cycle-associated proteins in neuronal death: a mandatory or dispensable path? *Trends Neurosci*, 24(1):25–31, 2001.

J. M. Craig. Heterochromatin–many flavours, common themes. *Bioessays*, 27(1): 17–28, 2005.

V. T. Cunliffe. Histone deacetylase 1 is required to repress notch target gene expression during zebrafish neurogenesis and to maintain the production of motoneurones in response to hedgehog signalling. *Development*, 131(12):2983–95, 2004.

A. J. de Ruijter, A. H. van Gennip, H. N. Caron, S. Kemp, and A. B. van Kuilenburg. Histone deacetylases (hdacs): characterization of the classical hdac family. *Biochem J*, 370(Pt 3):737–49, 2003.

F. Doetsch, I. Caille, D. A. Lim, J. M. Garcia-Verdugo, and A. Alvarez-Buylla. Subventricular zone astrocytes are neural stem cells in the adult mammalian brain. *Cell*, 97(6):703–16, 1999.

F. Doetsch, L. Petreanu, I. Caille, J. M. Garcia-Verdugo, and A. Alvarez-Buylla. Egf converts transit-amplifying neurogenic precursors in the adult brain into multipotent stem cells. *Neuron*, 36(6):1021–34, 2002.

2nd Dorn, G. W. and T. Force. Protein kinase cascades in the regulation of cardiac hypertrophy. *J Clin Invest*, 115(3):527–37, 2005.

J. A. Eisen, K. S. Sweder, and P. C. Hanawalt. Evolution of the snf2 family of proteins: subfamilies with distinct sequences and functions. *Nucleic Acids Res*, 23(14):2715–23, 1995.

P. Ellis, B. M. Fagan, S. T. Magness, S. Hutton, O. Taranova, S. Hayashi, A. McMahon, M. Rao, and L. Pevny. Sox2, a persistent marker for multipotential neural stem cells derived from embryonic stem cells, the embryo or the adult. *Dev Neurosci*, 26(2-4):148–65, 2004.

B. Eroglu, G. Wang, N. Tu, X. Sun, and N. F. Mivechi. Critical role of brg1 member of the swi/snf chromatin remodeling complex during neurogenesis and neural crest induction in zebrafish. *Dev Dyn*, 235(10):2722–35, 2006.

V. Filippov, G. Kronenberg, T. Pivneva, K. Reuter, B. Steiner, L. P. Wang, M. Yamaguchi, H. Kettenmann, and G. Kempermann. Subpopulation of nestin-expressing progenitor cells in the adult murine hippocampus shows electrophysiological and morphological characteristics of astrocytes. *Mol Cell Neurosci*, 23(3):373–82, 2003.

M. S. Finnin, J. R. Donigian, A. Cohen, V. M. Richon, R. A. Rifkind, P. A. Marks, R. Breslow, and N. P. Pavletich. Structures of a histone deacetylase homologue bound to the tsa and saha inhibitors. *Nature*, 401(6749):188–93, 1999.

A. Fischer, F. Sananbenesi, X. Wang, M. Dobbin, and L. H. Tsai. Recovery of learning and memory is associated with chromatin remodelling. *Nature*, 447(7141): 178–82, 2007.

K. Frederiksen and R. D. McKay. Proliferation and differentiation of rat neuroepithelial precursor cells in vivo. *J Neurosci*, 8(4):1144–51, 1988.

F. H. Gage. Stem cells of the central nervous system. *Curr Opin Neurobiol*, 8(5): 671–6, 1998.

F. H. Gage, P. W. Coates, T. D. Palmer, H. G. Kuhn, L. J. Fisher, J. O. Suhonen, D. A. Peterson, S. T. Suhr, and J. Ray. Survival and differentiation of adult

neuronal progenitor cells transplanted to the adult brain. *Proc Natl Acad Sci U S A*, 92(25):11879–83, 1995.

F. H. Gage, G. Kempermann, T. D. Palmer, D. A. Peterson, and J. Ray. Multipotent progenitor cells in the adult dentate gyrus. *J Neurobiol*, 36(2):249–66, 1998.

L. Gao, M. A. Cueto, F. Asselbergs, and P. Atadja. Cloning and functional characterization of hdac11, a novel member of the human histone deacetylase family. *J Biol Chem*, 277(28):25748–55, 2002.

J. M. Garcia-Verdugo, S. Ferron, N. Flames, L. Collado, E. Desfilis, and E. Font. The proliferative ventricular zone in adult vertebrates: a comparative study using reptiles, birds, and mammals. *Brain Res Bull*, 57(6):765–75, 2002.

S. Ge, E. L. Goh, K. A. Sailor, Y. Kitabatake, G. L. Ming, and H. Song. Gaba regulates synaptic integration of newly generated neurons in the adult brain. *Nature*, 439(7076):589–93, 2006.

M. Gotz. Glial cells generate neurons–master control within cns regions: developmental perspectives on neural stem cells. *Neuroscientist*, 9(5):379–97, 2003.

M. Gotz and W. B. Huttner. The cell biology of neurogenesis. *Nat Rev Mol Cell Biol*, 6(10):777–88, 2005.

M. Gotz, A. Stoykova, and P. Gruss. Pax6 controls radial glia differentiation in the cerebral cortex. *Neuron*, 21(5):1031–44, 1998.

H. Grandel, J. Kaslin, J. Ganz, I. Wenzel, and M. Brand. Neural stem cells and neurogenesis in the adult zebrafish brain: origin, proliferation dynamics, migration and cell fate. *Dev Biol*, 295(1):263–77, 2006.

I. V. Gregoretti, Y. M. Lee, and H. V. Goodson. Molecular evolution of the histone deacetylase family: functional implications of phylogenetic analysis. *J Mol Biol*, 338(1):17–31, 2004.

L. Guarente. Sir2 links chromatin silencing, metabolism, and aging. *Genes Dev*, 14 (9):1021–6, 2000.

H. Guo, S. Hong, X. L. Jin, R. S. Chen, P. P. Avasthi, Y. T. Tu, T. L. Ivanco, and Y. Li. Specificity and efficiency of cre-mediated recombination in emx1-cre knock-in mice. *Biochem Biophys Res Commun*, 273(2):661–5, 2000.

M. A. Hack, M. Sugimori, C. Lundberg, M. Nakafuku, and M. Gotz. Regionalization and fate specification in neurospheres: the role of olig2 and pax6. *Mol Cell Neurosci*, 25(4):664–78, 2004.

M. A. Hack, A. Saghatelyan, A. de Chevigny, A. Pfeifer, R. Ashery-Padan, P. M. Lledo, and M. Gotz. Neuronal fate determinants of adult olfactory bulb neurogenesis. *Nat Neurosci*, 8(7):865–72, 2005.

L. Haegele, B. Ingold, H. Naumann, G. Tabatabai, B. Ledermann, and S. Brandner. Wnt signalling inhibits neural differentiation of embryonic stem cells by controlling bone morphogenetic protein expression. *Mol Cell Neurosci*, 24(3):696–708, 2003.

S. H. Hendry, E. G. Jones, S. Hockfield, and R. D. McKay. Neuronal populations stained with the monoclonal antibody cat-301 in the mammalian cerebral cortex and thalamus. *J Neurosci*, 8(2):518–42, 1988.

R. A. Henry, S. M. Hughes, and B. Connor. Aav-mediated delivery of bdnf augments neurogenesis in the normal and quinolinic acid-lesioned adult rat brain. *Eur J Neurosci*, 25(12):3513–25, 2007.

W. His. Die neuroblasten und deren entstehung im embrionalen mark. *Abh Kgl sachs Ges Wissensch math phys Kl*, 15(1):311–372, 1889. 0890-9369 (Print) Book Chapter.

J. Hsieh and F. H. Gage. Epigenetic control of neural stem cell fate. *Curr Opin Genet Dev*, 14(5):461–9, 2004.

J. Hsieh, K. Nakashima, T. Kuwabara, E. Mejia, and F. H. Gage. Histone deacetylase inhibition-mediated neuronal differentiation of multipotent adult neural progenitor cells. *Proc Natl Acad Sci U S A*, 101(47):16659–64, 2004.

B. H. Huang, M. Laban, C. H. Leung, L. Lee, C. K. Lee, M. Salto-Tellez, G. C. Raju, and S. C. Hooi. Inhibition of histone deacetylase 2 increases apoptosis and p21cip1/waf1 expression, independent of histone deacetylase 1. *Cell Death Differ*, 12(4):395–404, 2005.

T. Imura, H. I. Kornblum, and M. V. Sofroniew. The predominant neural stem cell isolated from postnatal and adult forebrain but not early embryonic forebrain expresses gfap. *J Neurosci*, 23(7):2824–32, 2003.

E. L. Jackson and A. Alvarez-Buylla. Characterization of adult neural stem cells and their relation to brain tumors. *Cells Tissues Organs*, 2008.

E. C. Jacobs, C. Campagnoni, K. Kampf, S. D. Reyes, V. Kalra, V. Handley, Y. Y. Xie, Y. Hong-Hu, V. Spreur, R. S. Fisher, and A. T. Campagnoni. Visualization of corticofugal projections during early cortical development in a tau-gfp-transgenic mouse. *Eur J Neurosci*, 25(1):17–30, 2007.

K. Jin, Y. Sun, L. Xie, S. Batteur, X. O. Mao, C. Smelick, A. Logvinova, and D. A. Greenberg. Neurogenesis and aging: Fgf-2 and hb-egf restore neurogenesis in hippocampus and subventricular zone of aged mice. *Aging Cell*, 2(3):175–83, 2003.

C. B. Johansson, S. Momma, D. L. Clarke, M. Risling, U. Lendahl, and J. Frisen. Identification of a neural stem cell in the adult mammalian central nervous system. *Cell*, 96(1):25–34, 1999.

L. J. Juan, W. J. Shia, M. H. Chen, W. M. Yang, E. Seto, Y. S. Lin, and C. W. Wu. Histone deacetylases specifically down-regulate p53-dependent gene activation. *J Biol Chem*, 275(27):20436–43, 2000.

D. Junghans, M. Heidenreich, I. Hack, V. Taylor, M. Frotscher, and R. Kemler. Postsynaptic and differential localization to neuronal subtypes of protocadherin beta16 in the mammalian central nervous system. *Eur J Neurosci*, 27(3):559–71, 2008.

S. Kadam and B. M. Emerson. Transcriptional specificity of human swi/snf brg1 and brm chromatin remodeling complexes. *Mol Cell*, 11(2):377–89, 2003.

R. Kageyama, T. Ohtsuka, J. Hatakeyama, and R. Ohsawa. Roles of bhlh genes in neural stem cell differentiation. *Exp Cell Res*, 306(2):343–8, 2005.

A. Kakita and J. E. Goldman. Patterns and dynamics of svz cell migration in the postnatal forebrain: monitoring living progenitors in slice preparations. *Neuron*, 23(3):461–72, 1999.

M. S. Kaplan and D. H. Bell. Mitotic neuroblasts in the 9-day-old and 11-month-old rodent hippocampus. *J Neurosci*, 4(6):1429–41, 1984.

C. Kellendonk, F. Tronche, E. Casanova, K. Anlag, C. Opherk, and G. Schutz. Inducible site-specific recombination in the brain. *J Mol Biol*, 285(1):175–82, 1999.

G. Kempermann, S. Jessberger, B. Steiner, and G. Kronenberg. Milestones of neuronal development in the adult hippocampus. *Trends Neurosci*, 27(8):447–52, 2004.

T. Kouzarides. Histone acetylases and deacetylases in cell proliferation. *Curr Opin Genet Dev*, 9(1):40–8, 1999.

A. R. Kriegstein and M. Gotz. Radial glia diversity: a matter of cell fate. *Glia*, 43 (1):37–43, 2003.

G. Kronenberg, K. Reuter, B. Steiner, M. D. Brandt, S. Jessberger, M. Yamaguchi, and G. Kempermann. Subpopulations of proliferating cells of the adult hippocampus respond differently to physiologic neurogenic stimuli. *J Comp Neurol*, 467(4): 455–63, 2003.

P. W. Laird, A. Zijderveld, K. Linders, M. A. Rudnicki, R. Jaenisch, and A. Berns. Simplified mammalian dna isolation procedure. *Nucleic Acids Res*, 19(15):4293, 1991.

C. Lange, E. Mix, K. Rateitschak, and A. Rolfs. Wnt signal pathways and neural stem cell differentiation. *Neurodegener Dis*, 3(1-2):76–86, 2006.

A. Lavado and G. Oliver. Prox1 expression patterns in the developing and adult murine brain. *Dev Dyn*, 236(2):518–24, 2007.

J. E. Lee, S. M. Hollenberg, L. Snider, D. L. Turner, N. Lipnick, and H. Weintraub. Conversion of xenopus ectoderm into neurons by neurod, a basic helix-loop-helix protein. *Science*, 268(5212):836–44, 1995.

U. Lendahl, L. B. Zimmerman, and R. D. McKay. Cns stem cells express a new class of intermediate filament protein. *Cell*, 60(4):585–95, 1990.

J. Lessard, J. I. Wu, J. A. Ranish, M. Wan, M. M. Winslow, B. T. Staahl, H. Wu, R. Aebersold, I. A. Graef, and G. R. Crabtree. An essential switch in subunit composition of a chromatin remodeling complex during neural development. *Neuron*, 55(2):201–15, 2007.

D. C. Lie, H. Song, S. A. Colamarino, G. L. Ming, and F. H. Gage. Neurogenesis in the adult brain: new strategies for central nervous system diseases. *Annu Rev Pharmacol Toxicol*, 44:399–421, 2004.

D. A. Linseman, C. M. Bartley, S. S. Le, T. A. Laessig, R. J. Bouchard, M. K. Meintzer, M. Li, and K. A. Heidenreich. Inactivation of the myocyte enhancer factor-2 repressor histone deacetylase-5 by endogenous ca(2+) //calmodulin-dependent kinase ii promotes depolarization-mediated cerebellar granule neuron survival. *J Biol Chem*, 278(42):41472–81, 2003.

A. Liu, Y. R. Han, J. Li, D. Sun, M. Ouyang, M. R. Plummer, and P. Casaccia-Bonnefil. The glial or neuronal fate choice of oligodendrocyte progenitors is modulated by their ability to acquire an epigenetic memory. *J Neurosci*, 27(27):7339–43, 2007.

J. Luo, F. Su, D. Chen, A. Shiloh, and W. Gu. Deacetylation of p53 modulates its effect on cell growth and apoptosis. *Nature*, 408(6810):377–81, 2000.

C. A. Lyssiotis, J. Walker, C. Wu, T. Kondo, P. G. Schultz, and X. Wu. Inhibition of histone deacetylase activity induces developmental plasticity in oligodendrocyte precursor cells. *Proc Natl Acad Sci U S A*, 104(38):14982–7, 2007.

N. Majdzadeh, L. Wang, B. E. Morrison, R. Bassel-Duby, E. N. Olson, and S. R. D'Mello. Hdac4 inhibits cell-cycle progression and protects neurons from cell death. *Dev Neurobiol*, 68(8):1076–92, 2008.

P. Malatesta, E. Hartfuss, and M. Gotz. Isolation of radial glial cells by fluorescent-activated cell sorting reveals a neuronal lineage. *Development*, 127(24):5253–63, 2000.

P. Malatesta, M. A. Hack, E. Hartfuss, H. Kettenmann, W. Klinkert, F. Kirchhoff, and M. Gotz. Neuronal or glial progeny: regional differences in radial glia fate. *Neuron*, 37(5):751–64, 2003.

M. Marin-Husstege, M. Muggironi, A. Liu, and P. Casaccia-Bonnefil. Histone deacetylase activity is necessary for oligodendrocyte lineage progression. *J Neurosci*, 22(23):10333–45, 2002.

S. Matsumoto, F. Banine, J. Struve, R. Xing, C. Adams, Y. Liu, D. Metzger, P. Chambon, M. S. Rao, and L. S. Sherman. Brg1 is required for murine neural stem cell maintenance and gliogenesis. *Dev Biol*, 289(2):372–83, 2006.

M. McCarthy, D. Auger, and S. R. Whittemore. Human cytomegalovirus causes productive infection and neuronal injury in differentiating fetal human central nervous system neuroepithelial precursor cells. *J Hum Virol*, 3(4):215–28, 2000.

M. McCarthy, D. H. Turnbull, C. A. Walsh, and G. Fishell. Telencephalic neural progenitors appear to be restricted to regional and glial fates before the onset of neurogenesis. *J Neurosci*, 21(17):6772–81, 2001.

F. T. Merkle, A. D. Tramontin, J. M. Garcia-Verdugo, and A. Alvarez-Buylla. Radial glia give rise to adult neural stem cells in the subventricular zone. *Proc Natl Acad Sci U S A*, 101(50):17528–32, 2004.

J. P. Misson, M. A. Edwards, M. Yamamoto, and Jr. Caviness, V. S. Mitotic cycling of radial glial cells of the fetal murine cerebral wall: a combined autoradiographic and immunohistochemical study. *Brain Res*, 466(2):183–90, 1988.

T. Miyata, T. Maeda, and J. E. Lee. Neurod is required for differentiation of the granule cells in the cerebellum and hippocampus. *Genes Dev*, 13(13):1647–52, 1999.

A. V. Molofsky, S. He, M. Bydon, S. J. Morrison, and R. Pardal. Bmi-1 promotes neural stem cell self-renewal and neural development but not mouse growth and survival by repressing the p16ink4a and p19arf senescence pathways. *Genes Dev*, 19(12):1432–7, 2005.

R. L. Montgomery, C. A. Davis, M. J. Potthoff, M. Haberland, J. Fielitz, X. Qi, J. A. Hill, J. A. Richardson, and E. N. Olson. Histone deacetylases 1 and 2 redundantly regulate cardiac morphogenesis, growth, and contractility. *Genes Dev*, 21(14):1790–802, 2007.

S. Morettini, V. Podhraski, and A. Lusser. Atp-dependent chromatin remodeling enzymes and their various roles in cell cycle control. *Front Biosci*, 13:5522–32, 2008.

T. Mori, K. Tanaka, A. Buffo, W. Wurst, R. Kuhn, and M. Gotz. Inducible gene deletion in astroglia and radial glia–a valuable tool for functional and lineage analysis. *Glia*, 54(1):21–34, 2006.

B. E. Morrison, N. Majdzadeh, X. Zhang, A. Lyles, R. Bassel-Duby, E. N. Olson, and S. R. D'Mello. Neuroprotection by histone deacetylase-related protein. *Mol Cell Biol*, 26(9):3550–64, 2006.

B. E. Morrison, N. Majdzadeh, and S. R. D'Mello. Histone deacetylases: focus on the nervous system. *Cell Mol Life Sci*, 64(17):2258–69, 2007.

C. M. Morshead, B. A. Reynolds, C. G. Craig, M. W. McBurney, W. A. Staines, D. Morassutti, S. Weiss, and D. van der Kooy. Neural stem cells in the adult mammalian forebrain: a relatively quiescent subpopulation of subependymal cells. *Neuron*, 13(5):1071–82, 1994.

C. Muchardt, B. Bourachot, J. C. Reyes, and M. Yaniv. ras transformation is associated with decreased expression of the brm/snf2alpha atpase from the mammalian swi-snf complex. *Embo J*, 17(1):223–31, 1998.

G. J. Narlikar, H. Y. Fan, and R. E. Kingston. Cooperation between complexes that regulate chromatin structure and transcription. *Cell*, 108(4):475–87, 2002.

J. Ninkovic and M. Gotz. Signaling in adult neurogenesis: from stem cell niche to neuronal networks. *Curr Opin Neurobiol*, 17(3):338–44, 2007.

J. Ninkovic, T. Mori, and M. Gotz. Distinct modes of neuron addition in adult mouse neurogenesis. *J Neurosci*, 27(40):10906–11, 2007.

S. C. Noctor, A. C. Flint, T. A. Weissman, W. S. Wong, B. K. Clinton, and A. R. Kriegstein. Dividing precursor cells of the embryonic cortical ventricular zone have morphological and molecular characteristics of radial glia. *J Neurosci*, 22(8): 3161–73, 2002.

C. Nolte, M. Matyash, T. Pivneva, C. G. Schipke, C. Ohlemeyer, U. K. Hanisch, F. Kirchhoff, and H. Kettenmann. Gfap promoter-controlled egfp-expressing transgenic mice: a tool to visualize astrocytes and astrogliosis in living brain tissue. *Glia*, 33(1):72–86, 2001.

A. Novak, C. Guo, W. Yang, A. Nagy, and C. G. Lobe. Z/eg, a double reporter mouse line that expresses enhanced green fluorescent protein upon cre-mediated excision. *Genesis*, 28(3-4):147–55, 2000.

R. S. Nowakowski, S. B. Lewin, and M. W. Miller. Bromodeoxyuridine immunohistochemical determination of the lengths of the cell cycle and the dna-synthetic phase for an anatomically defined population. *J Neurocytol*, 18(3):311–8, 1989.

M. C. Nunes, N. S. Roy, H. M. Keyoung, R. R. Goodman, 2nd McKhann, G., L. Jiang, J. Kang, M. Nedergaard, and S. A. Goldman. Identification and isolation

of multipotential neural progenitor cells from the subcortical white matter of the adult human brain. *Nat Med*, 9(4):439–47, 2003.

K. Ono, H. Takebayashi, K. Ikeda, M. Furusho, T. Nishizawa, K. Watanabe, and K. Ikenaka. Regional- and temporal-dependent changes in the differentiation of olig2 progenitors in the forebrain, and the impact on astrocyte development in the dorsal pallium. *Dev Biol*, 2008.

L. Ooi, N. D. Belyaev, K. Miyake, I. C. Wood, and N. J. Buckley. Brg1 chromatin remodeling activity is required for efficient chromatin binding by repressor element 1-silencing transcription factor (rest) and facilitates rest-mediated repression. *J Biol Chem*, 281(51):38974–80, 2006.

D. S. Ory, B. A. Neugeboren, and R. C. Mulligan. A stable human-derived packaging cell line for production of high titer retrovirus/vesicular stomatitis virus g pseudotypes. *Proc Natl Acad Sci U S A*, 93(21):11400–6, 1996.

D. F. Owens and A. R. Kriegstein. Is there more to gaba than synaptic inhibition? *Nat Rev Neurosci*, 3(9):715–27, 2002.

T. D. Palmer, J. Takahashi, and F. H. Gage. The adult rat hippocampus contains primordial neural stem cells. *Mol Cell Neurosci*, 8(6):389–404, 1997.

T. D. Palmer, A. R. Willhoite, and F. H. Gage. Vascular niche for adult hippocampal neurogenesis. *J Comp Neurol*, 425(4):479–94, 2000.

J. A. Payne, C. Rivera, J. Voipio, and K. Kaila. Cation-chloride co-transporters in neuronal communication, development and trauma. *Trends Neurosci*, 26(4): 199–206, 2003.

W. S. Pear, G. P. Nolan, M. L. Scott, and D. Baltimore. Production of high-titer helper-free retroviruses by transient transfection. *Proc Natl Acad Sci U S A*, 90 (18):8392–6, 1993.

L. Pinto, M. T. Mader, M. Irmler, M. Gentilini, F. Santoni, D. Drechsel, R. Blum, R. Stahl, A. Bulfone, P. Malatesta, J. Beckers, and M. Gotz. Prospective isolation of functionally distinct radial glial subtypes–lineage and transcriptome analysis. *Mol Cell Neurosci*, 38(1):15–42, 2008.

T. Prozorovski, U. Schulze-Topphoff, R. Glumm, J. Baumgart, F. Schroter, O. Ninnemann, E. Siegert, I. Bendix, O. Brustle, R. Nitsch, F. Zipp, and O. Aktas. Sirt1

contributes critically to the redox-dependent fate of neural progenitors. *Nat Cell Biol*, 10(4):385–94, 2008.

C. Ramirez-Castillejo, F. Sanchez-Sanchez, C. Andreu-Agullo, S. R. Ferron, J. D. Aroca-Aguilar, P. Sanchez, H. Mira, J. Escribano, and I. Farinas. Pigment epithelium-derived factor is a niche signal for neural stem cell renewal. *Nat Neurosci*, 9(3):331–9, 2006.

J. M. Rhee, M. K. Pirity, C. S. Lackan, J. Z. Long, G. Kondoh, J. Takeda, and A. K. Hadjantonakis. In vivo imaging and differential localization of lipid-modified gfp-variant fusions in embryonic stem cells and mice. *Genesis*, 44(4):202–18, 2006.

S. J. Riedl and Y. Shi. Molecular mechanisms of caspase regulation during apoptosis. *Nat Rev Mol Cell Biol*, 5(11):897–907, 2004.

J. D. Rothstein, L. Martin, A. I. Levey, M. Dykes-Hoberg, L. Jin, D. Wu, N. Nash, and R. W. Kuncl. Localization of neuronal and glial glutamate transporters. *Neuron*, 13(3):713–25, 1994.

A. Salminen, T. Tapiola, P. Korhonen, and T. Suuronen. Neuronal apoptosis induced by histone deacetylase inhibitors. *Brain Res Mol Brain Res*, 61(1-2):203–6, 1998.

U. B. Schambra, J. Silver, and J. M. Lauder. An atlas of the prenatal mouse brain: gestational day 14. *Exp Neurol*, 114(2):145–83, 1991.

A. Schaper. The earliest differentiation in the central nervous system of vertebrates. *Science*, 5(1):430–431, 1897. 0890-9369 (Print) Book Chapter.

R. Seidenfaden, A. Desoeuvre, A. Bosio, I. Virard, and H. Cremer. Glial conversion of svz-derived committed neuronal precursors after ectopic grafting into the adult brain. *Mol Cell Neurosci*, 32(1-2):187–98, 2006.

S. Seo and K. L. Kroll. Geminin's double life: chromatin connections that regulate transcription at the transition from proliferation to differentiation. *Cell Cycle*, 5 (4):374–9, 2006.

S. Seo, A. Herr, J. W. Lim, G. A. Richardson, H. Richardson, and K. L. Kroll. Geminin regulates neuronal differentiation by antagonizing brg1 activity. *Genes Dev*, 19(14):1723–34, 2005a.

S. Seo, G. A. Richardson, and K. L. Kroll. The swi/snf chromatin remodeling protein brg1 is required for vertebrate neurogenesis and mediates transactivation of ngn and neurod. *Development*, 132(1):105–15, 2005b.

B. Seri, J. M. Garcia-Verdugo, B. S. McEwen, and A. Alvarez-Buylla. Astrocytes give rise to new neurons in the adult mammalian hippocampus. *J Neurosci*, 21 (18):7153–60, 2001.

B. Seri, J. M. Garcia-Verdugo, L. Collado-Morente, B. S. McEwen, and A. Alvarez-Buylla. Cell types, lineage, and architecture of the germinal zone in the adult dentate gyrus. *J Comp Neurol*, 478(4):359–78, 2004.

M. Shaked, K. Weissmuller, H. Svoboda, P. Hortschansky, N. Nishino, S. Wolfl, and K. L. Tucker. Histone deacetylases control neurogenesis in embryonic brain by inhibition of bmp2/4 signaling. *PLoS ONE*, 3(7):e2668, 2008.

S. Shen, J. Li, and P. Casaccia-Bonnefil. Histone modifications affect timing of oligodendrocyte progenitor differentiation in the developing rat brain. *J Cell Biol*, 169(4):577–89, 2005.

F. A. Siebzehnrubl, R. Buslei, I. Y. Eyupoglu, S. Seufert, E. Hahnen, and I. Blumcke. Histone deacetylase inhibitors increase neuronal differentiation in adult forebrain precursor cells. *Exp Brain Res*, 176(4):672–8, 2007.

S. Sif, A. J. Saurin, A. N. Imbalzano, and R. E. Kingston. Purification and characterization of msin3a-containing brg1 and hbrm chromatin remodeling complexes. *Genes Dev*, 15(5):603–18, 2001.

M. T. Stockhausen, J. Sjolund, C. Manetopoulos, and H. Axelson. Effects of the histone deacetylase inhibitor valproic acid on notch signalling in human neuroblastoma cells. *Br J Cancer*, 92(4):751–9, 2005.

T. Storck, S. Schulte, K. Hofmann, and W. Stoffel. Structure, expression, and functional analysis of a na(+)-dependent glutamate/aspartate transporter from rat brain. *Proc Natl Acad Sci U S A*, 89(22):10955–9, 1992.

B. D. Strahl and C. D. Allis. The language of covalent histone modifications. *Nature*, 403(6765):41–5, 2000.

P. Sudarsanam and F. Winston. The swi/snf family nucleosome-remodeling complexes and transcriptional control. *Trends Genet*, 16(8):345–51, 2000.

C. Sumi-Ichinose, H. Ichinose, D. Metzger, and P. Chambon. Snf2beta-brg1 is essential for the viability of f9 murine embryonal carcinoma cells. *Mol Cell Biol*, 17(10):5976–86, 1997.

G. Sun, R. T. Yu, R. M. Evans, and Y. Shi. Orphan nuclear receptor tlx recruits histone deacetylases to repress transcription and regulate neural stem cell proliferation. *Proc Natl Acad Sci U S A*, 104(39):15282–7, 2007.

N. U. Takemura. Evidence for neurogenesis within the white matter beneath the temporal neocortex of the adult rat brain. *Neuroscience*, 134(1):121–32, 2005.

A. Tashiro, V. M. Sandler, N. Toni, C. Zhao, and F. H. Gage. Nmda-receptor-mediated, cell-specific integration of new neurons in adult dentate gyrus. *Nature*, 442(7105):929–33, 2006.

C. M. Trivedi, Y. Luo, Z. Yin, M. Zhang, W. Zhu, T. Wang, T. Floss, M. Goettlicher, P. R. Noppinger, W. Wurst, V. A. Ferrari, C. S. Abrams, P. J. Gruber, and J. A. Epstein. Hdac2 regulates the cardiac hypertrophic response by modulating gsk3 beta activity. *Nat Med*, 13(3):324–31, 2007.

M. Vignali, A. H. Hassan, K. E. Neely, and J. L. Workman. Atp-dependent chromatin-remodeling complexes. *Mol Cell Biol*, 20(6):1899–910, 2000.

A. K. Voss, T. Thomas, and P. Gruss. Compensation for a gene trap mutation in the murine microtubule-associated protein 4 locus by alternative polyadenylation and alternative splicing. *Dev Dyn*, 212(2):258–66, 1998.

P. A. Wade. Methyl cpg binding proteins: coupling chromatin architecture to gene regulation. *Oncogene*, 20(24):3166–73, 2001.

B. P. Williams and J. Price. Evidence for multiple precursor cell types in the embryonic rat cerebral cortex. *Neuron*, 14(6):1181–8, 1995.

Z. Xu, X. Meng, Y. Cai, M. J. Koury, and S. J. Brandt. Recruitment of the swi/snf protein brg1 by a multiprotein complex effects transcriptional repression in murine erythroid progenitors. *Biochem J*, 399(2):297–304, 2006.

M. Yamaguchi, N. Tonou-Fujimori, A. Komori, R. Maeda, Y. Nojima, H. Li, H. Okamoto, and I. Masai. Histone deacetylase 1 regulates retinal neurogenesis in zebrafish by suppressing wnt and notch signaling pathways. *Development*, 132(13):3027–43, 2005.

Y. Yang, T. Stopka, N. Golestaneh, Y. Wang, K. Wu, A. Li, B. K. Chauhan, C. Y. Gao, K. Cveklova, M. K. Duncan, R. G. Pestell, A. B. Chepelinsky, A. I. Skoultchi, and A. Cvekl. Regulation of alphaa-crystallin via pax6, c-maf, creb and a broad domain of lens-specific chromatin. *Embo J*, 25(10):2107–18, 2006.

M. Yoshida and T. Beppu. Reversible arrest of proliferation of rat 3y1 fibroblasts in both the g1 and g2 phases by trichostatin a. *Exp Cell Res*, 177(1):122–31, 1988.

T. Yoshimura, Y. Kawano, N. Arimura, S. Kawabata, A. Kikuchi, and K. Kaibuchi. Gsk-3beta regulates phosphorylation of crmp-2 and neuronal polarity. *Cell*, 120 (1):137–49, 2005.

M. Zerlin, A. Milosevic, and J. E. Goldman. Glial progenitors of the neonatal subventricular zone differentiate asynchronously, leading to spatial dispersion of glial clones and to the persistence of immature glia in the adult mammalian cns. *Dev Biol*, 270(1):200–13, 2004.

Y. Zhang, H. H. Ng, H. Erdjument-Bromage, P. Tempst, A. Bird, and D. Reinberg. Analysis of the nurd subunits reveals a histone deacetylase core complex and a connection with dna methylation. *Genes Dev*, 13(15):1924–35, 1999.

C. Zhao, W. Deng, and F. H. Gage. Mechanisms and functional implications of adult neurogenesis. *Cell*, 132(4):645–60, 2008.

X. Zhao, T. Ueba, B. R. Christie, B. Barkho, M. J. McConnell, K. Nakashima, E. S. Lein, B. D. Eadie, A. R. Willhoite, A. R. Muotri, R. G. Summers, J. Chun, K. F. Lee, and F. H. Gage. Mice lacking methyl-cpg binding protein 1 have deficits in adult neurogenesis and hippocampal function. *Proc Natl Acad Sci U S A*, 100 (11):6777–82, 2003.

Y. Zhou, E. Takahashi, W. Li, A. Halt, B. Wiltgen, D. Ehninger, G. D. Li, J. W. Hell, M. B. Kennedy, and A. J. Silva. Interactions between the nr2b receptor and camkii modulate synaptic plasticity and spatial learning. *J Neurosci*, 27(50): 13843–53, 2007.

S. Zimmermann, F. Kiefer, and M. Goettlicher. Reduced body size and decreased intestinal tumor rates in hdac2-mutant mice. *Cancer Res 2007*, 67(19):1–8, 2007.